Modelling of Complex Plasmas

Modellering van Complexe Plasma's

(met een samenvatting in het Nederlands)

PROEFSCHRIFT

TER VERKRIJGING VAN DE GRAAD VAN DOCTOR AAN DE
UNIVERSITEIT UTRECHT, OP GEZAG VAN DE
RECTOR MAGNIFICUS, PROF. DR. W.H. GISPEN, INGEVOLGE
HET BESLUIT VAN HET COLLEGE VOOR
PROMOTIES IN HET OPENBAAR TE VERDEDIGEN OP
VRIJDAG 26 SEPTEMBER 2003 DES OCHTENDS TE 10.30 UUR

DOOR

MOHAMED REDA AKDIM

GEBOREN OP 27 JANUARI 1976, TE UTRECHT

Dit proefschrift is goedgekeurd door de promotoren:

Prof. dr. F.C. Schüller
Faculteit Natuur- en Sterrenkunde Universiteit Utrecht
Copromotor:
Dr. W.J. Goedheer
FOM-instituut voor Plasmafysica Rijnhuizen

And it is We who have built the universe
with our power; and, verily, it is We who are
steadily expanding it.

The Qur'an (51:47)

Contents

1. Introduction

1.1   Historical background

Tonks and Langmuir (1929) were the first ones who used the term 'plasma' to describe the inner region of a glowing ionized gas produced by means of an electric discharge in a tube. The term plasma represents a gas containing many interacting charged particles (electrons and ions) and neutrals. In outer space, a lot of matter exists in the form of a plasma, e.g. stars and nebulas. In some cases the plasma coexists with dust particles (nebulas). These particles can range from nanometers up to microns in diameter. They are also seen as building blocks for planet formation. These dust particles are in most cases not neutral, they obtain either a positive or negative charge due to interaction with the surrounding plasma and photon flux. In space the dust particles usually obtain a positive charge due to photo-ionization. A dust particle embedded in a plasma becomes generally negatively charged by the collection of electrons. A mixture of charged dust particles, electrons, ions and neutrals is called a 'dusty' or complex plasma. The historical background of dusty plasmas is quite old. In old manuscripts, bright comets have been described, like the famous comet of Halley. These comets are excellent examples for the study of dust-plasma interactions in space. A simple and nice example of dust-plasma interaction on a laboratory scale is an ordinary flame. The fact that a flame is considered as a plasma may seem as a surprise. However, strictly it is not. What makes it it close to being a plasma is the presence of very small particles ($\sim 100 \mathring{A}$) of unburnt carbon. The yellow light emitted by the typical hydrocarbon flames is due to incandescence of these small dust particles heated to well over 1000 degrees Celsius. The thermionic emission of electrons from the dust particles elevates the degree of ionization within the flame to several orders of magnitude above what is predicted by the Saha equation for air at that temperature. There are more recent examples of dusty plasmas. These are ion thrusters used for propagation of satellites, processing plasmas used in device fabrication (e.g. amorphous silicon solar cells, microchips for computers), dusty plasmas created in laboratories for studying collective processes, plasma crystals, etc. In thermonuclear fusion plasmas dust formation takes place in the cool edge layers in contact with material walls. The dust has become a safety issue for future fusion reactors (ITER). The dust particles may retain a large fraction of hydrogen which will lead to considerable tritium inventories [1]. Furthermore, these fine dispersed dust particles may be chemically reactive and may spontaneously react with oxygen or water vapor in the case of a vacuum or coolant leak. Another

aspect is the migration of dust particles. Due to thermophoretic forces and due to repetitive evaporation and condensation they may accumulate at cold areas of the device and they may block spacings and fill gaps which were introduced for engineering reasons.

1.2 Complex plasmas

In the previous paragraph some examples of dusty plasmas have been given. In the case of a processing plasma, e.g. for the fabrication of amorphous silicon solar cells, a mixture of silane and hydrogen gas is injected in a reactor. These gases are decomposed by making a plasma. A plasma with a low degree of ionization (typically 10^{-5}) is usually made in a reactor containing two electrodes driven by a radio-frequency (RF) power source in the megahertz regime. In that case a RF plasma is made in which a lot of species (ions, radicals, neutrals and electrons) are formed. Under the right circumstances the radicals, neutrals and ions can react further to produce nanometer sized dust particles. These particles can stick to the surface and thereby contribute to a higher deposition rate (increase with 100 %) which is often seen when the plasma enters the so-called γ'-regime. Still no definitive explanation has been found for this large increase in deposition rate. Another possibility is that these nanometer sized particles coagulate and form larger micron sized particles. These particles obtain a high negative charge, due to their large radius and are usually trapped in a radio-frequency plasma, because of there interaction with the electric field present in the discharge sheaths which is directed towards the electrodes (fig. 1.1)

When the interaction of the dust particles with the plasma changes considerably the plasma quantities as e.g. electric potential, electron density and temperature, ion densities and gas temperature, the plasma is called a dusty or complex plasma. Others [2] have studied complex plasmas by injection of spherical micron sized particles in noble gas plasmas. On earth usually a two-dimensional dust crystal is formed containing several lattices. In these crystals the dust particles hold each other at regular distances due to the Coulomb force. Electrons, ions and neutrals can still move freely through the lattices. In some of these dust crystals a dust free region (void) has been observed [3] which is usually surrounded by a crystalline region. Similar experiments have been carried out on the MIR, International Space Station (ISS) and TEXUS rocket experiments to observe dust crystals under microgravity. These microgravity experiments show three-dimensional crystals with a void in the middle. The appearance of this void was a mystery for quite some time. Modelling efforts from our side have shed some light on this issue.
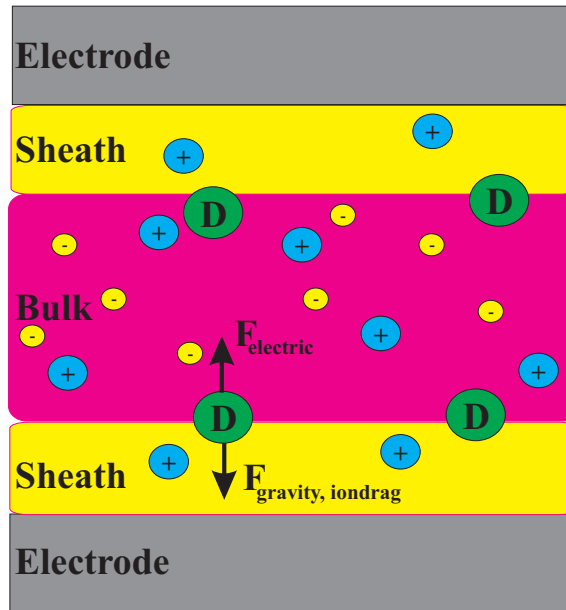
Figure 1.1: Schematic drawing of RF plasma with dust.

1.3 Previous work, Contribution of this thesis

Prior to the work in this thesis, modelling has already addressed the behavior of dust in radio frequency plasmas [4, 5, 6] . However these models can not be used to model discharges which contain a large amount of dust (million of dust particles) as in the experiments carried out under microgravity. Usually important processes like, e.g. recombination on the surface of the dust, dust transport, accounting for the dust charge in the Poisson equation and heating of a dust particle are neglected. The main contribution of this thesis is the self-consistent modelling of complex plasmas including the important processes mentioned above. For this two previously developed fluid models (silane and argon) [7, 8] have been extended with a dust fluid to model a complex plasma. The one-dimensional silane fluid model has been extended with dust as an additional species to find a possible mechanism which could explain the large increase in deposition rate seen in the experiments when the plasma enters the dusty regime. To model the experiments performed at the ISS, a two dimensional argon fluid model has been extended with dust. Both extended models are special in the sense, that these where the first models which could deal with the transport of large quantities of dust. The main problem behind modelling the transport of dust is the large difference in time scales between the highly mobile electrons (10^{-9} s) and the slow, heavy dust particles ($10^{-2} - 1$ s)

1.4   Outline thesis

This thesis deals with numerical fluid models which have been extended to model complex radio-frequency discharges. In the models dust is also treated as a fluid. The models are based on a combination of particle and energy balance equations for the plasma and neutral species, the Boltzmann equation to solve the electron energy distribution function and important processes which are triggered by the dust species. In chapter 2, the relevant basic theory of complex plasmas is reviewed. In chapter 3, the one-dimensional silane model extended with a dust fluid is described. Also results, e.g., for the electric potential, densities and deposition rates obtained for silane plasmas containing different amounts of dust are discussed. In chapter 4, the two-dimensional argon-dust fluid model has been used to give some insight in the formation of the void seen in the dust crystal experiments carried under microgravity. In chapter 5, the two-dimensional argon model extended with a dust fluid is described. Results obtained for situations where the dust fluid has a significant influence on the plasma properties are shown. In chapter 6, the two-dimensional argon-dust fluid model has been extended with a particle tracking module to take the inertia of the dust particle into account. The particle tracking module is described. Results obtained with this extended model show vortices which usually appear in dusty plasma experiments carried out under microgravity. In Chapter 7, the two-dimensional particle tracking model in which the forces are taken from the argon-dust fluid model is compared with a three-dimensional particle tracking model where the forces are modelled via a harmonic potential. Chapter 8, deals with the extension of the model described in chapter 5 to a multi dust fluid model. In this model different sized dust species can be followed. Results are shown for situations where the different sized species interact with each other. In chapter 9, the argon-dust fluid model described in chapter 5 is extended to a model that can deal with discharges containing positive ions, negative ions and dust. Comparisons are made for dusty electropositive and dusty electronegative discharges. The chapters 3 through 9 are approximately one to one copies of the papers listed below.

1.5   Publications related to this thesis

1.5.1   Publications related to chapters of this thesis

- M. R. Akdim and W. J. Goedheer, Modelling of dust in a silane/hydrogen plasma, Journal of Applied Physics, Vol 94, 1 (2003) (Chapter 3).
- M. R. Akdim and W. J. Goedheer, Modelling of voids in a colloidal plasmas, Physical Review E, Vol 65, 015401(R) (2002) (Chapter 4).

- M. R. Akdim and W. J. Goedheer, Modelling the effect of dust on the plasma parameters in a dusty argon discharge, Physical Review E, Vol 67, 066407 (2003), (Chapter 5).
- M. R. Akdim and W. J. Goedheer, Modelling of self-excited dust vortices in complex plasmas under microgravity, Physical Review E, Vol 67, 056405 (2003) (Chapter 6).
- W. J. Goedheer and M. R. Akdim, Vortices in dust clouds under microgravity: a simple explanation, Physical Review E, accepted, (2003) (Chapter 7).
- M. R. Akdim, W. J. Goedheer and R. P. Dahiya, Modelling of two differently sized dust species in plasmas under micro-gravity, New Journal of Physics, Focus issue: Complex plasmas, Vol 5, 20 (2003) (Chapter 8).
- M. R. Akdim and W. J. Goedheer, Modelling of voids in electronegative discharges under microgravity, submitted to IEEE, (2003) (Chapter 9).
- M. R. Akdim, Stof tot nadenken, Nederlands Tijdschrift voor Natuurkunde, January 2002.

1.5.2   Contributions to work of others

- A. C. W. Biebericher, W. F. Van der Weg, J. K. Rath, M. R. Akdim and W. J. Goedheer, Gas-efficient deposition of device quality hydrogenated amorphous silicon using low gas flows and power modulated radio frequency discharges, J. Vac. Sci. Technol. A, Vol 21, (2003).
- W. J. Goedheer, M. R. Akdim and Yu. I. Chutov, Hydrodynamic and kinetic modelling of dust free and dust radio-frequency discharges, submitted to Contr. Plasma. Phys., (2003).

1.5.3   Contributions to various international workshops and conferences

- M. R. Akdim and W. J. Goedheer, Modelling of dust in a silane/hydrogen plasma, IVth European Workshop on Dusty and Colloidal Plasmas, Lisbon, (2000) (Poster contribution).
- M. R. Akdim and W. J. Goedheer, Modelling of voids in colloidal plasmas, 9th Workshop on the Physics of Dusty Plasmas, Iowa, (2001) (Poster contribution).
- M. R. Akdim and W. J. Goedheer, Modelling of PKE-Nefedov dusty plasma microgravity experiments, Proceedings, 29th EPS conference on plasma Phys. and Contr. Fusion, Montreux, (2002) (Oral contribution).
- M. R. Akdim and W. J. Goedheer, Modelling of voids in electronegative discharges under microgravity, 10th Workshop on the Physics of Dusty Plasmas, Virgin Islands, (2003) (Oral contribution) .

References

[1] J. Winter, Plasma Phys. Control. Fusion, **40**, 1201 (1998).

[2] G. E. Morfill et al, Phys. Rev. Lett., **83**, 1598 (1999).

[3] R. P. Dahiya et al, Phys. Rev. Lett., **89**, 125001 (2002).

[4] V. Vyas et al, J. Appl. Phys., **92**, 6451 (2002).

[5] T. Nitter , Plasma Sources Sci. Technol., **5**, 93 (1996).

[6] P. Belenguer et al, Phys. Rev. A., **46**, 7923 (1992).

[7] G. J. Nienhuis et al, J. Appl. Phys., **82**, 2060 (1997).

[8] J. D. P. Passchier et al, J. Appl. Phys., **73**, 1073 (1993).

2. Basic theory

2.1 Characteristics of complex plasmas

2.1.1 Charging of a dust particle: the floating potential

The charge and potential of a dust particle immersed in a plasma is determined by the balance between the electron and ion current towards the dust particle's surface. Since electrons are more mobile than ions, a dust particle in a plasma will acquire a negative charge and thus a negative potential with respect to the surrounding plasma potential. The floating potential of the dust particle's adjusts itself in such a way that, by repelling the mobile electrons and attracting positive ions, the dust particle on average collects no net charge at steady state. Dust particles in a plasma behave as a microscopic probe. The general aspects of probe theory are therefore important for dusty plasmas. To determine the charge and floating potential of a dust particle in a plasma, descriptions of the electron and ion transport towards the dust particle's surface in the perturbed potential around the particle are required. In most approximations it is assumed that the width of the sheath region around a dust particle is smaller than electron-neutral or ion-neutral collision mean free path. This means that the charged particle transport is collisionless in the sheath. If the effect of individual Coulomb collisions is neglected in comparison to collective phenomena, the problem reduces tot the solutions of the charged particle Vlasov equations:

$$\boldsymbol{v} \cdot \boldsymbol{\nabla}_r f_e(\boldsymbol{r}, \boldsymbol{v}) - \frac{e}{m_e} \boldsymbol{E} \cdot \boldsymbol{\nabla}_v f_e(\boldsymbol{r}, \boldsymbol{v}) = 0 \tag{2.1}$$

and

$$\boldsymbol{v} \cdot \boldsymbol{\nabla}_r f_i(\boldsymbol{r}, \boldsymbol{v}) + \frac{e}{m_i} \boldsymbol{E} \cdot \boldsymbol{\nabla}_v f_i(\boldsymbol{r}, \boldsymbol{v}) = 0 \tag{2.2}$$

where $\boldsymbol{E} = -\boldsymbol{\nabla} V$, V is the electric potential, m_e and m_i are the electron and ion masses and e the elementary charge. The solution of the Poisson equation is given by:

$$-\nabla^2 V = \boldsymbol{\nabla} \cdot \boldsymbol{E} = \frac{e}{\epsilon_0} \left(n_+ - n_e \right). \tag{2.3}$$

For a plasma, the charged particle distributions $f_e(\boldsymbol{r}, \boldsymbol{v})$ and $f_+(\boldsymbol{r}, \boldsymbol{v})$ are related to electron (n_e) and (n_+) ion densities by

$$n_{e,+}(\boldsymbol{r}) = \int f_{e,+}(\boldsymbol{r}, \boldsymbol{v}) d^3 v, \tag{2.4}$$

If the loss of electrons to the dust particle does not affect the electron density and if the electron distribution function in the unperturbed plasma is a Maxwellian, a good approximate solution to the Vlasov equation for electrons in a repulsive potential (i.e. potential of a negatively charged dust particle), is a Boltzmann distribution,

$$n_e(r) = n_\infty \exp\left(\frac{e\left[V(r) - V_\infty\right]}{k_B T_e} \right),$$
(2.5)

where n_∞ is the density and V_∞ is the potential of the unperturbed plasma far away from the dust particle, k_B is the Boltzmann constant and T_e is the electron temperature. Usually in low-temperature plasmas the electron distribution function is non-Maxwellian and the above expression may be inaccurate.

Orbital motion limited theory for a spherical dust particle

We assume that the electron density around a spherical dust particle is given by a Boltzmann distribution,

$$n_e(r) = n_\infty \exp\left(\frac{eV(r)}{k_B T_e} \right).$$
(2.6)

V_∞ has been taken equal to 0 in equation 2.6. The problem to be solved is the spatial distribution of ions around the dust particle and the collected ion current. The first expressions of the ion current towards the dust particle's surface in the sheath regime were obtained by Mott-Smith and Langmuir (1926). This OML (orbit motion limited) theory assumes that for every ion energy there exists an ion impact parameter that makes the ion hit the dust particle with a grazing incidence. The trajectory of an ion can be derived as in the classical collision theory except that, due to the finite radius of the dust particle, the ion can be collected if its radial position reaches the radius of the dust particle r=a. In case of an ion with an energy E_0 and angular momentum J_0 at infinity, and a dust particle with radius a is placed at r=0, the conservation of energy and angular momentum gives

$$E_0 = \frac{1}{2} m_+ \dot{r}^2 + \frac{1}{2} \frac{J_0^2}{m_+ r^2} + eV(r),$$
(2.7)

the ion impact parameter b is related to J_0 by $J_0 = m_+ v_0 b$ (v_0 is the initial ion velocity). Equation 2.7 can be transformed into

$$b = r \left[1 - \frac{eV(r)}{E_0} - \frac{1}{2} \frac{m_+ \dot{r}^2}{E_0} \right]^{1/2}.$$
(2.8)

The ions whose impact parameter is b_{coll} with

$$b_{coll} = a \left[1 - \frac{eV(a)}{E_0} \right]^{1/2}$$
(2.9)

will hit the dust particle with zero radial velocity. Therefore all ions of energy E_0 whose impact parameter is less than b_{coll} will hit and be collected by the dust particle. The cross-section σ_{coll} for ion collection by the dust particle can be defined as:

$$\sigma_{coll} = \pi b_{coll}^2 = \pi a^2 \left[1 - \frac{eV(a)}{E_0} \right]^{1/2} \tag{2.10}$$

For monoenergetic ions, the ion current to the dust particle is then

$$I_+ = n_\infty e v_0 \sigma_{coll} = \pi a^2 n_\infty e \left(\frac{2E_0}{m_+} \right)^{1/2} \left[1 - \frac{eV(a)}{E_0} \right] \tag{2.11}$$

This expression gives the OML current, i.e. the maximum ion current that a spherical dust particle can collect assuming collisionless and stationary plasma conditions. In the derivation above the existence of ion trajectories reflected by an 'absorption barrier' due to possible secondary maxima in the effective potential energy curves are neglected.

In these conditions the positive ion density can be formulated as:

$$n_+ = \frac{1}{2} n_\infty \left(\left[1 - \frac{eV(r)}{E_0} \right]^{1/2} + \left[1 - \frac{eV(r)}{E_0} - \frac{I_+}{I_r} \right]^{1/2} \right) \tag{2.12}$$

where I_r is given by

$$I_r = \pi r^2 n_\infty e \left(\frac{2E_0}{m_+} \right). \tag{2.13}$$

Equation 2.12 shows that positive ion density increases from the plasma toward the dust particle, assuming that the potential becomes more negative when the particle is approached.

Substituting equation 2.12 and equation 2.6 in the Poisson equation gives

$$\Delta V = -\frac{e}{\epsilon_0} n_\infty \left\{ \frac{1}{2} \left(\left[1 - \frac{eV(r)}{E_0} \right]^{1/2} + \left[1 - \frac{eV(r)}{E_0} - \frac{I_+}{I_r} \right]^{1/2} \right) \right.$$
$$\left. - \exp \left[\frac{eV(r)}{k_B T_e} \right] \right\}. \tag{2.14}$$

Equation 2.14 can be linearized for large values of r/a. This results in

$$\left(\Delta - \lambda_L^{-2} \right) V = 0, \tag{2.15}$$

where λ_L is the linearized Debye length given by

$$\lambda_L = \left[\frac{e n_\infty}{\epsilon_0} \left(\frac{1}{k_B T_e} + \frac{1}{2E_0} \right) \right]^{-1/2}. \tag{2.16}$$

Solving equation 2.15 gives the Debye-Hückel potential or so-called screened Coulomb potential

$$V(r) = V(a)\frac{a}{r}\exp\left(-\frac{r-a}{\lambda_{\mathrm{L}}}\right).$$
(2.17)

Daugherty et al. [1] have shown that for small values of a/λ_L the exact solution of the Poisson equation is very close to the Debye-Hückel solution for $eV/kT_{e,+} \ll 1$, which is not true near the dust particle. Several radii from the dust particle the real solution is given by the Coulomb potential. This is predicted by the screened Coulomb expression.

In the discussion above we assumed that the ions are monoenergetic. For a Maxwellian ion distribution, the ion current to the dust particle has a similar form as the one derived for the monoenergetic ions:

$$I_+ = \frac{\pi a^2 n_\infty e}{4}\left(\frac{8kT_+}{\pi m_+}\right)^{1/2}\left[1 - \frac{eV(a)}{k_B T_+}\right].$$
(2.18)

For the electrons we take the Boltzmann distribution for the electron density, this gives an electron current

$$I_e = -\frac{\pi a^2 n_\infty e}{4}\left(\frac{8kT_e}{\pi m_e}\right)^{1/2}\exp\left[\frac{eV(a)}{k_B T_e}\right].$$
(2.19)

At steady state the total current towards the dust particle becomes equal to zero. The charge Q_d for a total current of zero can be obtained from

$$Q_d = 4\pi a^2 \sigma$$
(2.20)

where σ is the surface charge density of the dust particle related to the electric field normal to the dust particle surface by

$$\sigma = \epsilon_0 E_r(a) = -\epsilon_0 (\nabla V)|_{r=a}.$$
(2.21)

Using the expression for the Debye-Hückel potential, the charge of a dust particle becomes

$$Q_d = 4\pi\epsilon_0 a\left(1 + \frac{a}{\lambda_L}\right)V(a)$$
(2.22)

As mentioned previously, the OML theory assumes that all the ions with an impact parameter less than b_{coll} are collected by the dust particle. This may be not true because of the specific potential distributions around the dust particle which can reflect ions that would not be reflected in a simpler Coulomb-like potential. The OML theory therefore gives an upper limit to the ion current collected by the dust particle. It is important to know when the OML theory is valid or is

a good approximation since the calculation of the collected ion current is much more complicated in the general case. Usually the OML theory can be used if the Debye-Hückel potential is a good approximation to the potential distribution around the dust particle. This is the case when $a/\lambda_L \ll 1$. Daugherty et al. [1] found that the OML theory for dust particles is a good approximation even when the particle radius is comparable to the electron Debye length.

Non-Maxwellian distribution function

In the OML theory the electron velocity distribution function is assumed to be Maxwellian. This assumption is usually made to obtain simple analytical expressions for the electron current to the dust particle. In a non-equilibrium, low temperature plasma the electron distribution function is often non-Maxwellian. Therefore it is good to estimate the errors made on the charge of a dust particle in these conditions. For a given electron energy distribution function $f(\epsilon)$ (EEDF) the electron current can be obtained from the integral:

$$I_e = -en_e \int_0^\infty \pi b_e^2 \sqrt{\frac{\epsilon}{2m_e}} f_e d\epsilon \tag{2.23}$$

where the cross-section πb_e^2 is calculated from

$$\pi b_e^2 = \begin{cases} \pi a^2 \left(1 - \frac{2eV(a)}{m_e v_e^2}\right), & \text{if} \quad \frac{1}{2}m_e v_e^2 > -eV(a); \\ 0, & \text{if} \quad \frac{1}{2}m_e v_e^2 \leq -eV(a). \end{cases} \tag{2.24}$$

For Maxwellian electrons, this gives the electron current of equation 2.19. Matsoukas and Russell [2] have derived an analytical expression for the electron current for a Druyvesteyn electron distribution. As expected, the number of negatives charges is smaller for a Druyvesteyn distribution than for a Maxwellian, the difference is in the order of 20 %. The explanation lies in the fact that for the same mean energy, the tail of the Druyvesteyn distribution is less populated, the balance of electron and ion current to the particle is achieved with a lower repulsive potential $V(a)$, and the number of charges carried by the dust particle decreases.

Charging time

A dust particle injected or formed in a plasma will charge up, if stochastic effects are neglected, according to the law:

$$\frac{dQ_d}{dt} = I_+ - I_e \tag{2.25}$$

Equation 2.25 gives the time evolution of the number of charges carried by a dust particle. The evolution of the charging time of a dust particle does not have an exponential behavior, this is due to the non-linear dependence of the currents I_e and I_+ on the dust particle potential and charge. Bouchoule [3] has derived a characteristic charging time τ for a dust particle. Using a reduced potential y defined by

$$y = \frac{eV(a)}{kT_e} \tag{2.26}$$

as a new variable, the relation between charge and floating potential $Q_d = 4\pi\epsilon_0 a V(a)$, and the expression for I_e and I_+ of the OML theory results in the following differential equation

$$\frac{dy}{dt} = -A\left[1 + y\frac{T_e}{T_+} - \frac{v_{th,e}}{v_{th,+}}\exp(-y)\right] \quad \text{with} \quad A = \frac{e}{4\epsilon_0}an_\infty\frac{e}{kT_e}v_{th,+} \tag{2.27}$$

At equilibrium ($t \to \infty$), $\frac{dy}{dt} \to 0$. y is the solution of

$$1 + y\frac{T_e}{T_+} - \frac{v_{th,e}}{v_{th,+}}\exp(-y) = 0 \tag{2.28}$$

We take y^* as the equilibrium of y. y^* usually has a value between 1 and 4. Bouchoule [3] has defined the time τ characterizing the evolution of y to its equilibrium values after a perturbation ($y^* + \epsilon$) around the equilibrium value y^*:

$$\tau = \frac{\epsilon}{d\epsilon/dt} \tag{2.29}$$

This gives

$$\tau = \frac{1}{A\left[1 + (T_e/T_+)(1 + y^*)\right]} \tag{2.30}$$

Usually $T_e \gg T_+$, and the charging time simplifies to

$$\tau = 4\frac{\epsilon_0}{e}\left(\frac{\pi m_+}{8e}\right)^{1/2}\frac{(kT_+/e)^{1/2}}{an_\infty(1 + y^*)} \tag{2.31}$$

From equation 2.31 it can be seen that the charging time is inversely proportional to the plasma density and dust particle radius and proportional to the square root of the ion temperature. Punset and Boeuf [3] have shown with their Monte Carlo simulation that the charging time is in the order of 20 μs for a 100 nm radius dust particle in a $5\text{x}10^{15}$ m^{-3} argon plasma, and for T_+/T_e=0.1 and T_e= 3 eV. These times are considerably longer than the RF cycle time but considerably shorter than the time needed for a dust particle to find its equilibrium position.

2.1.2 Coulomb coupling parameter

One other important characteristic of a dusty plasma is its Coulomb coupling parameter which determines the possibility of the formation of dusty plasma crystals. If two dust grains with the same charge are separated form each other by a distance a, the screened Coulomb potential energy is given by

$$E_c = \frac{q_d^2}{a} \exp\left(-\frac{a}{\lambda_D}\right) \qquad (2.32)$$

and the dust thermal energy is $k_B T_d$. The Coulomb coupling parameter is defined as the ratio of the dust potential energy to the dust thermal energy and is represented by

$$\Gamma_c = \frac{q_d^2}{a k_B T_d} \exp\left(-\frac{a}{\lambda_D}\right). \qquad (2.33)$$

A dusty plasma is a weakly coupled system when $\Gamma_c \ll 1$, while it is strongly coupled when $\Gamma_c \gg 1$. The number of charges residing on the grain, the ratio of the inter-grain distance to the Debye screening length and the dust thermal energy play decisive roles in deciding whether a dusty plasma will be strongly coupled or weakly coupled.

2.2 Forces acting on spherical dust particles

In capacitively coupled radio frequency plasmas dust particles which have obtained charge are usually trapped by an electrostatic force present in the discharge. Usually the potential in these plasmas is higher than the surrounding walls. This results in an electric field pointing towards the reactor walls and acting as an effective trap for the negatively charged dust particles. This section will give a review of the various forces acting on dust particles in radio frequency plasmas.

2.2.1 Electric force

In this paragraph important results form Daugherty, Porteous and Graves (1993) [4] and Hamaguchi and Farouki (1994) [5] will be summarized. Daugherty et al. have shown that the electric force acting on the dust particle in the presence of an external electric field is very well approximated by the vacuum force $Q_d \boldsymbol{E}_0$ when the dust particle radius is small with respect to the linearized Debye length. The most important result is that although the sheath around a dust particle shields it from the surrounding plasma, it does not screen the particle from an externally applied electric field. Hamaguchi and Farouki (1994) have pointed out that the Debye sheath is not 'attached' to the dust particle and represents only a local

perturbation of the background plasma. This means that the ions and electrons composing the sheath do not travel with the dust particle. The resulting force found by Daugherty et al is in the direction of the applied electric field $\boldsymbol{E}_0$ and is given by

$$\boldsymbol{F}_e = Q_d\boldsymbol{E}_0\left[1 + \frac{(a/\lambda_L)^2}{3(1 + a/\lambda_L)}\right] \tag{2.34}$$

The first term of equation 2.34 is the force that would be experienced by the dust particle under the electric field $\boldsymbol{E}_0$ in vacuum. The second term corresponds to the dipolar force due to polarization of the surface charge. This means that the polarized surface charge creates an electric field which in turn exerts an electric force. Since in general $a \ll \lambda_L$, the electric force can be approximated by $Q_d\boldsymbol{E}_0$. Hamaguchi et al. have shown that for a uniform plasma the electric field resulting from the polarization of the dust particle also exerts a force on the plasma, increasing the ion pressure on the dust particle. They have shown, assuming a Boltzmann ion density in the sheath, that the ion pressure force exactly cancels the force due to surface charge polarization resulting in the vacuum electrostatic force

$$\boldsymbol{F}_e = Q_d\boldsymbol{E}_0 \tag{2.35}$$

Hamaguchi et al. also found another force due to the deformation of the Debye sheath induced by a spatially dependent Debye length like in the pre-sheath. Bouchoule [3] has shown that this so-called 'polarization' field is negligible under usual conditions, ($a \ll \lambda_L$).

2.2.2   Ion drag force

The ion drag force is due to the momentum transfer between the positive ions and the dust particle. This force becomes important in regions where the ion flux is large. It has two components one due to the momentum transfer if the positive ion is collected (collection force) and the other due to the electrostatic Coulomb interaction between a dust particle and a positive ion deflected by the potential around it (orbit force). For monoenergetic ions the collection cross-section is given by

$$\sigma_{coll} = \pi b_{coll}^2 = \pi a^2\left[1 - \frac{2eV(a)}{m_+u_+^2}\right] \tag{2.36}$$

where u_+ is the ion drift velocity. This results in a collection force

$$\boldsymbol{F}_{ion}^{col} = \pi a^2 n_+ m_+ u_+ \boldsymbol{u}_+\left[1 - \frac{2eV(a)}{m_+u_+^2}\right] \tag{2.37}$$

Barnes et al. [6] (1992) have given an approximate collection force for a more general ion velocity distribution function by replacing directed velocity u_+ by the

total velocity, i.e. the velocity $v_{+,tot}$ related to the ion total mean energy:

$$u_+ \rightarrow v_{+,tot} = (u_+^2 + v_{+,th}^2)^{1/2} = \left(u_+^2 + \frac{8k_B T_+}{\pi m_+} \right)^{1/2} \qquad (2.38)$$

To estimate the orbit force for a monoenergetic ion beam, the potential distribution around a dust particle has to be known. To obtain analytical expressions the potential around the dust particle is approximated by a classical Coulomb distribution (reasonable approximation for $a \ll \lambda_L$). The momentum cross-section for the orbit force can derived by solving the following integral

$$\sigma^{orb} = 4\pi \int_{b_{coll}}^{\lambda_L} \frac{p dp}{1 + (p/b_{\pi/2})^2} \qquad (2.39)$$

where p is the impact parameter and $b_{\pi/2}$ is the parameter whose angle is $\pi/2$:

$$b_{\pi/2} = a \frac{-eV(a)}{2E_+} \qquad (2.40)$$

E_+ is the ion energy given by $\frac{1}{2} m_+ u_+^2$. The integration is performed between the collection impact parameter b_{coll} and the Debye length λ_L. The parameter b_{coll} is given by

$$b_{coll} = a \left[1 - \frac{eV(a)}{E_+} \right] \qquad (2.41)$$

The cut-off for the upper integration limit is introduced because of the divergence of the integral for an infinite upper limit. Shielding is assumed to suppress the potential for larger impact parameters. The corresponding Coulomb potential is therefore called the cut-off Coulomb potential. Solving the integral Eq. 2.39 above gives the following expression for the orbit cross-section

$$\sigma^{orb} = 2\pi b_{\pi/2}^2 ln \left(\frac{\lambda_L^2 + b_{\pi/2}^2}{b_{coll}^2 + b_{\pi/2}^2} \right) \qquad (2.42)$$

For non-monoenergetic ions, Barnes et al. used the following expression for the orbit force

$$\boldsymbol{F}_{ion}^{orb} = n_+ m_+ \sigma^{orb} v_{+,tot} \boldsymbol{u}_+ \qquad (2.43)$$

the directed velocity has been replaced by the total velocity and E_+ replaced by the total mean energy.

2.2.3   Neutral drag force

A dust particle moving in a neutral gas experiences a drag due to momentum transfer during collisions with atoms or molecules. For laboratory plasmas, the relative velocity between the dust particles and molecules is smaller than the thermal velocity of the gas. The neutral drag force can then be approximated by the Epstein relations for the neutral drag force

$$\boldsymbol{F}_n = -\frac{4}{3}\pi a^2 m_n n_n v_{th,n}(\boldsymbol{u}_d - \boldsymbol{u}_n) \tag{2.44}$$

where m_n is the mass of the atom or molecule, n_n is the gas density, $v_{th,n} = (8kT_{gas}/\pi m_n)^{1/2}$ is the thermal velocity of the gas, $\boldsymbol{u}_d$ is the dust particle velocity and $\boldsymbol{u}_n$ is the velocity of the neutral atom or molecule.

2.2.4   Thermophoretic force

When the neutral gas temperature is not uniform, a dust particle will experience a net resulting force due to collisions with the surrounding gas molecules. Gas molecules or atoms impinging on the hot side of the dust particles will transfer more momentum to the dust particle than gas molecules or atoms impinging for the cooler side. This gives a net resulting force which is called the thermophoretic force in the direction of the heat flux. Talbot et al. [7] have derived an analytical expression for the thermophoretic force

$$\boldsymbol{F}_{th} = -\frac{32}{15}\frac{a^2}{v_{th,n}}\left[1 + \frac{5\pi}{32}(1 - \alpha)\right]\kappa_T \boldsymbol{\nabla} T_n \tag{2.45}$$

where κ_T is the translational thermal conductivity of the gas and T_n is the gas temperature. Talbot et al. [7] have shown that for gas and dust particle temperatures less then 500 K the accommodation coefficient α is approximately 1.

2.2.5   Gravity

If a dusty plasma is considered on earth the gravitational force has to be taken into account. For micron sized dust particles the gravitational force is usually a dominant force. In experimental cases where the gravitational force is dominant the balance of forces acting on a dust particle is mainly made by the electric and gravitational force. The gravitational force is proportional to the particle mass, i.e. to the mass density ρ and to the dust particle volume:

$$\boldsymbol{F}_g = m_d \boldsymbol{g} = \frac{4}{3}\pi r_d^3 \rho \boldsymbol{g} \tag{2.46}$$

where g is the gravitational acceleration.

References

[1] J.E. Daugherty et al, J. Appl. Phys., **78**, 3934 (1992).

[2] T. Matsoukas et al, J. Appl. Phys., **77**, 4285 (1995).

[3] A. Bouchoule, Dusty Plasmas, Wiley, (1999).

[4] J.E. Daugherty et al, J. Appl. Phys., **73**, 1617 (1993).

[5] S. Hamaguchi et al, Phys. Rev. E., **49**, 4430 (1994).

[6] M. S. Barnes et al, Phys. Rev. Lett., **68**, 313 (1992).

[7] L. Talbot et al, J. Fluid Mech., **101**, 737 (1980).

3. Modelling of Dust in a Silane/Hydrogen Plasma

Abstract. *A dusty radio-frequency silane/hydrogen discharge is simulated, with the use of a one-dimensional fluid model. In the model, discharge quantities like the fluxes, densities and electric field are calculated self-consistently. A radius and an initial density profile for the spherical dust-particles are given and the charge and the density of the dust are calculated with an iterative method. During the transport of the dust, its charge is kept constant in time. The dust influences the electric field distribution through its charge and the density of the plasma through recombination of positive ions and electrons at its surface. In the model this process gives an extra production of silane radicals, since the growth of dust is not included. Results are presented for situations in which the dust significantly changes the discharge characteristics, both by a strong reduction of the electron density and by altering the electric field by its charge. Simulations for dust with a radius of 2 μm show that the stationary solution of the dust density and the average electric field depend on the total amount of the dust. The presence of dust enhances the deposition rate of amorphous silicon at the electrodes because of the rise in the average electron energy associated with the decrease of the electron density and the constraint of a constant power input.*

3.1 Introduction

A radio-frequency discharge in a mixture of SiH_4 and H_2 is often used to deposit thin films of amorphous hydrogenated silicon (a-Si:H), which is used for instance in solar cells and in thin film transistors. The properties of these films can be influenced by changing the plasma process parameters such as RF power, pressure, RF frequency and gas mixture. Study of the complicated chemistry in a SiH_4/H_2 discharge is of importance to optimize the material properties. For economical reasons a high deposition rate and efficient gas usage is desired.

A higher deposition rate can be achieved by increasing the pressure, RF power or frequency. By increasing these parameters complicated chemical reactions involving different ionic and neutral species can be ignited. An important process is the formation of big (molecular) clusters (dust). These clusters, ranging from a few nm to a few μm in radius, can significantly alter the discharge characteristics, and thus the formation of the deposited material. A discharge enters the so-called γ'-regime when the formation of dust becomes significant. With increasing radius the dust particle becomes more and more negatively charged. When the total charge on the dust is large enough, it alters the electric field locally. Here, we report on an investigation of situations in which the dust influences the discharge, by means of numerical simulations with a one-dimensional (1D) fluid model. An important extension compared to existing models [1, 2, 3] is that the behavior of the dust fluid is modelled self-consistently.

The structure of this paper is as follows. The description of the model is given in section 3.2. In section 3.3 simulation results for the γ'-regime are presented and the dependence of the discharge characteristics on the plasma process parameters (e.g. dust density, frequency) are studied. Conclusions are presented in section 3.4.

3.2 Description of the model

3.2.1 SiH_4/H_2 fluid model

To model the dynamics of a dusty plasma, we have used a self-consistent fluid model. This model is an extension of a previously described one-dimensional model [4]. Only the most important aspects of the model will be summarized here. It consists of particle balance equations for the different species (electrons, different ions and different neutrals) and an energy balance equation for the electrons. Ion-neutral collisions have been included to simulate a possible gas heating mechanism. For this we have used a simple approximation by assuming that the energy taken up from the electric field by the ions is dissipated locally in colli-

sions with the background gas [5]. The electric field is calculated by solving the Poisson equation.

In the model the density balance for each species is replaced by the drift-diffusion approximation. The source terms of the electron impact collisions (e.g. dissociation, ionisation) are derived from the electron energy distribution function (EEDF) and expressed as a function of the average electron energy. The EEDF is calculated by solving the Boltzmann equation in the two-term approximation.

In the model the density balance for each species j is:

$$\frac{dn_j}{dt} + \frac{d\Gamma_j}{dx} = S_j, \tag{3.1}$$

where n_j is the particle's density, Γ_j the flux of the species and S_j, the sink or source terms.

The momentum balance is replaced by the drift-diffusion approximation, where the particle flux consist of a diffusive term and a drift term,

$$\Gamma_j = \mu_j n_j E - D_j \frac{dn_j}{dx}, \tag{3.2}$$

where μ_j and D_j are the mobility and diffusion coefficient of species j. E is the electric field.

The drift-diffusion approximation assumes that the charged particles will react instantaneously to a change in the electric field. For the ions this is not a valid assumption, because of the low momentum transfer frequency. Therefore an effective electric field is calculated for the ions, to compensate for inertia effects due to the non-instantaneous reaction to a change in the electric field. An expression for the effective electric field, replacing the instantaneous field in Eq. 3.2 is obtained by neglecting the diffusive transport and inserting the expression $\Gamma_i = \mu_i n_i E_{eff}$ in the simplified momentum balance

$$\frac{d\Gamma_i}{dt} = \frac{en_i}{m_i} E - \nu_{m,i} \Gamma_i, \tag{3.3}$$

where $\nu_{m,i}$ is the momentum transfer frequency of ions given by:

$$\nu_{m,i} = \frac{e}{\mu_i m_i}. \tag{3.4}$$

Here e is the elementary charge and m_i the mass of the ion. The effective electric field is then given by:

$$\frac{dE_{eff,i}}{dt} = \nu_{m,i} \left(E - E_{eff,i} \right) \tag{3.5}$$

The electric field E and potential V are calculated using the Poisson equation:

$$\frac{d^2V}{dx^2} = -\frac{e}{\epsilon_0}\left(\sum n_i - n_e - Q_d n_d\right), \tag{3.6}$$

$$E = -\frac{dV}{dx}, \tag{3.7}$$

where ϵ_0 is the permittivity of vacuum space, n_e the electron density, n_i the ion density, Q_d the charge on a dust particle and n_d the dust density.

The electron energy density $w_e = n_e\epsilon$ (i.e. the product of the electron density and average electron energy ϵ) is calculated self-consistently from the second moment of the Boltzmann equation:

$$\frac{dw_e}{dt} + \frac{d\Gamma_w}{dx} = -e\Gamma_e \cdot E + S_w, \tag{3.8}$$

where Γ_w is the electron energy density flux:

$$\Gamma_w = \frac{5}{3}\mu_e w_e E - \frac{5}{3}D_e\frac{dw_e}{dx}, \tag{3.9}$$

and μ_e and D_e are the electron mobility and electron diffusion coefficients. The term S_w in the electron energy balance equation is the loss of electron energy due to electron impact collisions, including recombination of electrons on the dust particle's surface.

The plasma-wall interaction is taken into account by introducing a sticking model, each neutral particle has a certain surface reaction probability when it hits the wall. For the chemistry neutral-neutral, electron-neutral, electron-ion, and ion-ion reactions are taken into account; the chemistry is described in detail in a previous article [4]. The plasma is connected in series to an RLC circuit via the surface charge on the electrodes.

3.2.2 Dust in the fluid model

Charging of dust

When a dust particle exceeds a certain size it can collect more than one electron and be charged up to the floating potential relative to the surrounding plasma. This potential depends on the local ion and electron density and energy distribution. For a spherical dust particle with a radius r_d, the Orbital-Motion-Limited theory (OML) [6] predicts a positive ion and electron current:

$$I_i = 4\pi r_d^2 e n_i \sqrt{\frac{k_B T_i}{2\pi m_i}}\left(1 - \frac{eV_{fl}}{k_B T_i}\right), \tag{3.10}$$

$$I_e = 4\pi r_d^2 e n_e \sqrt{\frac{k_B T_e}{2\pi m_e}} \exp\left(\frac{eV_{fl}}{k_B T_e}\right). \tag{3.11}$$

Here, n_i the positive ion density, k_B Boltzmann's constant, T_i the positive ion temperature , T_e the electron temperature, m_e the electron mass and V_{fl} the floating potential. All species are assumed to have a Maxwellian energy distribution.

When the ions enter the plasma sheaths, they get a drift velocity v_i due to the electric field. Therefore, we have replaced $k_B T_i$ in the expression for the ion current by the mean energy E_i, which is:

$$E_i = \frac{4 k_B T_{gas}}{\pi} + \frac{1}{2} m_i v_i^2. \tag{3.12}$$

In the model the charge $Q_d = 4\pi\epsilon_0 r_d V_{fl}$ on the dust is calculated by equating these currents, where of course the ion current has been summed over all positive ionic species. The current of negative ions towards the dust particle's surface is neglected, the negative ions do not have enough kinetic energy to overcome the negative floating potential of the dust particle.

The floating potential of the dust is assumed to be constant during an RF cycle. This assumption is justified by the fact that the currents towards the dust particle surface are too small to change the charge significantly during an rf cycle.

Recombination on dust particles

When a dust particle becomes negatively charged, it will attract positive ions, these will recombine with an electron that has to be replaced again by an electron from the discharge to maintain the floating potential. As a result the equilibrium fluxes of positive ions and electrons arriving at the dust surface will recombine. The electron flux (Eq. 3.11) results in a recombination rate:

$$R = 4\pi r_d^2 n_d n_e \sqrt{\frac{k_B T_e}{2\pi m_e}} \exp\left(\frac{eV_{fl}}{k_B T_e}\right). \tag{3.13}$$

Forces acting on a dust particle

In a plasma dust particles undergo a wide variety of forces. Assuming that a dust particle is a perfect sphere the gravitational force can be written as:

$$F_g = \frac{4}{3}\pi r_d^3 \rho_d g, \tag{3.14}$$

where ρ_d is the mass density and g is the gravitational acceleration. For amorphous silicon ρ_d is approximately $2.1 \cdot 10^3 \ kg/m^3$.

When a dust particle has a velocity relative to the neutral gas, it will experience a drag force due to momentum transfer from/to the gas. This neutral drag force has been discussed in detail by Graves et al [7]. It can be approximated by,

$$F_n = -\frac{4}{3}\pi r_d^2 n_n \left(v_d - v_n\right) v_{th} m_n, \tag{3.15}$$

where n_n is the density of the neutral with mass m_n, v_d the drift velocity of the dust particle, v_n the velocity of the gas and v_{th} the average thermal velocity of the gas. Because advection of the neutral gas is not included in the model, $v_n=0$, this force will only be present as a damping force on the velocity of the dust particles.

Another force caused by momentum transfer is the ion drag. This force results from the positive ion current that is driven by the electric field. It consists of two components. The collection force represents the momentum transfer of all the ions that are collected by the dust particle and is given by:

$$F_i^c = \pi b_c^2 n_i v_s m_i v_i, \tag{3.16}$$

where v_s the mean speed of the ions and b_c the collection impact parameter.

The second component is the orbit force given by:

$$F_i^o = 4\pi b_{\pi/2}^2 \Gamma n_i v_s m_i v_i, \tag{3.17}$$

with $b_{\pi/2}$ the impact parameter that corresponds to a deflection angle $\pi/2$ and Γ the Coulomb logarithm.

$$\Gamma = \frac{1}{2}\ln\left(\frac{\lambda_L^2 + b_{\pi/2}^2}{b_c^2 + b_{\pi/2}^2}\right), \tag{3.18}$$

$\lambda_L = ((1/\lambda_e)^2 + (1/\lambda_i)^2)^{-1/2}$ is the linearized Debye length, which is a combination of the electron Debye length, λ_e, and the ion Debye length, λ_i. The ion drag is discussed in more detail by Barnes et al [8].

Due to their charge, dust particles will experience an electric force. Daugherty et al [9] derived the following expression:

$$F_e = Q_d E \underbrace{\left(1 + \frac{\kappa r_d}{3(1 + \kappa r_d)}\right)}_{\approx 1}, \tag{3.19}$$

where Q_d is the charge on the dust particle, E is the electric field and $\kappa = 1/\lambda_L$. In a discharge the dust particle radius is much smaller than the linearized Debye length, therefore the term between the bracket is approximately 1 and the electric force is given by:

$$F_e = Q_d E. \tag{3.20}$$

This expression holds for situations where the dust particles are not shielded from the plasma by positive ions trapped in orbitals around the dust particle [10]. In that case the particle plus ion cloud will behave as some kind of dipole.

When a temperature gradient is present in a discharge, for instance due to cooling or heating of the electrodes a third force driven by momentum transfer will occur. This force is called the thermophoretic force. Atoms impinging from the hot side have more momentum than their companions of the cold side, this can result in a force pointing in the direction $-\frac{dT_{gas}}{dx}$.

For large Knudsen numbers Talbot et al [11] derived the following expression:

$$F_{th} = -\frac{32}{15}\frac{r_d^2}{v_{th}}\left(1 + \frac{5\pi}{32}(1-\alpha)\right)\kappa_T\frac{dT_{gas}}{dx}, \tag{3.21}$$

κ_T is the translation part of the thermal conductivity. α, the thermal accommodation coefficient of the gas is taken equal to 1. In our case, the total thermophoretic force has been calculated as the summation over the two inlet gasses.

Implementing dust in SiH_4/H_2 fluid model

To obtain a suitable expression for the flux of dust particles, we assume that the neutral drag force is in equilibrium with the sum of the other forces. This assumption is valid when the final steady state is approached, but should be relaxed, for instance, when the dust is injected at a high velocity. In that case the inertia of the dust should not be neglected. With the introduction of a momentum loss frequency and a mobility and diffusion coefficient for the dust particles given by:

$$\nu_{md} = \sqrt{2}\frac{p_{tot}}{k_B T_{gas}}\pi r_d^2\sqrt{\frac{8k_B T_{gas}}{\pi m_d}}, \tag{3.22}$$

$$\mu_d = \frac{Q_d}{m_d\nu_{md}}, \tag{3.23}$$

$$D_d = \mu_d\frac{k_B T_{gas}}{Q_d}, \tag{3.24}$$

it is possible to define a "drift-diffusion" expression for the flux of the dust particles,

$$\begin{aligned}
\Gamma_d \quad &= \quad -\mu_d n_d E_{eff} - D_d\frac{dn_d}{dx} - \frac{n_d}{\nu_{md}}g \\
&+ \sum_{ions}\frac{n_d m_i v_s}{m_d\nu_{md}}\left(4\pi b_{\pi/2}^2\Gamma + \pi b_c^2\right)\Gamma_i \\
&- \frac{32}{15}\frac{n_d r_d^2}{m_d\nu_{md}v_{th}}\kappa_T\frac{dT_{gas}}{dx}
\end{aligned} \tag{3.25}$$

and treat them with the same numerical procedures as the other charged particles in the fluid model. Note that the ion drag force is summed over all the positive ionic species. Because of the low mobility of the dust particles the effective field E_{eff} is approximated by the time averaged RF field. The diffusion originates from the pressure gradient, $k_B T_d \frac{dn_d}{dx}$. The Einstein relation couples the diffusion and the mobility coefficients, see equation 3.24.

The internal pressure of the crystal due to the inter-particle interaction has been included by means of a density dependence of the diffusion coefficient for the dust. The diffusion coefficient of the dust is increased by a factor $\exp(N_d/N_c)$ where the reference density N_c is chosen such that the dust density saturates at a value N_{crys}. This models the incompressibility of the crystal. Actually, the (yet unknown) equation of state of the dust crystal should be used to account for the internal pressure. Since we were not primarily interested in the precise structure of the crystallized regions, we have chosen for the simple and computationally robust exponential increase of D_d.

The drift velocity and the diffusion coefficient of the dust fluids are much smaller than those of the ions and electrons. Therefore it would require a large computational effort to achieve a steady state solution for the dust when it is followed during an RF cycle. We therefore have developed a method to speed up the convergence toward the steady state solution by introducing a different calculation cycle with a different time step for the dust. Our model thus consists of two calculation cycles. In the first one, the transport equations of the ions, electrons and the Poisson equation are solved during a number of rf cycles, during the RF cycles the dust does not move. After that, the transport equation of the dust is solved with a greater time step, using the time averaged electric field, and electron and positive ion fluxes. During the second calculation, space charge regions are created, because the electron and positive ion densities do not change. These space charge regions will lead to instabilities in the solution of Poisson equation and the electron transport. To solve this problem, we correct the artificially generated space charge by adapting the positive ion density distributions prior to the next series of RF cycles, in which the ion and electron density profiles adapt themselves to the new dust density profile. With this method the required speed-up is established.

3.3   Results and discussion

In this section the results, obtained with the 1D numerical code are presented. A comparison is made between two almost identical initial situations. The only parameter that varies is the total amount of dust.

Other plasma process parameters, i.e., the gas temperature (400 K), gas flows (30 sccm SiH_4 and 30 sccm H_2), RF frequency (50 MHz), RF power (5 W), pres-

sure (40 Pa), electrode spacing (2.7 cm) and the dust particle radius (2 μm) are kept constant. Gravity is neglected. The simulation starts with a fourth order polynomial for the initial dust density profile. Figure 3.1 shows the dust density
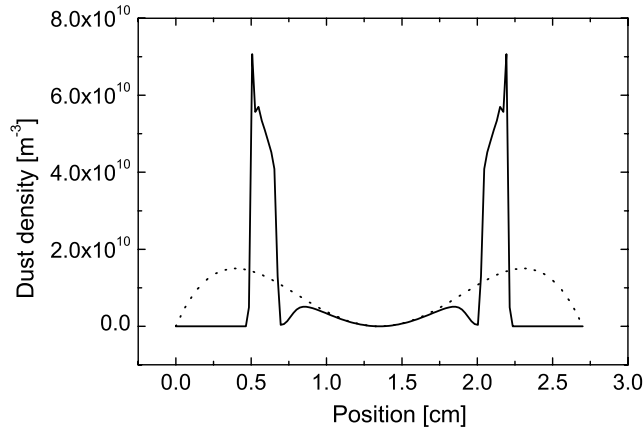

Figure 3.1: Dust density m^{-3} as function of the position. The line integrated amount of dust is $2.15 \cdot 10^8\ m^{-2}$. Dotted curve is the initial dust density profile.

profile for a line integrated amount of $2.15 \text{x} 10^8\ m^{-2}$. It shows that the steady state profile differs significantly from the initial profile. The high peaks formed in the dust density profile are result of the balance between the electric force, ion drag and thermophoretic force at these positions [12, 13].

Figure 3.2 shows the density profile of the dust in case of a low $(7.2 \cdot 10^4\ m^{-2})$ and high $(8.47 \cdot 10^8\ m^{-2})$ line integrated amount of dust. This figure shows clearly that the position where the resulting force acting on the dust particles vanishes, depending on the line integrated amount of dust in the reactor. This shows that the dust considerably influences the discharge. Figure 3.3 shows the charge on a dust particle. It varies through the discharge according to the local ion and electron densities and the electron temperature. In the sheaths there are almost no electrons (Fig. 3.4), this results in a strong decrease of the dust particle's charge. In the pre-sheaths a reasonable number of electrons is available with a high energy. This results in maxima of the grain charge at the pre-sheaths. In the center of the discharge the electron energy is very low, this makes it for the electrons difficult to overcome the repulsive Coulomb force caused by the charge on the dust particle's surface. This effect represents itself in a minimum of the grain charge at the center. For the case of a high amount of dust (see the dashed line), the dust is also influencing its own charge by enhancing the positive ion

density and thus increasing the ion flux towards its surface at the positions where the dust density peaks appear, this results in local minima in the charge profile.
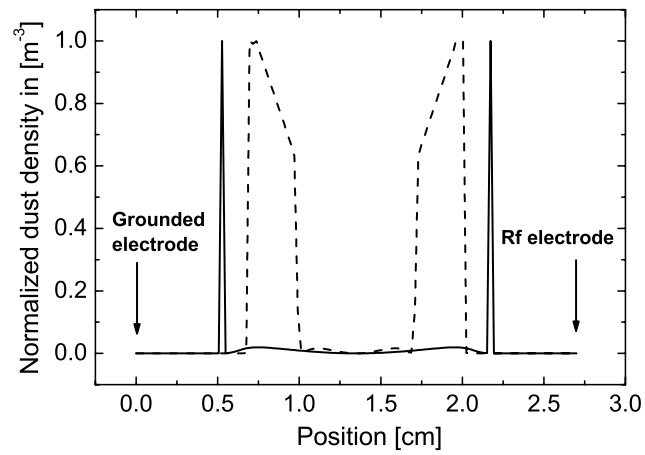

Figure 3.2: Dust density in m^{-3} as function of the position. The solid curve represents a dust density profile with an integrated amount of dust of $7.2 \cdot 10^4$ m^{-2}, the du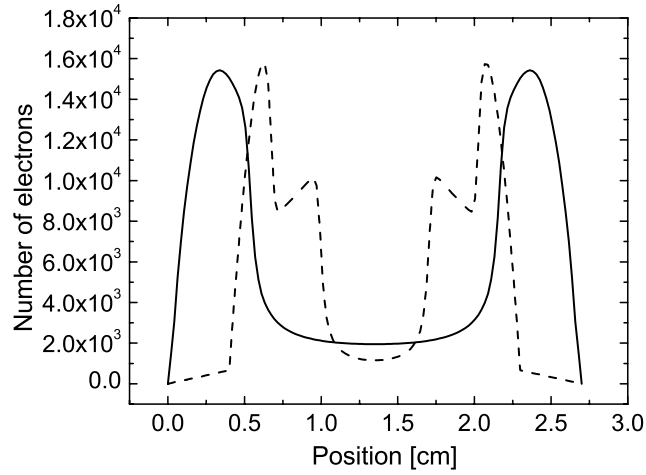st density is normalized with a of factor $1.27 \cdot 10^8$. The dashed curve represents a dust density profile with an integrated amount of dust of $8.47 \cdot 10^8$ m^{-2}, the dust density is normalized with a factor of $1.66 \cdot 10^{11}$.

Figure 3.3: Charge on a dust particle in number of electrons as function of the position. The line integrated amount of dust differs between the two curves. The solid curve: $7.2 \cdot 10^4$ m^{-2}, dashed curve: $8.47 \cdot 10^8$ m^{-2}.
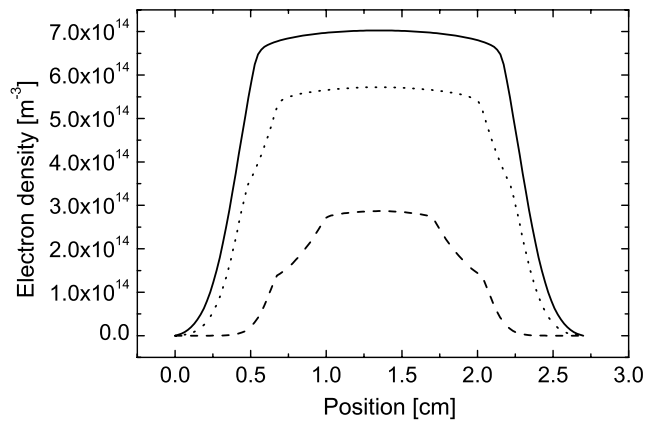

Figure 3.4: The time-averaged electron density in m^{-3} as function of the position. The line integrated amount of dust differs between the three curves. The solid curve: No dust. Dotted curve: $2.15 \cdot 10^8$ m^{-2}. Dashed curve: $8.47 \cdot 10^8$ m^{-2}.
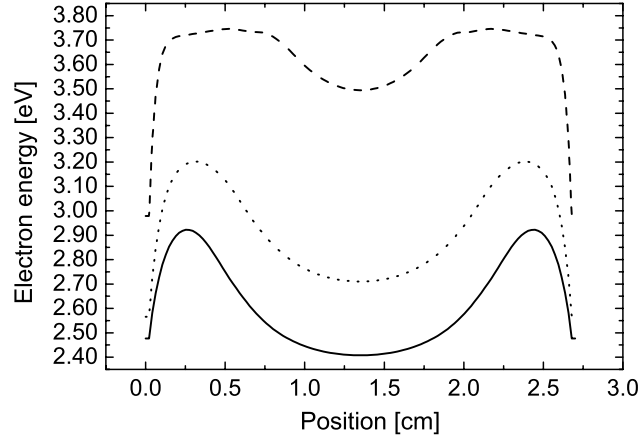
Figure 3.5: The time-averaged electron energy in eV as function of the position. The line integrated amount of dust differs between the three curves. The solid curve: No dust. Dotted curve: $2.15 \cdot 10^8 \ m^{-2}$. Dashed curve: $8.47 \cdot 10^8 \ m^{-2}$.

According to equation 3.13, the large surface area of the dust particles leads to a significant recombination rate. As result the electron density will drop (Fig. 3.4) and the average electron temperature will increase because the applied power is constant. This is shown in figure 3.5.

When the line integrated amount of dust is low its influence can be neglected, and the electron temperature is low in the quasi-neutral bulk, this is due to the lack of electric field. Only in the plasma-sheath transition zone the electrons can gain energy, as shown by the two peaks in figure 3.5. When the line integrated amount of dust particles is large (dashed curve in fig. 3.5), the heating is more uniform, this is due to the electron density drop which enhances the Debye length and therefore the electric field can penetrate much further into the discharge. Also the oscillating field in the center increases. Figure 3.6 shows the electric potential for different integrated amounts of dust. For a large amount the potential increases. This is a result of the constraint of a constant power, because the electron density decreases (Fig. 3.4) the displacement current also decreases. To compensate for this effect, the RF voltage has to increase, which results in a higher plasma potential.

The higher electron temperature in this case will lead to an increase in the ionization rate (needed to compensate for the recombination on the dust) and dissociation rate. The dissociation rate increases even if the electron density decreases because the rate coefficient almost exponentially increases with the electron energy. Therefore the deposition rate also increases with the dust density. This is
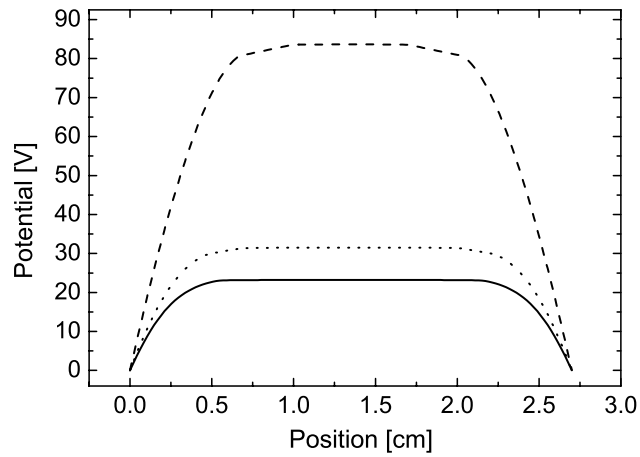
Figure 3.6: The time-averaged electric potential in V as function of the position. The line integrated amount of dust differs between the three curves. The solid curve: No dust. Dotted curve: $2.15 \cdot 10^8 \ m^{-2}$. Dashed curve: $8.47 \cdot 10^8 \ m^{-2}$.
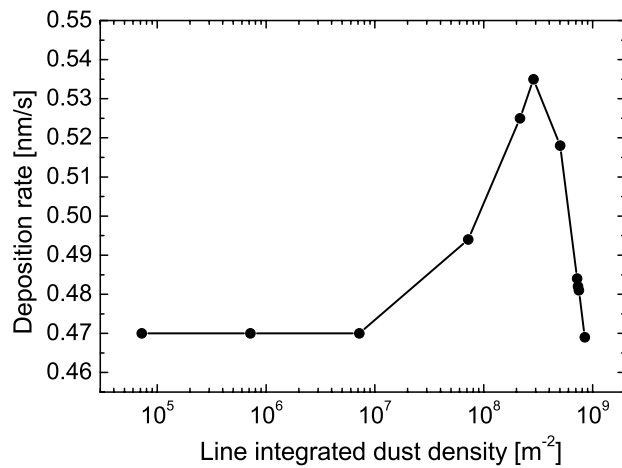

Figure 3.7: The deposition rate in nm/s as function of the line integrated dust density.

shown in figure 3.7. This increase in the deposition rate can not explain the significant increase which occurs in the experiments [4]. This may be caused by neglecting the contribution of dust in the sticking model. For large amounts of dust, the deposition rate again decreases because the gain in electron temperature can no longer compensate for the loss of electrons, therefore the dissociation of SiH_4 and ionization will drop. At still higher amounts of dust, the discharge cannot be maintained any longer and the simulation crashes.
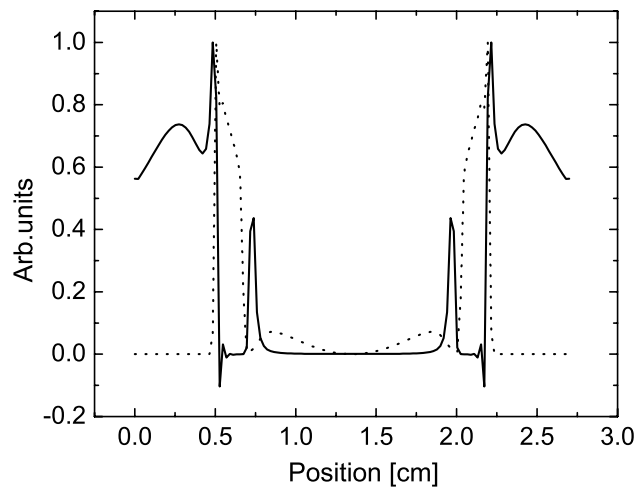

Figure 3.8: The net space charge in elementary charges as function of the position for a line integrated amount of dust of $2.15 \cdot 10^8$ m^{-2}, represented by the solid curve and normalized with a factor $1.82 \cdot 10^{14}$. The dotted curve represents the dust density profile in m^{-3} for a line integrated dust density of $2.15 \cdot 10^8$ m^{-2}, normalized with a factor $7.07 \cdot 10^{10}$.

Figure 3.8 shows the net space charge for a line integrated amount of dust of $2.15 \cdot 10^8$ m^{-2}. As expected, positive space charge regions appear close to the electrodes. At the center between the electrodes a quasi-neutral region can be observed. An interesting phenomenon induced by the dust can be observed. A double space charge layer appears around the sharp boundary of the dust crystal. The positive space charge layer in front of the dust crystal boundary is caused by the recombination on the dust particle's surfaces of ions and electrons entering the crystal. As in front of an absorbing wall, the difference in mobility between the ions and the electrons results in a net positive space charge that enhances the electric field which in turn accelerates the ions from the center of discharge towards the dust crystal to compensate for the mobility difference. The negative

space charge layer appears very close to the sharp edges inside the dust crystal. It appears due to the fact that the diffusion of the ions prohibits a full compensation of the fast rising negative charge of the dust crystal.

3.4   Conclusions

Simulations with the one-dimensional fluid model show that the deposition rate in SiH_4/H_2 can be increased by the presence of dust particles with a considerable size (2 μm). The recombination on these particles alters the radio-frequency SiH_4/H_2 discharge in such a way, that the electron temperature increases and the electron density decreases. This process leads to an increase in the dissociation and ionization rates. The modelled increase in deposition rate underestimates the increase observed in the experiments [4] during the α-$\gamma^{'}$ transition. Depending on the total amount of dust the width of the plasma sheaths may change considerably, thus altering the position where the dust will settle. An other interesting phenomenon is the appearance of a double space charge layer at the edge of the dust crystal which is formed by the difference in mobility between the ions and electrons and the diffusive transport of the ions caused by the steep density gradient imposed by the dust.

Acknowledgments

References

[1] P. Belenguer et al, Phys. Rev. A., **46**, 7923 (1992).

[2] T. Nitter , Plasma Sources Sci. Technol., **5**, 93 (1996).

[3] V. Vyas et al, J. Appl. Phys., **92**, 6451 (2002).

[4] G. J. Nienhuis et al, J. Appl. Phys., **82**, 2060 (1997).

[5] I. Revel et al, J. Appl. Phys., **88**, 2234 (2000).

[6] J. E. Allen et al, J. Plasma. Phys., **63**, 299 (2000).

[7] D. B. Graves et al, Plasma Sources Sci. Technol., **3**, 433 (1994).

[8] M. S. Barnes et al, Phys. Rev. Lett., **68**, 313 (1992).

[9] J. E. Daugherty J E al, J. Appl. Phys., **73**, 1617 (1994).

[10] M. Lampe et al, Phys. Rev. Lett., **86**, 5278 (2001).

[11] L. Talbot et al, J. Fluid Mech., **101**, p.737 (1980).

[12] G. E. Morfill et al, Phys. Rev. Lett., **83**, 1598 (1999).

[13] H. Thomas et al, Phys. Rev. Lett., **73**, 652 (1994).

4. Modelling of Voids in Colloidal plasmas

Abstract. *A two dimensional fluid model for a dusty argon plasma in which the plasma and dust parameters are solved self-consistently, is used to study the behavior of voids, i.e., dust-free regions inside dust clouds. These voids appear in plasma crystal experiments performed under microgravity conditions. The ion drag force turns out to be the most promising driving force behind these voids. The contribution of the thermophoretic force, driven by the temperature gradient induced by gas heating from ion-neutral collisions, can be neglected in the quasi-neutral center of the plasma.*

4.1 Introduction

Plasma crystal experiments performed under microgravity conditions have shown three dimensional structures, which exhibit stable voids surrounded by a crystalline region. In their PKE chamber Morfill et al, for instance, observed a centimeter-size void that was usually stable[1]. Other authors have reported on various theoretical studies of the creation of these voids [1, 2, 3]. None of these, however, fully explain the mechanism behind the appearance of the void.

Theoretical and numerical studies up to now have basically followed single dust particles in the electric field and particle fluxes of an undisturbed discharge. An important aspect not covered is the influence of the dust on the discharge. For this a fully self-consistent model is needed. We have developed such a model for a dust containing radio frequency [RF] discharge in argon and used it to investigate the behavior of voids.

In this two-dimensional fluid model the particle balances, the electron energy balance and the Poisson equation are solved, including the transport of the dust fluid. Problems related to the huge difference in the timescale of the dust motion (1-10 s) and the RF period (100 ns) have been solved by timesplitting and an iterative procedure. Ion-neutral collisions have been included to simulate a possible gas heating mechanism. For a dust-free argon discharge the model gives the same results as the two-dimensional model of Boeuf [4]. The charge on a dust particle is calculated by using the Orbital-Motion-Limited [OML] probe theory. This OML theory assumes a uniform charge distribution on a spherical dust particle and is only valid if $r_d << \lambda_L$, where r_d is the radius of the dust particle and $\lambda_L = ((1/\lambda_e)^2 + (1/\lambda_i)^2)^{-1/2}$ the linearized Debye length [2], which is a combination of the electron Debye length, λ_e, and the ion Debye length, λ_i. The (constant) charge on the dust particle is obtained from the balance of the (OML) electron and ion currents collected by the particle. Recombination of ions and electrons on the dust particle surface is also taken into account.

4.2 Forces acting on a dust particle

The dust particle motion is affected by the gravitational force, $\boldsymbol{F_g} = m_d\boldsymbol{g}$, where g is the gravitational acceleration and m_d the mass of the dust particle, and the electrostatic force, $\boldsymbol{F_e} = Q_d\boldsymbol{E}$, with Q_d the charge on the dust particle and $\boldsymbol{E}$ the electric field. On earth, the gravitational force reduces the crystal to consist of only a few horizontal lattice planes above the electrode [5]. This force has been neglected in our microgravity simulations.

Also a number of drag forces are present. The drag exerted by collisions with the neutral gas is opposite to the relative velocity. In the model the neutral flow is

neglected, therefore the neutral drag is a damping force. It is approximated by:

$$\boldsymbol{F}_{nd} = -\frac{4}{3}\pi r_d^2 n_d \boldsymbol{v}_d v_{th} m_n = -m_d \nu_{md} \boldsymbol{v}_d \tag{4.1}$$

where n_n is the neutral density, m_n the neutral mass, v_d the drift velocity of the dust particle, v_{th} the average thermal velocity of the gas. ν_{md} is the neutral-dust collision frequency. The neutral drag force is described in more detail by Graves et al [6]. The ion drag, as discussed by Barnes et al [7], results from the positive ion current that is driven by the electric field. It consists of two components. The collection force represents the momentum transfer of all the ions that are collected by the dust particle and is given by:

$$\boldsymbol{F}_i^c = \pi b_c^2 n_i v_s m_i \boldsymbol{v}_i \tag{4.2}$$

where n_i is the ion density, v_s the mean speed of the ions, v_i the ion drift velocity and b_c the collection impact parameter. The second component is the orbit force, caused by deflected ions. It given by:

$$\boldsymbol{F}_i^o = 4\pi b_{\pi/2}^2 \Gamma n_i v_s m_i \boldsymbol{v}_i \tag{4.3}$$

with $b_{\pi/2}$ the impact parameter that corresponds to a deflection angle $\pi/2$ and Γ the Coulomb logarithm:

$$\Gamma = \frac{1}{2}\ln\left[\frac{\lambda_L^2 + b_{\pi/2}^2}{b_c^2 + b_{\pi/2}^2}\right] \tag{4.4}$$

When a temperature gradient is present in the discharge, for instance due to cooling or heating of the electrodes or due to ion-neutral collisions, the thermophoretic force will act upon the dust. Atoms impinging from the hot side have more momentum than their companions of the cold side, this results in a force pointing in the direction $-\boldsymbol{\nabla} T_{gas}$. For large Knudsen numbers Talbot et al derived the following expression [8]:

$$\boldsymbol{F}_T = -\frac{32}{15}\frac{r_d^2}{v_{th}}\left(1 + \frac{5\pi}{32}(1-\alpha)\right)\kappa_T \boldsymbol{\nabla} T_{gas} \tag{4.5}$$

where κ_T is the translation part of the thermal conductivity. The thermal accommodation coefficient of the gas, α, is taken equal to 1. Neglecting inertia, the balance of all forces leads to the following expression for the flux of dust particles:

$$\boldsymbol{\Gamma}_d = -\mu_d n_d \boldsymbol{E} - D_d \boldsymbol{\nabla} n_d - \frac{n_d}{\nu_{md}}\boldsymbol{g}$$

$$+ \quad \frac{n_d m_i v_s}{m_d \nu_{md}} \left(4\pi b_{\pi/2}^2 \Gamma + \pi b_c^2 \right) \mathbf{\Gamma}_i \tag{4.6}$$

$$- \quad \frac{32}{15} \frac{n_d r_d^2}{m_d \nu_{md} v_{th}} \kappa_T \mathbf{\nabla} T_{gas}$$

Where Γ_d is the flux of dust particles, μ_d the mobility of the dust, n_d the dust density, and D_d the diffusion coefficient of the dust. Diffusion is added, using Fick's law and the Einstein relation to couple the electrical mobility and the diffusion coefficient. The internal pressure of the crystal due to the inter-particle interaction has been included by means of a density dependence of the diffusion coefficient for the dust. Plasma crystal experiments [1] have shown an inter-particle distance of about 300 microns. This results in an average "crystal" density N_{crys} of $3.7 \cdot 10^{10}$ m^{-3}. The diffusion coefficient of the dust is increased by a factor $\exp(N_d/N_c)$ where the reference density N$_c$ is chosen such that the dust density saturates at a value N$_{crys}$. This models the incompressibility of the crystal. Actually, the (yet unknown) equation of state of the dust crystal should be used to account for the internal pressure. Since we were not primarily interested in the precise structure of the crystallized regions, we have chosen for the simple and computationally robust exponential increase of D$_d$.
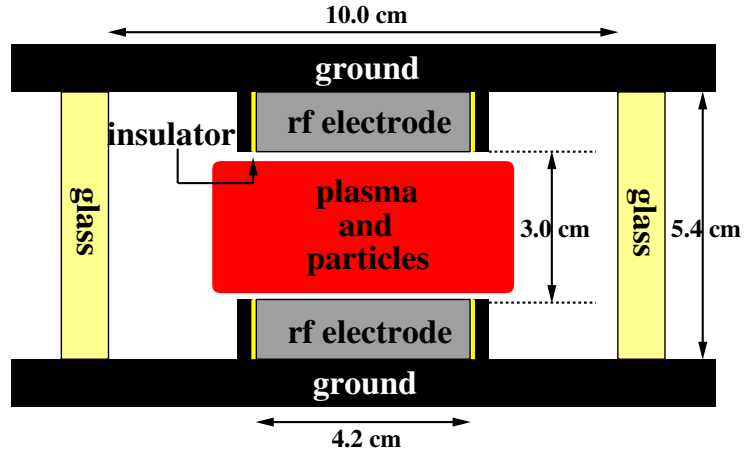
4.3 Results and discussion

Figure 4.1: A schematic drawing of the PKE chamber.

The PKE chamber used by Morfill et al [1] has been modelled (Fig. 4.1). The reactor is cylindrically symmetric. The simulation starts with a quadratic initial dust density profile which has a maximum in between the electrodes on the

z-axis. A number of times during the simulation the dust density profile is multiplied with a certain factor to increase the amount of dust in the reactor. Eventually a total amount of between 0.94 and 3.8 million dust particles is reached. The electrodes are both driven by a radio-frequency power source at a frequency of 13.56 MHz. The peak-to-peak voltage is 70 volts, this results in a power dissipation of about 0.04 W. The pressure is 40 Pa. The dust particles have a diameter of 15 microns. The equation of motion for the dust particles, Eq.4.6, is solved for the time-averaged electric field, plasma densities and fluxes.

Figure 4.2 shows the time-averaged potential distribution V(r,z). The potential has its maximum in the bulk of the plasma between the electrodes, so the electric field points in the direction of the electrodes. This means that the negatively charged particles will be trapped due to the electrostatic force, while the positive ion flux, pointing toward the electrodes results in an ion drag force that expels the particles. Figure 4.3 shows the charge on a dust particle as a function of the position. Dust particles that are in the pre-sheath regions have a maximum number of electrons on their surface. The charge decreases toward the center because the average electron energy decreases and toward the electrode because the electron density becomes less than the ion density in the space charge sheaths. The number of electrons varies between 0 and 55000. In Fig. 4.4 the gas temperature
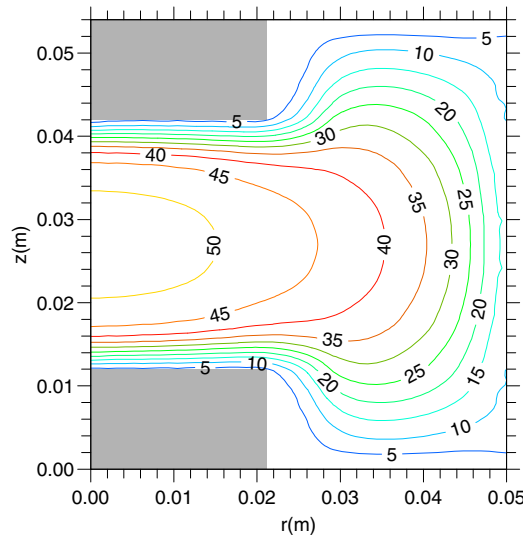

Figure 4.2: The time-averaged electric potential in volts in a dust-free discharge.

is plotted. We have assumed that the power consumed by the ions is completely transferred to the gas by ion-neutral collisions. This overestimates the heating, as the ions will take part of this power to the electrodes. The wall is assumed to
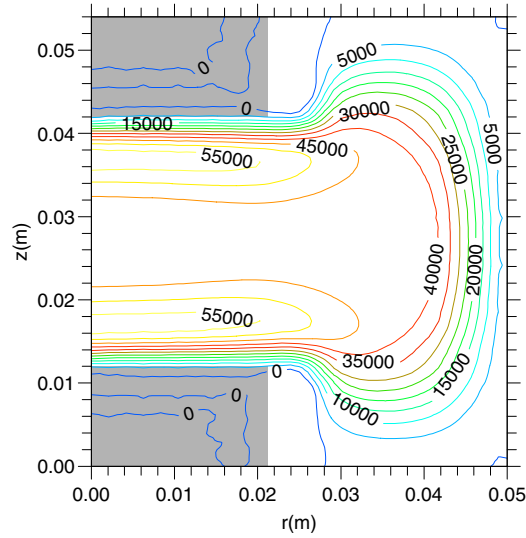
Figure 4.3: The number of electrons on a dust particle in a dust-free discharge.

have a constant temperature of 273 K. The results show that ion-neutral collisions give rise to a temperature gradient in the discharge of 2 K/cm at maximum. The temperature profile is almost uniform in the bulk. This results in a thermophoretic force in the bulk which is insufficient to explain the appearance of the void in the plasma crystal experiments.

The dust particles will accumulate at positions where the forces are in balance and the velocity of the dust fluid vanishes. From figure 4.5, it can be seen that the dust particles accumulate in the bulk of the discharge. The electrostatic force is dominant and forces the particles to move to the bulk of the plasma.

The linearized Debye length is in the order of 30 microns in the bulk of the plasma, thus the OML theory becomes questionable in the bulk, which has consequences for the contribution of the ion drag force. The small Debye length results from the very small ion contribution in the bulk, where the ions have a small drift velocity because of the low electric field. In the sheaths, however, the ions gain energy from the high electric field. This results in a linearized Debye length of the same order of magnitude as the electron Debye length (Fig. 4.6).

The simulation results above can not explain the appearance of the void in the plasma crystal experiment. To study the conditions which are needed to create a void, we have artificially enhanced the ion drag force. There are several reasons why one may expect an ion drag exceeding that of equations 4.2 and 4.3. The OML theory does not account for trapped ions [9] and the particles are not isolated, but interact, which influences the screening length. The ion drag had to be scaled up with at least a factor 10 before a void with a reasonable size appeared.
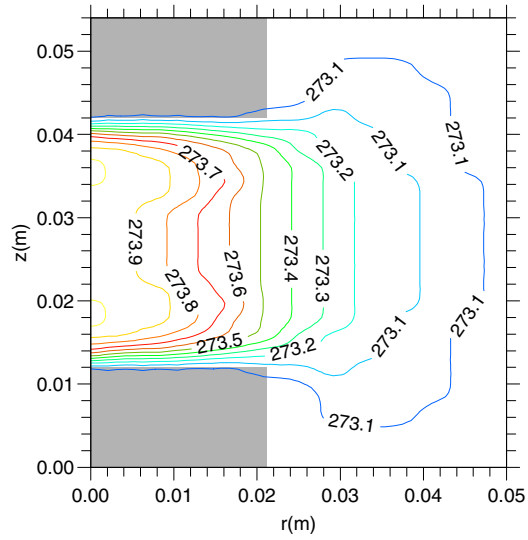
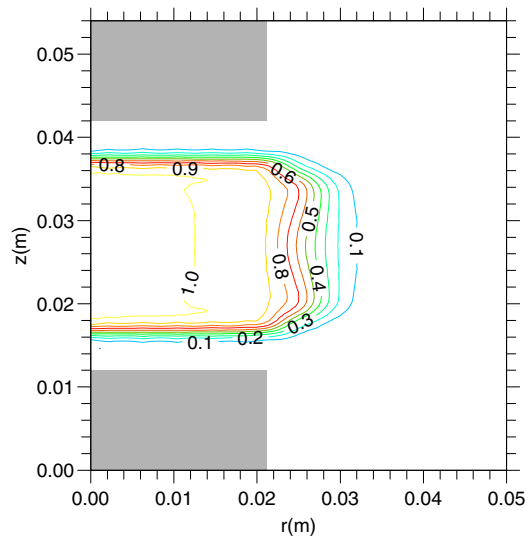Figure 4.4: Gas temperature profile in K in dust-free discharge.

Figure 4.5: The dust density in m^{-3}, normalized with a factor of $1.6 \cdot 10^{10}$. The total amount of particles is 940.000.
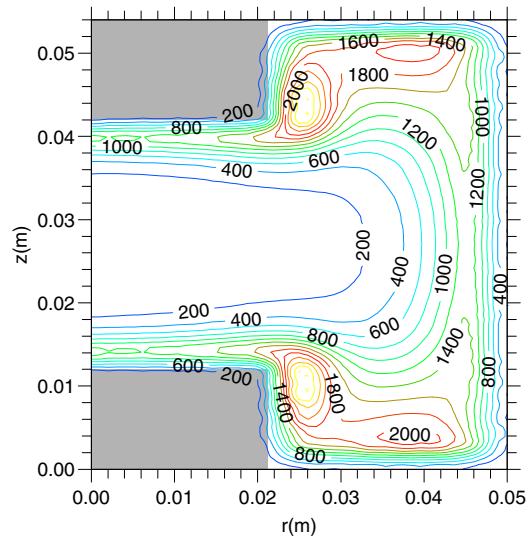
Figure 4.6: The linearized Debye length in μm in a dust-free discharge.

After the void has appeared the scale factor can be decreased again. This is due to the large temperature gradient between the sheaths and the electrodes which causes the thermophoretic force to act in the same direction as the ion drag force. The scale factor can be decreased to a value of 5, if it is decreased further the void collapses.

The results presented in Fig. 4.7 are obtained for the dust density profile. Also in case only the electron Debye length is used in equation 4.4, a void appears. The electron Debye length is of the order of the 200 microns which is the screening length needed to explain the inter-particle distance observed in the experiments. This increase of the screening length results in an enhancement of the ion drag to an extent where it exceeds the electric force in the bulk plasma.

4.4 Effects of recombination

Modelling results show also that a different initial condition with a large amount of dust particles in the bulk results in crystalline region instead of a void. This is due to the recombination on the dust particles that can cause the ion flux and drag force to reverse sign. In the experiments, however, the dust particles are injected through the electrodes.
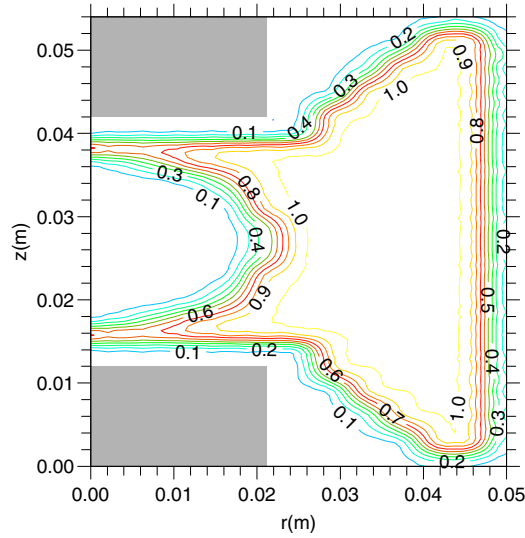
Figure 4.7: The dust density in m^{-3}, normalized with a factor of $1.5 \cdot 10^{10}$. Five times enhanced ion drag force. The total amount of particles is $3.8 \cdot 10^6$.

4.5   Conclusions

The numerical simulation results show that the ion-neutral collisions increase the gas temperature by a maximum of 1 K and that the thermophoretic force plus the ion drag force can not fully explain the appearance of the void. The OML theory becomes questionable in the bulk of the plasma, because of the small linearized Debye length. Enhancement of the ion drag by replacement of λ_L by the electron Debye length results in the appearance of a void. Enhancing the ion drag instead of replacing the linearized Debye length, requires a factor of at least 10. After the void has appeared, the scaling factor can be decreased until it equals 5. This is due to the temperature gradient between the sheaths and electrodes, which causes the thermophoretic force to act in the same direction as the ion drag force. A further decrease of the scaling factor results in a collapse of the void. The ion drag force can be seen as the most promising driving force behind the appearance of the void. Possibly a different dust injection scheme will lead to a large dust density in the bulk and a self-sustained crystal based on recombination and inversion of the ion flux. Thus, there is need for more experiments to verify the model. A systematic scan, varying the power, pressure, and RF frequency would show the behavior of the void while changing the various forces. A strongly electronegative background gas may lead to a change of sign of the ion drag in the plasma bulk, as the result of recombination with negative ions.

4.6 Addendum: Inclusion of the equation of state for the dust

In section 4.2 it has been shown that the diffusion coefficient of the dust has been enhanced by a factor $\exp(N_d/N_c)$ where the reference density N_c is chosen such that the dust density saturates at a value N_{crys}. This artificial enhancement has been used to model the incompressibility of the crystal.

Now the internal pressure of the crystal due to the inter-particle interaction has been taken into account by means of an equation of state for the dust. Gozadinos et al [10] have obtained an expression for the equation of state for a crystalline structure of dust particles. The crystalline pressure is given by:

$$P_{cr} = \frac{(1 + \beta\kappa)}{3\beta} N_{nn} \Gamma P_g \exp(-\beta\kappa) \qquad (4.7)$$

where $\Gamma = Q_d^2/4\pi\epsilon_0\Delta k_B T_d$ is the coupling parameter, $\Delta = n_d^{-1/3}$ is the mean inter-particle distance, $\kappa = \Delta/\lambda_e$, $P_g = n_d k_B T_d$, N_{nn} is the number of nearest neighbours (N_{nn}=8 and β=1.09 for bcc lattices, N_{nn}=12 and β=1.12 for fcc and hcp lattices). We take only a fcc and hcp lattices into account in our simulations. With the above equation the effective diffusion coefficient for the crystalline regions becomes

$$D_d = \frac{dP_{cr}/dn}{m_d\nu_m} \qquad (4.8)$$

Further details can be found in [10].

By including the above mentioned equation of state, the dust profile shown in figure 4.7 changes. In figure 4.8 the dust profile is shown for the same plasma settings, the only difference is the inclusion of the equation of state. It shows a much broader dust crystal with structure between the electrodes, the average dust density is $3.34 \cdot 10^{10} m^{-3}$, which is in agreement with the experiments. Also the
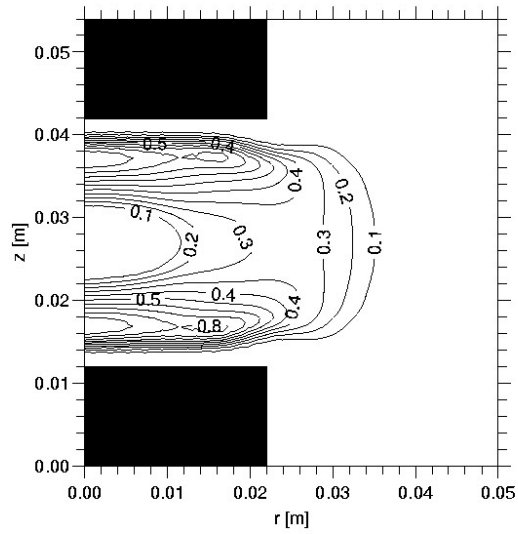
Figure 4.8: The dust density in m^{-3}, normalized with a factor of $3.34 \cdot 10^{10}$. The total amount of particles is $1.0 \cdot 10^6$.

dust crystal near the reactor wall has disappeared, which is also not seen in the experiments.

References

[1] G. E. Morfill et al, Phys. Rev. Lett., **83**, 1598 (1999).

[2] H. Thomas et al, Phys. Rev. Lett., **73**, 652 (1994).

[3] J. Goree et al, Phys. Rev. E., **59**, 7055 (1999).

[4] J. P. Boeuf et al, Phys. Rev. E., **51**, 1376 (1995).

[5] A. Homann et al, Phys. Rev. Lett., **242**, 173 (1998).

[6] D. B. Graves et al, Plasma Sources Sci. Technol., **3**, 433 (1994).

[7] M. S. Barnes et al, Phys. Rev. Lett., **68**, 313 (1992).

[8] L. Talbot et al, J. Fluid. Mech., **101**, 737 (1980).

[9] M. Lampe et al, Phys. Rev. Lett., **86**, 5278 (2001).

[10] G. Gozadinos et al, New J. Phys., **5**, (2003).

5. Modelling the Effect of Dust on the Plasma Parameters in a Dusty Argon Discharge under Microgravity

Abstract. *A dusty radio-frequency argon discharge is simulated with the use of a two-dimensional fluid model. In the model, discharge quantities as the fluxes, densities and electric field are calculated self-consistently. The charge and the density of the dust are calculated with an iterative method. During the transport of the dust, its charge is kept constant in time. The dust influences the electric potential distribution through its charge and the density of the plasma through recombination of positive ions and electrons on its surface. Results are presented for situations in which the dust significantly changes the discharge characteristics, both by a strong reduction of the electron density and by altering the electric potential by its charge. Simulations for dust with a radius of 7.5 microns show that a double space charge layer is created around the sharp boundary of the dust crystal. A central dust-free region (void) is created by the ion drag force. Inside this void a strong increase of the production of argon meta-stables is found. This phenomenon is in agreement with experimental observations, where an enhanced light emission is seen inside the void.*

5.1 Introduction

Plasma crystal experiments performed under microgravity conditions have shown dust particles which arrange in a crystal like structure. In their PKE chamber Morfill et al [1, 2], usually observed a stable void with two dust vortices near the edges of the electrodes . Also an increase of light emission emerging from center of the discharge has been observed.
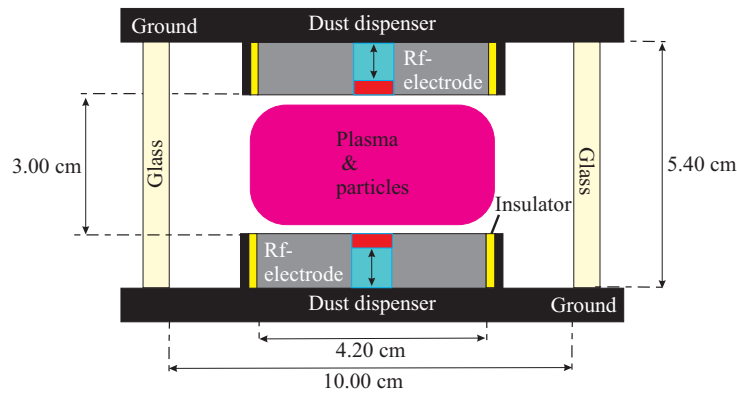

Figure 5.1: Schematic diagram of the PKE reactor.

Theoretical and numerical studies up to now have basically followed dust particles in the electric field and particle fluxes of an undisturbed discharge. An important aspect not covered is the influence of the dust on the discharge. For this a fully self-consistent model is needed. We have developed such a model for a dust containing radio frequency (RF) discharge in argon and used it to investigate the behavior of dust particles. The model contains a dust fluid part which has been described shortly in [3]. In existing models [4, 5, 6], the influence of the dust particles on the discharge due to recombination on their surface or the motion of the dust as a fluid is neglected. In case discharges contain a considerable amount of dust, like in the PKE experiments, this approximation is not correct. Our model accounts for the influence of the dust fluid on the plasma and for its transport as a fluid. This makes it a sophisticated tool for studying dusty discharges. In this paper we describe the results obtained with the argon-dust fluid model, studying in particular the dust-plasma interaction.

5.2   Description of the model

5.2.1   Fluid model for the plasma species

To model the dynamics of a dusty plasma, we have used an extension of a previously described two-dimensional model [7], of which only the most important aspects will be summarized here. It consists of particle balance equations for the different species (electrons, ions and meta-stables) and an energy balance equation for the electrons. Ion-neutral collisions have been included to simulate a possible gas heating mechanism. For this we have used a simple approximation by assuming that the energy taken up from the electric field by the ions is dissipated locally in collisions with the gas[8]. This gas heating mechanism has been refined by taking the heating of the dust particle surface into account [9, 10]. The dust particle (surface) temperature can affect the gas temperature which in turn could affect the other elementary processes in the discharge.

In the model the density balance for each species j is:

$$\frac{dn_j}{dt} + \boldsymbol{\nabla} \cdot \boldsymbol{\Gamma}_j = S_j, \tag{5.1}$$

where n_j is the particle's density, $\overrightarrow{\Gamma_j}$ the flux of the species, and S_j the local sink or source.

The momentum balance is replaced by the drift-diffusion approximation, where the particle flux consist of a diffusive term and a drift term,

$$\boldsymbol{\Gamma}_j = \mu_j n_j \boldsymbol{E} - D_j \boldsymbol{\nabla} n_j, \tag{5.2}$$

with μ_j and D_j the mobility and diffusion coefficient of species j. $\boldsymbol{E}$ is the electric field.

For ions the characteristic momentum transfer frequency is only a few megahertz (MHz). To use the drift-diffusion approximation for ions for RF frequencies higher than a few MHz the electric field field in equation 5.2 is replaced by an effective electric field. Using this effective electric field $\boldsymbol{E}_{eff}$, inertia effects are taken into account. An expression for the effective electric field is obtained by neglecting the diffusive transport and inserting the expression $\boldsymbol{\Gamma}_i = \mu_i n_i \boldsymbol{E}_{eff}$ in the simplified momentum balance

$$\frac{d\boldsymbol{\Gamma}_i}{dt} = \frac{en_i}{m_i} \boldsymbol{E} - \nu_{m,i} \boldsymbol{\Gamma}_i, \tag{5.3}$$

where $\nu_{m,i}$ is the momentum transfer frequency of the argon ions given by:

$$\nu_{m,i} = \frac{e}{\mu_i m_i}. \tag{5.4}$$

Here e is the elementary charge and m_i the mass of the argon ion. The effective electric field is then obtained by solving:

$$\frac{d\boldsymbol{E}_{eff,i}}{dt} = \nu_{m,i} \left(\boldsymbol{E} - \boldsymbol{E}_{eff,i} \right) \tag{5.5}$$

The electric field $\boldsymbol{E}$ and potential V are calculated using the Poisson equation:

$$\Delta V = -\frac{e}{\epsilon_0} \left(n_i - n_e - Q_d n_d \right), \tag{5.6}$$

$$\boldsymbol{E} = -\boldsymbol{\nabla} V, \tag{5.7}$$

where ϵ_0 is the permittivity of vacuum space, n_e the electron density, n_i the ion density, Q_d the charge on a dust particle and n_d the dust density.

The electron energy density $w_e = n_e \epsilon$ (i.e. the product of the electron density and average electron energy ϵ) is calculated self-consistently from the second moment of the Boltzmann equation:

$$\frac{dw_e}{dt} + \boldsymbol{\nabla} \cdot \boldsymbol{\Gamma}_w = -e\boldsymbol{\Gamma}_e \cdot \boldsymbol{E} + S_w, \tag{5.8}$$

with $\boldsymbol{\Gamma_w}$ the electron energy density flux:

$$\boldsymbol{\Gamma}_w = \frac{5}{3}\mu_e w_e \boldsymbol{E} - \frac{5}{3} D_e \boldsymbol{\nabla} w_e, \tag{5.9}$$

and μ_e and D_e the electron mobility and electron diffusion coefficients. The term S_w in the electron energy balance equation is the loss of electron energy due to electron impact collisions, including excitation, ionization and recombination of electrons on the dust particle's surface. To compute the sources as a function of ϵ, tables are generated using the two-term Boltzmann solver for the electron energy distribution function. Via the surface charge on the electrodes the plasma can be connected to an RLC circuit. Further details about the algorithms used to solve the above mentioned equations can be found in [7].

5.2.2 Implementing dust as a fluid

Charging of dust

When a dust particle exceeds a certain size it can collect more than one electron and be charged up to the floating potential relative to the surrounding plasma. This potential depends on the local ion and electron density and energy distribution. For a spherical dust particle with a radius r_d, much smaller than the linearized

Debye length, the Orbital-Motion-Limited theory (OML) [11] predicts a positive ion and electron current:

$$I_i = 4\pi r_d^2 e n_i \sqrt{\frac{k_B T_i}{2\pi m_i}} \left(1 - \frac{eV_{fl}}{k_B T_i} \right), \tag{5.10}$$

$$I_e = 4\pi r_d^2 e n_e \sqrt{\frac{k_B T_e}{2\pi m_e}} \exp\left(\frac{eV_{fl}}{k_B T_e} \right). \tag{5.11}$$

Here, n_e is the electron density, n_i the positive ion density, e the elementary charge, k_B Boltzmann's constant, T_i the positive ion temperature , T_e the electron temperature, m_i the ion mass, m_e the electron mass, and V_{fl} the floating potential. All species are assumed to have a Maxwellian energy distribution. The influence of neighboring dustparticles is neglected.

When the ions enter the plasma sheaths near the electrodes, they get a directed velocity v_i due to the electric field. Therefore, we have replaced $k_B T_i$ in the expression for the ion current by the mean energy E_i, which is:

$$E_i = \frac{4k_B T_{gas}}{\pi} + \frac{1}{2} m_i v_i^2. \tag{5.12}$$

Equation 5.12 is obtained by using the mean speed expression of Barnes et al [13] given by:

$$v_s = \left(\frac{8k_B T_{gas}}{\pi m_i} + v_i^2 \right)^{1/2}. \tag{5.13}$$

By calculating $\frac{1}{2} m_i v_s^2$, equation 5.12 is obtained. The directed velocity v_i is the drift velocity of the ions (Eq. 5.2).

In the model the charge $Q_d = 4\pi\epsilon_0 r_d V_{fl}$ on the dust is calculated from the equilibrium of the currents in equation 5.10 and 5.11.

The floating potential of the dust is assumed to be constant during an RF cycle. This assumption is justified by the fact that the currents towards the dust particle surface are too small to change the charge significantly during an RF cycle.

Recombination on dust particles

When a dust particle becomes negatively charged, it will attract positive ions, these will recombine with an electron that has to be replaced again by an electron from the discharge to maintain the floating potential. As a result the equilibrium fluxes of positive ions and electrons arriving at the dust surface will recombine and the released energy is used to heat up the dust particle surface [9, 10]. The electron flux (Eq. 5.11) results in a recombination rate:

$$R = 4\pi r_d^2 n_d n_e \sqrt{\frac{k_B T_e}{2\pi m_e}} \exp\left(\frac{eV_{fl}}{k_B T_e} \right), \tag{5.14}$$

Forces acting on a dust particle

In a plasma dust particles undergo a wide variety of forces. Assuming that a dust particle is a perfect sphere the gravitational force can be written as:

$$\boldsymbol{F}_g = \frac{4}{3}\pi r_d^3 \rho_d \boldsymbol{g}, \tag{5.15}$$

where r_d is the dust particle radius, ρ_d is the mass density and $\boldsymbol{g}$ is the gravitational acceleration. For the often used melamine-formaldehyde dust particle ρ_d is approximately $1.51 \cdot 10^3 \ kg/m^3$.

When a dust particle has a velocity relative to the neutral gas, it will experience a drag force due to momentum transfer from/to the gas. This neutral drag force has been discussed in detail by Graves et al [12]. It can be approximated by,

$$\boldsymbol{F}_n = -\frac{4}{3}\pi r_d^2 n_n \left(\boldsymbol{v}_d - \boldsymbol{v}_n\right) v_{th} m_n, \tag{5.16}$$

where n_n is the density of the neutral with mass m_n, $\boldsymbol{v}_d$ the drift velocity of the dust particle, $\boldsymbol{v}_n$ the velocity of the gas and v_{th} the average thermal velocity of the gas. Because advection of the neutral gas is not included in the model, $\boldsymbol{v}_n = \boldsymbol{0}$, this force will only be present as a damping force on the velocity of the dust particles.

Another force caused by momentum transfer is the ion drag. This force results from the positive ion current that is driven by the electric field. It consists of two components. The collection force represents the momentum transfer of all the ions that are collected by the dust particle and is given by:

$$\boldsymbol{F}_i^c = \pi b_c^2 n_i v_s m_i \boldsymbol{v}_i, \tag{5.17}$$

where v_s the mean speed of the ions, $\boldsymbol{v}_i$ the ion drift velocity and b_c the collection impact parameter.

The second component is the orbit force given by:

$$\boldsymbol{F}_i^o = 4\pi b_{\pi/2}^2 \Gamma n_i v_s m_i \boldsymbol{v}_i, \tag{5.18}$$

with $b_{\pi/2}$ the impact parameter that corresponds to a deflection angle $\pi/2$ and Γ the Coulomb logarithm.

$$\Gamma = \frac{1}{2} \ln \left(\frac{\lambda_L^2 + b_{\pi/2}^2}{b_c^2 + b_{\pi/2}^2} \right), \tag{5.19}$$

$\lambda_L = ((1/\lambda_e)^2 + (1/\lambda_i)^2)^{-1/2}$ is the linearized Debye length, which is a combination of the electron Debye length, λ_e, and the ion Debye length, λ_i. The ion drag

is discussed in more detail by Barnes et al [13]. Previous calculations have shown that the ion drag should be enhanced with at least a factor 5 or the linearized Debye length in the Coulomb logarithm (Eq. 5.19) should be replaced by the electron Debye length, in order to generate a void [3]. This factor is also included in the calculation presented here. Khrapak et al [14] have studied cases where the ion drag force is underestimated by using the ion drag expression of Barnes. These cases are quite similar to ours. Lampe et al [15] have shown that collisions with the background gas may enhance the collection of ions. This could explain the factor 5 needed in our simulations.

Due to their charge, dust particles will experience an electric force. Daugherty et al [16] derived the following expression:

$$\boldsymbol{F}_e = Q_d \boldsymbol{E} \underbrace{\left(1 + \frac{\kappa r_d}{3(1 + \kappa r_d)}\right)}_{\approx 1}, \qquad (5.20)$$

where Q_d is the charge on the dust particle, $\boldsymbol{E}$ is the electric field and $\kappa = 1/\lambda_L$. In a discharge the dust particle radius is much smaller than the linearized Debye length, therefore the term between the bracket is approximately 1 and the electric force is given by:

$$\boldsymbol{F}_e = Q_d \boldsymbol{E}. \qquad (5.21)$$

This expression holds for situations where the dust particles are not shielded from the plasma by positive ions trapped in orbitals around the dust particle [15]. In that case the particle plus ion cloud will behave as some kind of dipole.

When a temperature gradient is present in a discharge, for instance due to cooling or heating of the electrodes a third force driven by momentum transfer will occur. This force is called the thermophoretic force. Atoms impinging from the hot side have more momentum than their companions of the cold side, this can result in a force pointing in the direction $-\boldsymbol{\nabla} T_{gas}$.

For large Knudsen numbers Talbot et al [17] derived the following expression:

$$\boldsymbol{F}_{th} = -\frac{32}{15} \frac{r_d^2}{v_{th}} \left(1 + \frac{5\pi}{32}(1 - \alpha)\right) \kappa_T \boldsymbol{\nabla} T_{gas}, \qquad (5.22)$$

$v_{th} = [8k_B T_{gas}/(\pi m)]^{1/2}$ is the average thermal velocity of the gas. κ_T is the translation part of the thermal conductivity. α, the thermal accommodation coefficient of the gas is taken equal to 1.

To obtain a suitable expression for the flux of dust particles, we assume that the neutral drag force is in equilibrium with the sum of the other forces. This assumption is valid when the final steady state is approached, but should be relaxed, for instance, when the dust is injected at a high velocity. In that case the inertia

of the dust should not be neglected. With the introduction of a momentum loss frequency and a mobility and diffusion coefficient for the dust particles given by:

$$\nu_{md} = \sqrt{2}\frac{p_{tot}}{k_B T_{gas}}\pi r_d^2 \sqrt{\frac{8k_B T_{gas}}{\pi m_d}}, \tag{5.23}$$

where p_{tot} is the static pressure and m_d the dust particle's mass.

$$\mu_d = \frac{Q_d}{m_d \nu_{md}}, \tag{5.24}$$

$$D_d = \mu_d \frac{k_B T_{gas}}{Q_d}, \tag{5.25}$$

it is possible to define a "drift-diffusion" expression for the flux of the dust particles,

$$
\begin{aligned}
\boldsymbol{\Gamma}_d &= -\mu_d n_d \boldsymbol{E}_{eff} - D_d \boldsymbol{\nabla} n_d - \frac{n_d}{\nu_{md}}\boldsymbol{g} \\
&+ \frac{n_d m_i v_s}{m_d \nu_{md}}\left(4\pi b_{\pi/2}^2 \Gamma + \pi b_c^2\right)\boldsymbol{\Gamma}_i \\
&- \frac{32}{15}\frac{n_d r_d^2}{m_d \nu_{md} v_{th}}\kappa_T \boldsymbol{\nabla} T_{gas},
\end{aligned}
\tag{5.26}
$$

and treat them with the same numerical procedures as the other charged particles in the fluid model. Because of the low mobility of the dust particles the effective field $\boldsymbol{E}_{eff}$ is approximated by the time averaged RF field. The diffusion originates from the pressure gradient, $k_B T_d \boldsymbol{\nabla} n_d$. The Einstein relation couples the diffusion and the mobility coefficients, see equation 5.25.

The drift velocity and the diffusion coefficient of the dust fluids are much smaller than those of the ions and electrons. Therefore it would require a large computational effort to achieve a steady state solution for the dust when it is followed during an RF cycle. We therefore have developed a method to speed up the convergence toward the steady state solution by introducing a different calculation cycle with a different time step for the dust. Our model thus consists of two calculation cycles. In the first one, the transport equations of the ions, electrons and the Poisson equation are solved during a number of RF cycles, during the RF cycles the dust does not move. After that, the transport equation of the dust is solved with a greater time step, using the time averaged electric field, and electron and positive ion fluxes. During the second calculation, space charge regions are created, because the electron and positive ion densities do not change. These space charge regions will lead to instabilities in the solution of Poisson equation

and the electron transport. To solve this problem, we correct the artificially generated space charge by adapting the positive ion density distributions prior to the next series of RF cycles, in which the ion and electron density profiles adapt themselves to the new dust density profile. With this method the required speed-up is established. Both for the plasma species and for the dust fluids the transport equations are solved using the Sharfetter-Gummel exponential scheme [7]. To model the reactor (Fig. 5.1), we have used a grid of 24 radial gridpoints times 48 axial gridpoints. We make use of a non-equidistant grid. The radial spatial resolution is 0.21 cm and the axial resolution between the electrodes is 0.09 cm. More details about the used discretion schemes can be found in [7].

The internal pressure of the crystal due to the inter-particle interaction has been included by means of a density dependence of the diffusion coefficient for the dust. The diffusion coefficient of the dust is increased by a factor $\exp(N_d/N_c)$ where the reference density N_c is chosen such that the dust density saturates at a value N_{crys}. This models the incompressibility of the crystal. Actually, the (yet unknown) equation of state of the dust crystal should be used to account for the internal pressure. Since we were not primarily interested in the precise structure of the crystallized regions, we have chosen for the simple and computationally robust exponential increase of D_d. Plasma crystal experiments [1] have shown an inter-particle distance of about 300 μm for a dust particle with diameter of 15 μm. This results in an average "crystal" density N_{crys} of $3.7 \cdot 10^{10}$ m^{-3}.

5.3   Results and discussion

In this section the results, obtained with the 2D argon-dust fluid model are presented. The PKE chamber used by Morfill et al has been modelled (Fig. 5.1). The reactor is cylindrically symmetric. The simulation starts with a zero dust density profile. During the simulation the dust is injected from both electrodes by adding source terms in the dust particle balances for the first grid points below/above the electrodes. The injection rate is about 750.000 particles per second. Eventually a total amount of 0.7 million dust particles is reached, after that the sources switched off. The electrodes are both driven by a radio-frequency power source at a frequency of 13.56 MHz. The peak-to-peak voltage is 70 volts, this results in a power dissipation of about 0.04 W. The pressure is 40 Pa. The dust particles have a diameter of 15 μm. Comparisons of the plasma parameters are made for a dusty and a dust-free argon discharge.

Figure 5.2 shows the steady state dust density profile. In the center of the discharge a dust-free region, the so-called void appears, surrounded by a crystalline region of dust with an average density of $1.55 \cdot 10^{10}$ m^{-3}. This gives an inter-particle distance of about 400 microns.
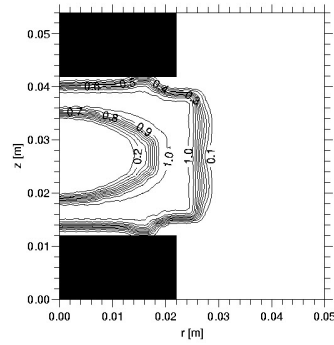
Figure 5.2: Dust density profile in m^{-3}, normalized with a factor of $1.55 \cdot 10^{10}$.
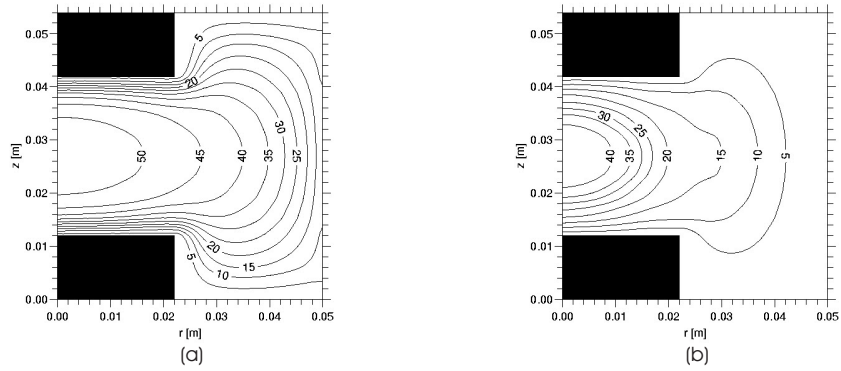

Figure 5.3: Time-averaged electric potential in volts in dust-free discharge (a) and for a dusty argon discharge (b).
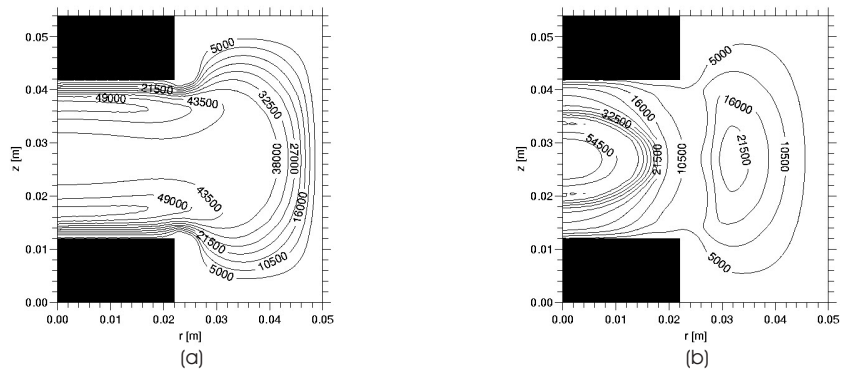

Figure 5.4: Number of electrons on a dust particle with diameter of 15 μm in a dust-free discharge (a) and for a dusty argon discharge (b).

Figures 5.3a and 5.3b show the time-averaged potential distribution V(r,z) in the dust-free and the dusty argon discharge. In both cases the potential has its maximum in the bulk of the plasma between the electrodes. Comparing the potential distributions, a significant change in the plasma potential can be observed. The plasma potential in the center of the dusty discharge has decreased compared with the dust-free case. This shows the importance of taking into account both the contribution of the charge on the dust (Fig. 5.4a and 5.4b) in the Poisson equation and the recombination on the dust particle surface. It can also be seen that if a dust particle would settle in the center of the discharge it would get a higher charge in a dusty discharge. This is mainly due to a higher electron energy. The non-uniform charge distribution is the result of the spatial distribution of the ions, electrons and electron energy. The enhanced ion density in the dust cloud reduces the dust charge.
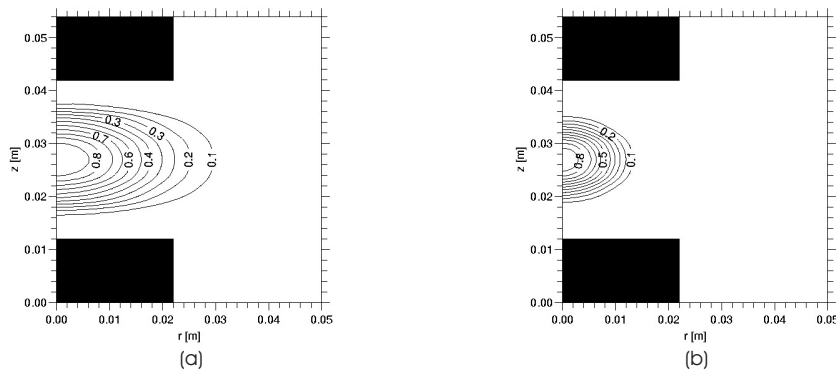

Figure 5.5: Time-averaged electron density in m^{-3} for a dust-free discharge, normalized with a factor of $2.59 \cdot 10^{15}$ (a) and for a dusty argon discharge, normalized with a factor of $2.61 \cdot 10^{15}$ (b).

Comparing Fig. 5.5a and Fig. 5.5b, it can be seen that indeed the recombination on the dust particle surface acts as a sink for the electrons. The same is observed for the argon ions (Fig. 5.6a and 5.6b). Due to a decrease in the electron and ion density, the remaining electrons can gain more energy from the larger oscillating electric field, this gives rise to a higher electron temperature in a dusty discharge (Fig. 5.7a and 5.7b). This increase in electron temperature enhances the production of the argon meta-stables with almost 25 percent. This is shown in figures 5.8a and 5.8b. In the experiments the enhanced electron temperature is seen via an increase of the intensity of the light emitted from inside the void due to excited argon atoms. However the meta-stables density could be used as an indirect indicator for the light emerging from the void.

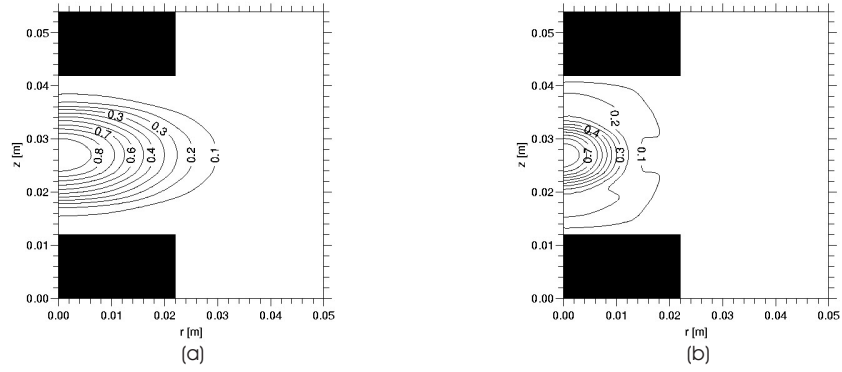Figure 5.9a shows the net space charge in a dust-free argon plasma. As ex-

Figure 5.6: Time-averaged ion density in m^{-3} for a dust-free discharge, normalized with a factor of $2.59 \cdot 10^{15}$ (a) and for a dusty argon discharge, normalized with a factor of $2.61 \cdot 10^{15}$ (b).
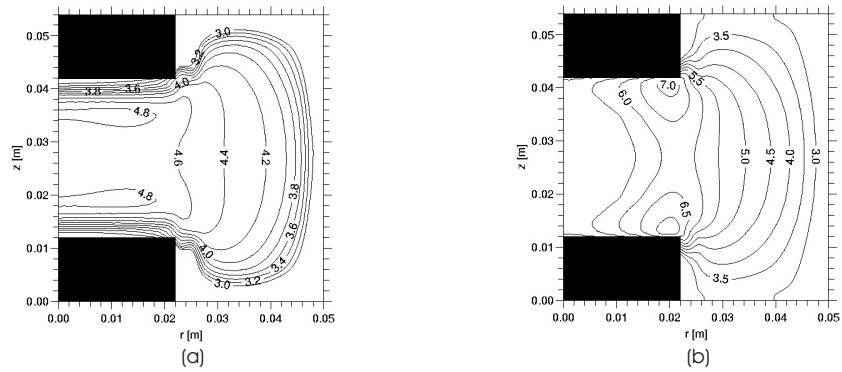

Figure 5.7: Time-averaged electron energy in eV for a dust-free discharge (a) and for a dusty argon discharge (b).
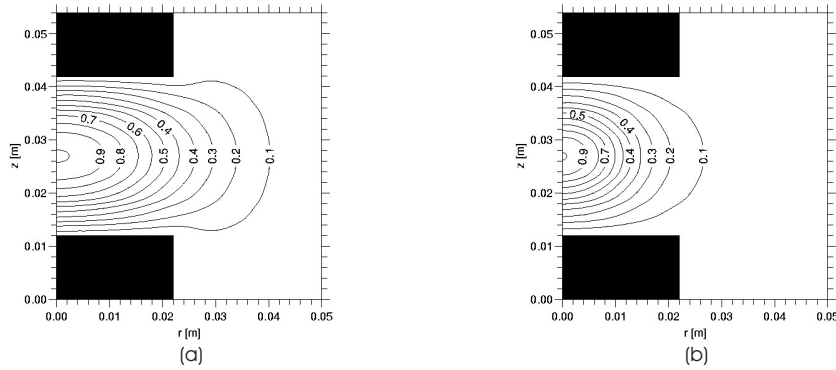
Figure 5.8: Time-averaged argon meta-stable density in m^{-3} for a dust-free discharge, normalized with a factor of $4.01 \cdot 10^{17}$ (a) and for a dusty argon discharge, normalized with a factor of $4.92 \cdot 10^{17}$ (b).

pected, positive space charge regions appear only close to the electrodes and the reactor wall. At the center between the electrodes a quasi-neutral region can be observed. For the dusty discharge case an interesting phenomenon can be observed. Figures 5.9b, 5.9c and 5.10 show a double space charge layer that appears around the sharp boundary of the dust crystal. This double space charge layer inside the void has been described by Annaratone et al [18]. The positive space charge layer in front of the dust crystal boundary is caused by the recombination on the dust particle's surfaces of ions and electrons entering the crystal. As in front of an absorbing wall, the difference in mobility between the ions and the electrons results in a net positive space charge that enhances the electric field which in turn accelerates the ions from the center of the void towards the dust crystal to compensate for the mobility difference. The negative space charge region appears very close to the sharp edges inside the dust crystal. It appears due to the fact that the diffusion of the argon ions prohibits a full compensation of the fast rising negative charge of the dust crystal. These double space charge layers could explain the repulsion effect of the generated dust clouds during the first stages of injection, which slows down the mixing of the dust clouds seen in the PKE experiments [1].

Figures 5.11a and 5.11b show the gas temperature for the dust-free and dusty discharge. The gas temperature profile in a dusty plasma has two maxima of 274.1 K in the sheaths, which is about 1 K higher than the reactor wall temperature that is kept at 273 K. In figures 5.12a and 5.12b the dust particle (surface) temperature is shown for the dust-free and dusty discharge, it can be observed that a dust particle would get a maximum temperature in the center of the plasma if it would settle there. This is due to the maximum in the ion and electron density in the middle of the discharge, giving a maximum recombination energy flux towards the
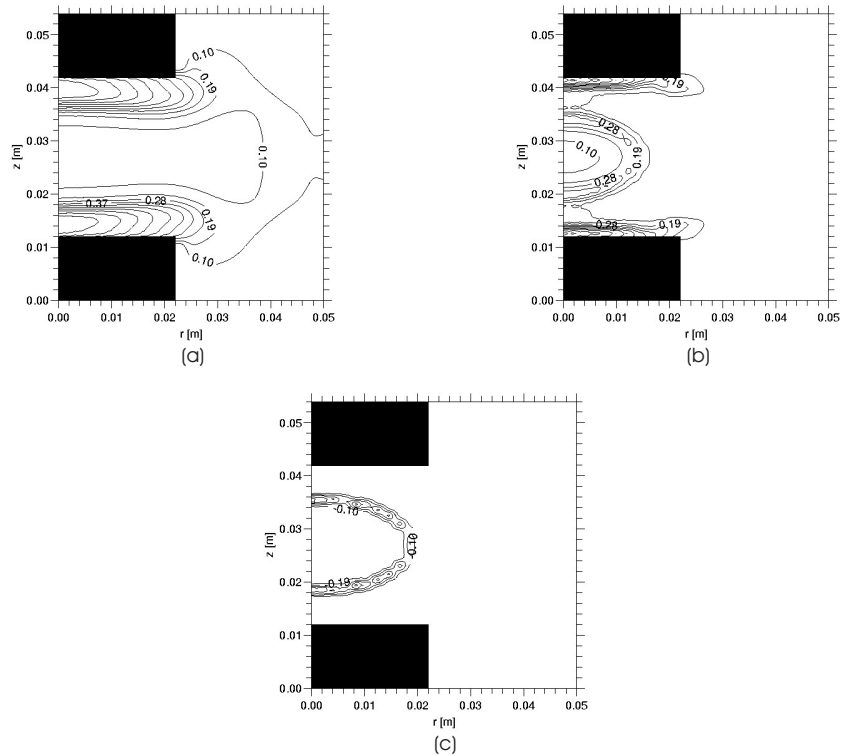
Figure 5.9: (a) Time-averaged net space charge in m^{-3} for a dust-free argon discharge in elementary charges, normalized with a factor of $1.42 \cdot 10^{14}$.
(b) Time-averaged positive space charge in m^{-3} for a dusty argon discharge in elementary charges, normalized with a factor of $2.16 \cdot 10^{14}$.
(c)Time-averaged negative space charge in m^{-3} for a dusty argon discharge in elementary charges, normalized with a factor of $5.78 \cdot 10^{13}$.
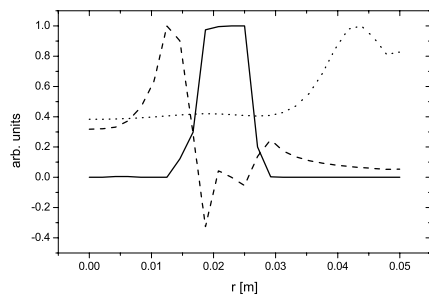
Figure 5.10: Dust density profile and the net space charge profile for a dust-free and dusty argon discharge at the axial symmetry axis. The thick curve represents dust density profile of the $15\mu m$ sized dust particles, normalized with a factor of $1.48 \cdot 10^{10}$. The dashed curve represents the net space charge in a dust argon discharge, normalized with a factor of $5.37 \cdot 10^{13}$. The dotted curve represents the net space charge for a dust-free discharge at the axial symmetry axis, normalized with a factor of $1.84 \cdot 10^{13}$.
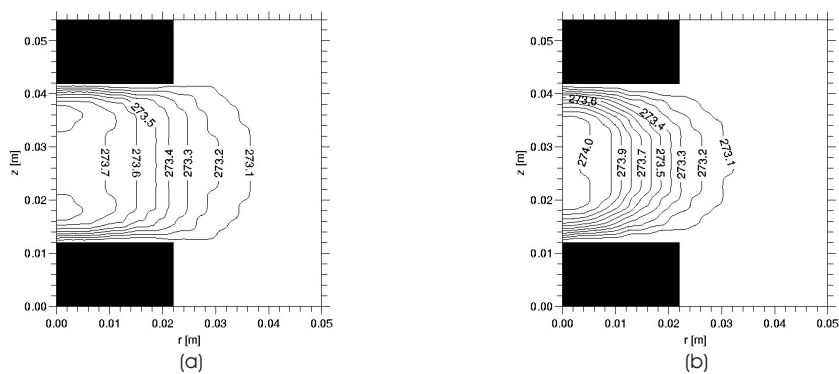

Figure 5.11: (a) Gas temperature in K for a dust-free discharge (a) and for a dusty argon discharge (b).
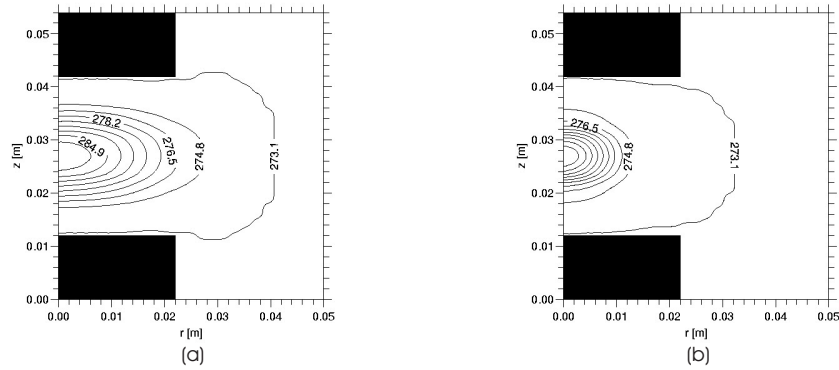
Figure 5.12: Dust particle surface temperature in K for a dust-free discharge (a) and for a dusty argon discharge (b).

dust particles surface. Note that the difference between the gas and dust particle surface temperature is about 9 K at the center of the discharge. Comparing the gas temperature for a dust free and dusty discharge (Fig. 5.11a and 5.11b) shows that the effect of the dust on the gas temperature profile is negligible.

5.4 Conclusions

The numerical simulation results show that self-consistent modelling of the plasma parameters in a dusty argon discharge is important. Both the contribution of the charge on the dust in the Poisson equation and the recombination on the dust particle surface must be taken into account. Recombination on the dust particle's surface results for instance in a significant difference in electron and ion densities between a dust-free and dusty argon discharge. Also the other plasma parameters are affected, like the electron temperature, the electric potential and the charge on the dust particles. An interesting phenomenon is the appearance of a double space charge at the edge of the dust crystal which is formed by the difference in mobility between the ions and electrons and the diffusive transport of the ions caused by the steep density gradients. The modelling results also show an increase of the density of the argon meta-stables inside the void, illustrating in an indirect way the increased light emission emerging from the void due to excited argon atoms, as observed in the PKE experiments [1].

Acknowledgments

References

[1] G. E. Morfill et al, Phys. Rev. Lett., **83**, 1598 (1999).

[2] H. Thomas et al, Phys. Rev. Lett., **73**, 652 (1994).

[3] M. R. Akdim et al, Phys. Rev. E., **65**, 015401(R) (2002).

[4] T. Nitter , Plasma Sources Sci. Technol., **5**, 93 (1996).

[5] P. Belenguer et al, Phys. Rev. A., **46**, 7923 (1992).

[6] V. Vyas et al, J. Appl. Phys., **92**, 6451 (2002).

[7] J. D. P. Passchier et al, J. Appl. Phys., **73**, 1073 (1993).

[8] I. Revel et al, J. Appl. Phys., **88**, 2234 (2000).

[9] M. R. Akdim et al, Phys. Rev. E., **67**, 056405 (2003).

[10] G. H. P. M. Swinkels et al, J. Appl. Phys., **88**, 1747 (2000).

[11] J. E. Allen et al, J. Plasma. Phys., **63**, 299 (2000).

[12] D. B. Graves et al, Plasma Sources Sci. Technol., **3**, 433 (1994).

[13] M. S. Barnes et al, Phys. Rev. Lett., **68**, 313 (1992).

[14] S. A. Khrapak et al, Phys. Rev. E., **66**, 046414 (2002).

[15] M. Lampe et al, Phys. Rev. Lett., **86**, 5278 (2001).

[16] J. E. Daugherty et al, J. Appl. Phys., **73**, 1617 (1994).

[17] L. Talbot et al, J Fluid Mech., **101**, 737 (1980).

[18] B. M. Annaratone et al, Phys. Rev. E., **66**, 056411 (2002).

6. Modelling of Self-Excited Dust Vortices in Complex Plasmas under Microgravity

Abstract. *A two dimensional hydrodynamic model for a dusty argon plasma in which the plasma and dust parameters are solved self-consistently, has been supplemented with a separate dust particle tracing module to study the behavior of dust vortices. These coherent vortices appear in plasma crystal experiments performed under microgravity conditions. The non-conservative total force exerted by the discharge on the dust particles is responsible for the generation of the vortices. The contribution of the thermophoretic force driven by the gas temperature gradient plays an insignificant role in the generation of the vortices, even when the gas heating via the dust particles is taken into account. The forces related to the electric field, including the ion drag force, are dominant.*

6.1 Introduction

Plasma crystal experiments performed under microgravity conditions have shown dust vortices which usually appear outside the crystalline regions. In their PKE (Plasmakristall-Experiment) chamber (Fig. 6.1) Morfill et al usually observed two stable dust vortices near the edges of the electrodes (Fig. 6.2), one rotating clockwise and the other counter-clockwise [1, 2]. Other authors have reported on
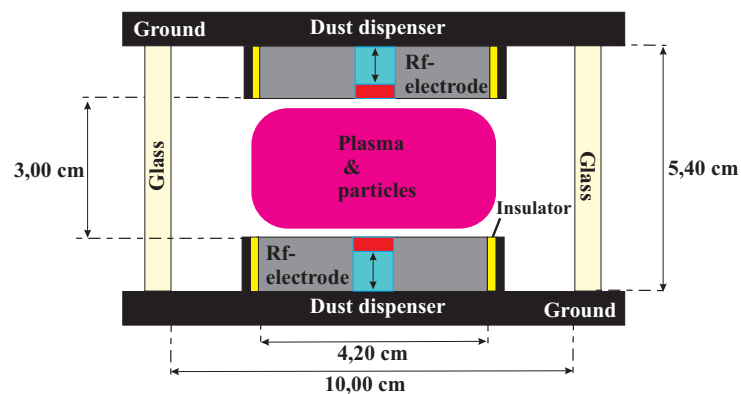

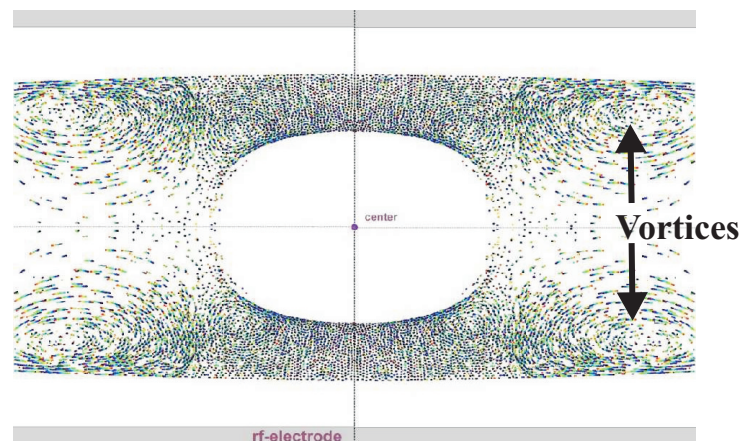Figure 6.1: A schematic diagram of the PKE chamber.

Figure 6.2: A dust crystal in a PKE experiment under microgravity conditions [2]. The vortices usually appear at the outer edges.

various theoretical and numerical studies of the driving mechanisms behind these vortices [3, 4]. None of these, however, fully explain the mechanism behind their creation under microgravity.

Theoretical and numerical studies up to now have basically followed dust particles in the electric field and particle fluxes of an undisturbed discharge. An important aspect not covered is the influence of the dust on the discharge. For this a fully self-consistent model is needed. We have developed such a model for a dust containing radio frequency (RF) discharge in argon and used it to investigate the behavior of dust particles. The model contains a dust-argon fluid part which has been described in a previous article [5] and a newly added part that takes the inertia and the screened-Coulomb interaction between the dust particles into account to trace dust particles in a dusty argon discharge. In existing models [6, 7], the influence of the dust particles on the discharge due to recombination on their surface or the motion of the dust is neglected. If a discharge contains a considerable amount of dust, like in the PKE experiments, this approximation is not correct. Our model accounts for the influence of the dust fluid on the plasma and for its transport as a fluid. This makes it a sophisticated tool for studying dusty discharges. The dust-argon fluid model provides the input data for a separate module which calculates the dust particle trajectories in the force field present in a dusty discharge. In this paper we describe the newly added particle tracing module and the results obtained with it, studying in particular the generation of vortices.

6.2   Fluid model

In the fluid part of our two-dimensional model the particle balances, the electron energy balance and the Poisson equation are solved, including the transport of the dust fluid. For each particle a density balance can be written as:

$$\frac{dn_j}{dt} + \boldsymbol{\nabla} \cdot \boldsymbol{\Gamma}_j = S_j, \tag{6.1}$$

where n_j is the particle's density, $\boldsymbol{\Gamma}_j$ the flux of the species and S_j, the sink or source terms.

The momentum balance is replaced by the drift-diffusion approximation, where the particle flux consist of a diffusive term and a drift term,

$$\boldsymbol{\Gamma}_j = \mu_j n_j \boldsymbol{E} - D_j \boldsymbol{\nabla} n_j, \tag{6.2}$$

where μ_j and D_j are the mobility and diffusion coefficient of species j. $\boldsymbol{E}$ is the electric field.

Also the flux of the dust particles can be written as a drift-diffusion expression. Setting the friction force exerted by the neutral gas equal to the sum of the other forces, including the force term from the dust pressure gradient, results in:

$$\boldsymbol{\Gamma}_d = \frac{\sum \boldsymbol{F}_d}{m_d \nu_{md}} - \frac{k_B T_d}{m_d \nu_{md}} \boldsymbol{\nabla} n_d, \tag{6.3}$$

with m_d the mass of the dust particle, ν_{md} the momentum loss frequency due to friction. The diffusion coefficient is enhanced at high dust densities in order to model the crystal formation [5].

For ions the characteristic momentum transfer frequency is only a few megahertz (MHz). To use the drift-diffusion approximation for ions for RF frequencies higher than a few MHz the electric field field in equation 6.2 is replaced by an effective electric field, using this effective electric field $\boldsymbol{E}_{eff}$, inertia effects are taken into account [8].

The electric field $\boldsymbol{E}$ and potential V are calculated using the Poisson equation:

$$\Delta V = -\frac{e}{\epsilon_0} \left(n_i - n_e - Q_d n_d \right), \tag{6.4}$$

$$\boldsymbol{E} = -\boldsymbol{\nabla} V, \tag{6.5}$$

where e is the elementary charge, ϵ_0 the permittivity of vacuum space, n_e the electron density, n_i the ion density, Q_d the charge on a dust particle and n_d the dust density.

The electron energy density $w_e = n_e \epsilon$ (i.e. the product of the electron density and average electron energy ϵ) is calculated self-consistently from the second moment of the Boltzmann equation:

$$\frac{dw_e}{dt} + \boldsymbol{\nabla} \cdot \boldsymbol{\Gamma}_w = -e\boldsymbol{\Gamma}_e \cdot \boldsymbol{E} + S_w, \tag{6.6}$$

where $\boldsymbol{\Gamma}_w$ is the electron energy density flux:

$$\boldsymbol{\Gamma}_w = \frac{5}{3} \mu_e w_e \boldsymbol{E} - \frac{5}{3} D_e \boldsymbol{\nabla} w_e, \tag{6.7}$$

and μ_e and D_e are the electron mobility and electron diffusion coefficients. The term S_w in the electron energy balance equation is the loss of electron energy due to electron impact collisions, for instance recombination of electrons on the dust particle's surface. Further details about the algorithms used to solve the above mentioned equations can be found in [8]. Problems related to the huge difference in the timescale of the dust motion (1-10 s) and the RF period (100 ns) have been solved by time splitting and an iterative procedure. The charge on a dust particle is calculated by using the Orbital-Motion-Limited (OML) probe theory [9]. The charge on the dust particle is assumed to be constant in time during an RF cycle and is obtained from the balance of the local (OML) time-averaged electron and ion currents collected by the particle. Recombination of ions and electrons on the dust particle surface is also taken into account. Ion-neutral collisions have been included to simulate a possible gas heating mechanism. For this we have used a simple approximation by assuming that the energy taken up from the electric field

by the ions is dissipated locally in collisions with the gas [10]. We have extended this gas heating mechanism by taking the heating of the dust particle surface into account. The dust particle (surface) temperature can affect the gas temperature which in turn could affect the other elementary processes in the discharge, relevant for the formation of vortices. The thermal balance of the particles can be written as an equality between the thermal influx Q_{in} and the outflux Q_{out}. For a stationary situation the thermal influx is given by $Q_{in} = J_{rec}$, where J_{rec} is the energy flux of the recombining ion-and electron flux arriving at the dust particle surface. For a Maxwellian electron energy distribution function J_{rec} is given by:

$$J_{rec} = n_d n_e \sqrt{\frac{k_B T_e}{2\pi m_e}} exp\left(\frac{eV_{fl}}{k_B T_e}\right)(E_i + eV_{fl}), \tag{6.8}$$

where T_e is the electron temperature, m_e the electron mass, V_{fl} the floating potential and E_i the ionisation energy which is 15.7 eV for argon. The outflux is given by $Q_{out} = J_{th} + J_{rad}$. For the pressure range in the PKE experiments, the thermal conduction of the gas J_{th} is governed by the Knudsen theory [11]. J_{rad} is the radiative cooling. J_{th} is given by:

$$J_{th} = \frac{\gamma + 1}{16(\gamma - 1)}\frac{p}{\sqrt{T_g}}\sqrt{\frac{8k_B}{\pi m_g}}\alpha(T_p - T_g), \tag{6.9}$$

where $\gamma = c_p/c_v$ is the heat capacity ratio, m_g the gas molecule mass, p the gas pressure, T_p the dust particle surface temperature, T_g the gas temperature and α the accommodation coefficient.

The radiative cooling term J_{rad} follows directly from the Stefan-Boltzmann law:

$$J_{rad} = \epsilon\sigma\left(T_p^4 - T_w^4\right), \tag{6.10}$$

where ϵ is the emissivity, σ the Stefan-Boltzmann constant and T_w the reactor wall temperature. For an argon discharge $\gamma = 5/3$ and $\alpha = 0.86$ have been suggested in the literature [12]. The emissivity of the melamine-formaldehyde (MF) particles that are used in the PKE experiments is supposed to be 0.9 [13]. Equation 6.9 and Eq. 6.10 are coupled to the temperature balance for the gas and solved with an iterative method.

6.3   Dust particle trajectories

In the fluid model [5], the transport of the dust fluid is solved by assuming that the forces acting on the dust particles are in balance with the neutral drag force. In that case the inertia of the dust particles is neglected and a so-called drift-diffusion expression is obtained for the flux of dust particles. This makes the fluid

model only useful to study the steady state behavior of dust clouds. To study the vortices that have been seen in the PKE experiments, the inertia and the interaction between the dust particles should be taken into account. The fluid model provides the force field and the linearized Debye length present in a dusty discharge. These are used by the dust particle trajectory model to solve the equation of motion of the dust particles. Neglecting the screened Coulomb interaction with the background dust crystal, the equation of motion is given by:

$$m_d\frac{d\boldsymbol{v}_d}{dt} = \boldsymbol{F}_E + \boldsymbol{F}_I + \boldsymbol{F}_T + \boldsymbol{F}_N + \boldsymbol{F}_{SC}, \tag{6.11}$$

where m_d is the mass of the dust particle, $\boldsymbol{v}_d$ its velocity, $\boldsymbol{F}_E$ the electric force, $\boldsymbol{F}_I$ the ion drag force, $\boldsymbol{F}_T$ the thermophoretic force, $\boldsymbol{F}_N$ the neutral drag force and $\boldsymbol{F}_{SC}$ the screened Coulomb force between the dust particles which are tracked in the dust particle trajectory module. For details about the expressions used for the above mentioned forces we refer to previous articles [5, 14].

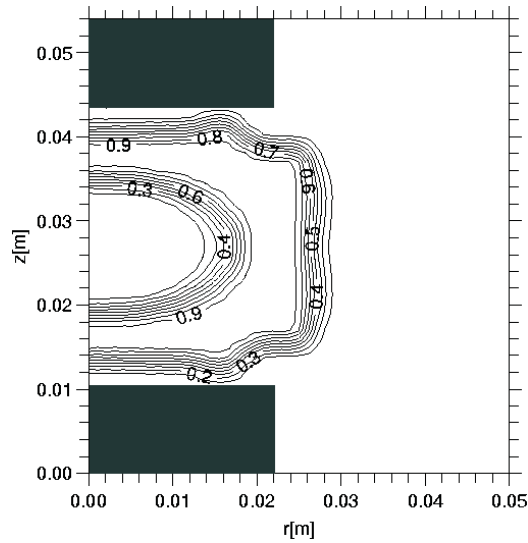## 6.4   Results and discussion

Figure 6.3: Simulated dust density profile in m^{-3} in an argon discharge, normalized with a factor $1.5 \cdot 10^{10}$.

The PKE chamber used by Morfill et al has been modelled. The reactor is cylindrically symmetric. The simulation starts with a zero dust density profile. During the simulation the dust is injected from both electrodes by adding source

terms in the dust particle balances for the first grid points below/above the electrodes, the injection rate is about 750.000 particles per second. Eventually a total amount of 0.7 million dust particles is reached; after that the sources are switched off. The electrodes are both driven by a radio-frequency power source at a frequency of 13.56 MHz. The peak-to-peak voltage is 70 volts. This results in a power dissipation of about 0.04 W. The pressure is 40 Pa. The dust particles have a diameter of 15 μm. The equation of motion for the dust fluid [5] is solved for the time-averaged electric field, plasma densities and fluxes.

Figure 6.3 shows the steady state dust density profile. In the center of the discharge a dust-free region, the so-called void appears, surrounded by a crystalline region of dust with an average density of $1.5 \cdot 10^{10} m^{-3}$.

Figures 6.4 and 6.5 show the time-averaged potential distribution V(r,z) in the dust-free and the dusty argon discharge. In both cases the potential has its maximum at the center of the plasma between the electrodes. Comparing the potential distributions, a significant difference in the plasma potential can be observed. The plasma potential decreases in the center of the discharge in the case of a dusty plasma. This shows the importance of taking into account both the contribution of the charge on the dust in the Poisson equation and the recombination on the dust particle surface, which leads to a lower electron density and a higher electron temperature.
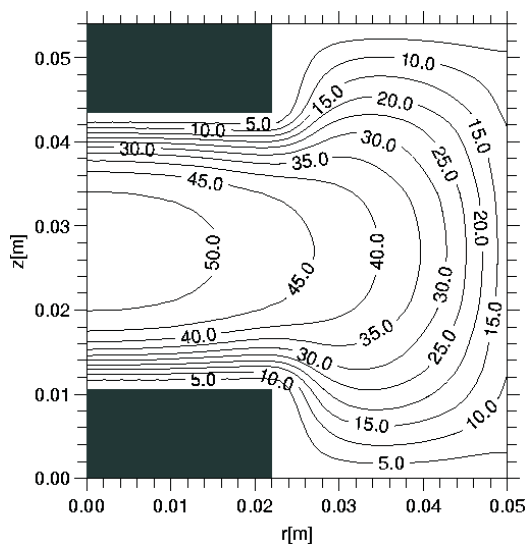

Figure 6.4: Time-averaged potential V(r,z) in volts in the dust-free argon discharge.

Figure 6.6 shows the gas temperature in a dusty discharge. The gas temperature profile has two maxima of 274.1 K in the sheaths, which is about 1 K higher than the reactor wall temperature that is kept at 273 K. In the regions where the
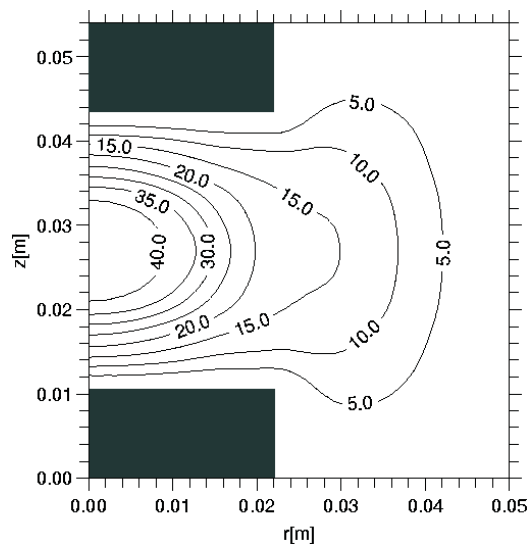
Figure 6.5: Time-averaged potential V(r,z) in volts the dusty argon discharge.
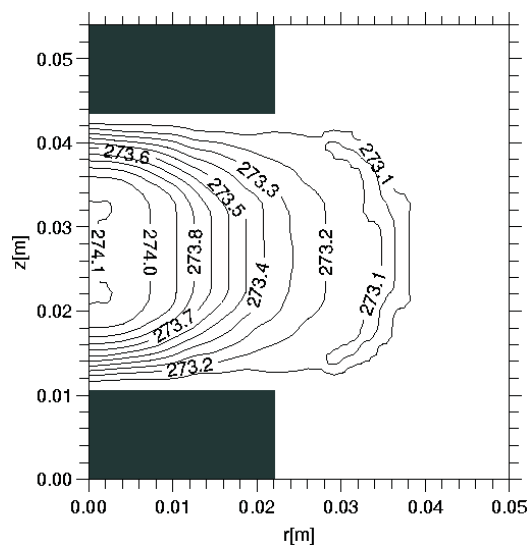

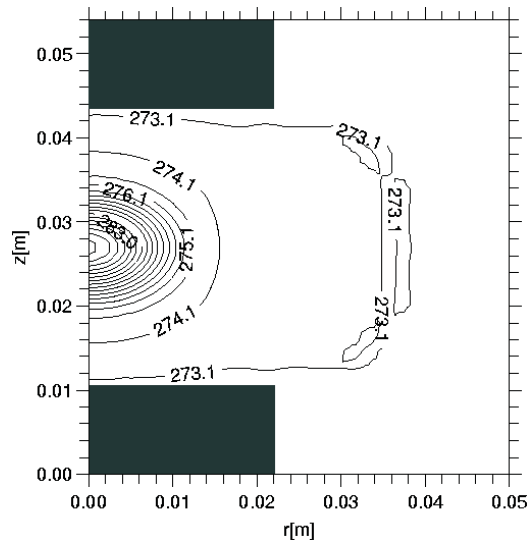Figure 6.6: Gas temperature in K in the dusty argon discharge.

Figure 6.7: Dust particle surface temperature in K in the dusty argon discharge.

dust vortices have been observed in the PKE experiments (Fig. 6.2) the thermal gradient is about 0.1 K/cm. This shows that the contribution of the thermophoretic force to the total force on the dust particles is negligible, typically 30 times smaller than the other forces. In figure 6.7 the dust particle (surface) temperature has been plotted. It can be observed that a dust particle would get a maximum temperature in the center of the plasma if it would settle there. This is due to the maximum in the ion and electron density in the middle of the discharge, giving a maximum recombination energy flux towards the dust particles surface. Note that the difference between the gas and dust particle temperature is about 9 K at the center of the discharge.

Figure 6.8 shows the dust particle trajectories of 12 particles which have been injected from the lower electrode in a dusty argon discharge. Apart from the negligible thermophoretic force (typical value $2 \cdot 10^{-13}$ N), the forces acting on a particle are 1) the ion drag force ($7 \cdot 10^{-12}$ N) that tends to push the particles up or down, away from the plane of symmetry (z=0.027), and radially outward, and 2) the electric force ($7 \cdot 10^{-12}$ N), that acts in the opposite direction. The total force is their sum. At a certain radius, in the plane of symmetry (where all axial forces are zero), there is a point where the total radial force becomes zero. This is where a single particle will go. The repulsing screened Coulomb force ($5 \cdot 10^{-13}$ N) prohibits this in case of more particles. The particles are then forced to stay in the lower or upper half of the reactor and/or inside and outside the radius where the total radial force vanishes. In these regions the total force is not conservative ($\oint \boldsymbol{F}_{tot} \cdot \boldsymbol{ds} \neq 0$) and the particles start to rotate in a direction
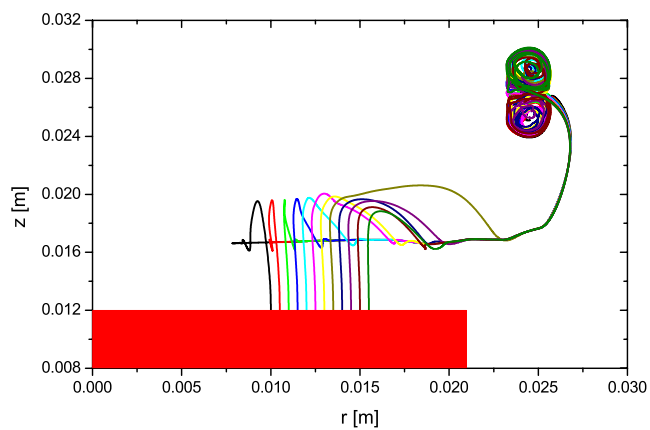
Figure 6.8: Trajectories of dust particles injected from the lower electrode in the dusty argon discharge. Two symmetric stable vortices are generated.
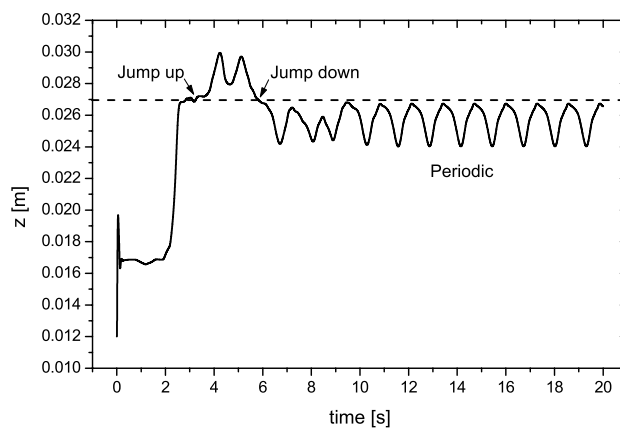

Figure 6.9: The axial position of the fourth dust particle injected from the lower electrode at the position $r = 0.012$ m as function of time, in the dusty argon discharge. The dashed line is the axial axis of symmetry.
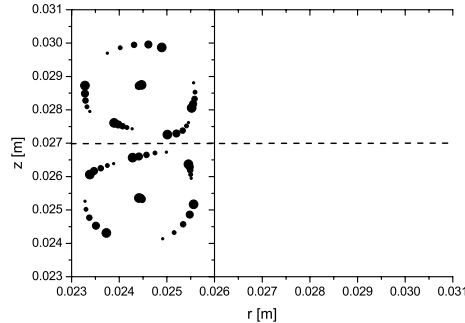
Figure 6.10: Positions of dust particles in the dusty argon discharge at different time steps, represented by growing dots. The solid circles shows the direction of rotation of the dust clouds. The dashed line is the axial axis of symmetry.

dictated by the sign of $\nabla \times \boldsymbol{F}_{tot}$. The neutral drag force ($5 \cdot 10^{-14}$ N) causes the particles to move in a closed orbit. These coherent vortices are permanently driven by the forces resulting from the plasma and therefore keep on turning for timescales much longer than the average rotation time. After injection, the system first has an irregular (chaotic) character, where particles can even jump from one cloud to the other (Fig. 6.9), and then it relaxes toward a self-organized state. Figure 6.10 shows the dust vortex motion after relaxation in more detail. Each dust cloud consist of 6 particles, of which five follow the same orbit and one in the middle has a small elliptic orbit. The vortices rotate in opposite directions, this has also been observed in the PKE experiments. The rotation in our case is mainly determined by the combination of ion drag and electric force acting on the dust particles. The ion drag force and the electric force are such that they push the particles axially toward the midplane $z = 0.027$ m and radially toward the plane $r = 0.0245$ m through the centers of the vortices. The screened Coulomb force however keeps the dust particles away from each other. The calculations made by Vaulina et al [3] show that negligible macro particle charge gradients could cause the dust clouds to rotate. Our calculation shows that no dust charge gradients are needed to get vortices, but that these vortices are driven by the force field dictated by the plasma. The changes in the particle charge in the course of one rotation due to the spatial variation of the plasma parameters are taken into account, but hardly influence its motion. Actually, the gradient in the particle charge is much larger at other positions, outside the vortices. Another difference with the analysis in [3] is the fact that in our case the most dominant forces all depend on the particle charge and gravity is not included.

6.5 Conclusions

The numerical simulation results show that self-consistent modelling of the plasma parameters in a dusty argon discharge is important. Both the contribution of the charge on the dust in the Poisson equation and the recombination on the dust particle surface must be taken into account. The dust-plasma interaction results in a significant difference in the time-averaged potential distributions V(r,z) between a dust-free and dusty argon discharge. Comparing the gas temperature and dust particle surface temperature in the center of the discharge, shows a considerable difference of 9 K, but this does not affect the gas temperature profile. In the region where the dust vortices appear the thermal gradient of the gas is small, the thermophoretic force is about 30 times smaller than the other forces acting on the dust particles. This fact lets us conclude that the generation of the dust vortices are generated by the combination of the ion drag force, electric force and the screened Coulomb force acting on the dust particles and not by the thermophoretic force. Our simulations show good agreement with the PKE experiments done under microgravity.

Acknowledgments

References

[1] G. E. Morfill et al, Phys. Rev. Lett., **83**, 1598 (1999).

[2] H. Thomas et al, Phys. Rev. Lett., **73**, 652-655 (1994).

[3] O.S. Vaulina et al, J. Exp. and Theor. Phys., **91**, 1147 (2000).

[4] D. A. Law et al, Phys. Rev. Lett., **80**, 4189 (1998).

[5] M. R. Akdim et al, Phys. Rev. E., **65**, 015401(R) (2002).

[6] T. Nitter , Plasma Sources Sci. Technol., **5**, 93 (1996).

[7] P. Belenguer et al, Phys. Rev. A., **46**, 7923 (1992).

[8] J. D. P. Passchier et al, J. Appl.Phys., **73**, 1073 (1993).

[9] J. E. Allen et al, J. Plasma.Phys., **63**, 299 (2000).

[10] I. Revel et al, J. Appl. Phys., **88**, 2234 (2000).

[11] M. Knudsen, Ann. Phys., **34**, 539 (1911).

[12] R. Piejak et al, Plasma Sources Sci. Technol., **7**, 590 (1998).

[13] CRC Handbook of Chemistry and Physics., **75th** ed., (1994).

[14] U. Konopka et al, Phys. Rev. Lett., **84**, 891 (2000).

7. Vortices in Dust Clouds under Microgravity: a simple explanation

Abstract. *Clouds of dust particles in radio frequency discharges often show a periodic vortex-like motion, especially near the edges of the electrodes or near the tip of an electrostatic probe. These vortices often last as long as the discharge is powered. In a previous paper we have followed a small number of individual dust particles in a discharge under microgravity conditions, moving under the influence of forces computed by means of a self-consistent two dimensional hydrodynamic model, and interacting via a screened Coulomb potential. The resulting motion showed the vortex-like rotation. In this paper we discuss this phenomenon in more detail, using a simplified model with harmonic forces, but extending the simulations to three dimensions. Stable vortices are observed that show a more chaotic behavior than in the two-dimensional situation. Particles frequently jump up and down between two counter-rotating vortices. The generation of the vortices can be ascribed to a non-zero rotation of the net global force vector field, that is the sum of the ion drag force, the electric force, and the thermophoretic force in case of the experiments. Comparison of experimental data with simulations using a model potential may open a way to unravel the forces inside a cloud of dust particles.*

7.1   Introduction

Plasma crystal experiments performed under microgravity conditions often show a coherent rotation of parts of the cloud of dust particles immersed in the discharge, while other parts stand still and eventually form a crystalline region. The driving mechanism behind this coherent rotation can not easily be unravelled because the forces acting on the dust particles are modified due to the presence of the dust and because the charge on the dust particles may vary in the course of their trajectory. Previously [1], we have reported on a simulation of the motion of individual particles in a dust cloud, using the net global force resulting from the ion drag, the electric and thermophoretic force exerted by the discharge, while adding the short range particle-particle interaction by means of a screened Coulomb potential as well as friction with the background gas. This simulation, however, was done in a two-dimensional (2D) (r,z) geometry, not allowing the particles to move in the ϕ-direction and also the number of particles was limited. In this paper we present similar simulations, but for a prescribed harmonic net axial and radial force, in three dimensions and with more particles. This approach is similar to those used to study ionic crystals [2, 3]
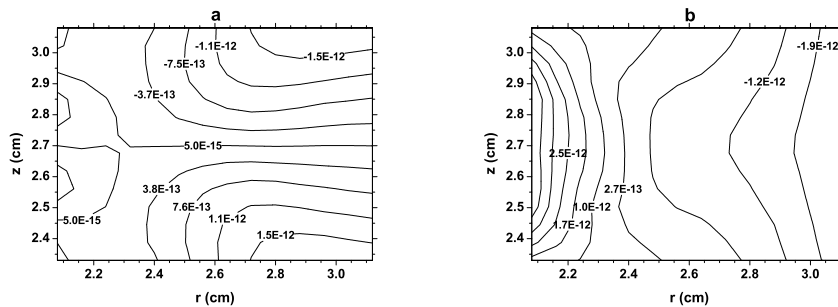
7.2   The forces included

Figure 7.1: The global net axial (a) and radial (b) force acting on a dust particle. Result from a 2D hydrodynamic simulation.

Figures 7.1a and 7.1b show the net force in the axial (a) and radial (b) direction acting on a dust particle according to one of the simulations with our 2D cylindrically symmetric hydrodynamic model for the Plasmakristall Experiment

(PKE) reactor under microgravity conditions [4, 5] for the region in r and z where the vortices appear. The force is the sum of the ion drag force (from the ions leaving the discharge), the electric force (from the net space charge distribution and the applied voltage), and the thermophoretic force (from the temperature gradient of the gas). The influence of the presence of the dust on the discharge is fully accounted for. Drawn in figures 7.1a and 7.1b are lines of constant force. Due to symmetry the axial force vanishes in the midplane of the reactor (z=2.7 cm) and, going up or down, the force tends to push the particles back to this plane in the outer regions and away from this plane in the central part of the discharge. The radial force changes direction from outward in the central part to inward in the outer part of the region considered. This behavior of the forces is responsible for the generation of a dustfree central void [5]. An important feature is that the lines of constant force are not straight, yielding a non-zero rotation of the net force vector field and thus the possibility that a particle gains energy in a periodic motion.

The complexity of this force and the fact that it is only known at a limited number of computational grid points prohibits a study of a dust particle cloud with a large number of particles in three dimensions. Therefore, we have turned to an analytical expression for the force that is easy to calculate at any particle position, while keeping the main features of the force in figures 7.1a and 7.1b. The force we have chosen is a harmonic force, $\boldsymbol{F}$, in both directions, but with the possibility that the axial position where the radial force vanishes becomes a function of the axial coordinate z:

$$\boldsymbol{F}_z = -\alpha_z m_p z \hat{e}_z, \tag{7.1}$$
$$\boldsymbol{F}_r = -\alpha_r m_p (r - r_0(z))\hat{e}_r \quad r_0(z) = r_{00} + \beta z^2,$$
$$\boldsymbol{F}_\phi = 0,$$

with m_p the mass of the particle. Thus, we can introduce a curvature of the lines with constant radial force by taking β different from zero and vary the force strength by means of the Hook constants α_z and α_r. r_{00} defines the point where the radial force vanishes in the plane of symmetry (z=0).

The particle-particle interaction is modelled according to the screened Coulomb potential, assuming a prescribed fixed charge, Q_p, screening distance, λ_{sc}, and a particle radius r_p that is much smaller than the screening length:

$$\boldsymbol{F}_{ij} = \frac{Q_p^2}{4\pi\epsilon_0 \|\boldsymbol{r}_i - \boldsymbol{r}_j\|^3}\Big(1 + \frac{\|\boldsymbol{r}_i - \boldsymbol{r}_j\|}{\lambda_{sc}}\Big) \exp\Big(-\frac{\|\boldsymbol{r}_i - \boldsymbol{r}_j\|}{\lambda_{sc}}\Big)(\boldsymbol{r}_i - \boldsymbol{r}_j). \tag{7.2}$$

This screened Coulomb interaction is usually observed in particle clouds in a discharge [6, 7]. The results of the simulations, however, will not change when an unscreened interaction is used. Friction with the background gas is accounted for

by the standard expression:

$$\boldsymbol{F}_f = -\alpha_f m_p \boldsymbol{v}_p, \tag{7.3}$$

where in reality the friction coefficient α_f will depend on the density of the background gas [8].

All this straightforward leads to the equation of motion for particle i:

$$m_p \frac{d\boldsymbol{v}_i}{dt} = \boldsymbol{F}(\boldsymbol{r}_i) + \sum_{j \neq i} \boldsymbol{F}_{ij} + \boldsymbol{F}_f(\boldsymbol{v}_i). \tag{7.4}$$

This equation is integrated in time with a leap-frog scheme, with a sufficiently small time step to avoid spurious heating. All particle-particle interactions are accounted for.

7.3   Results and Discussion
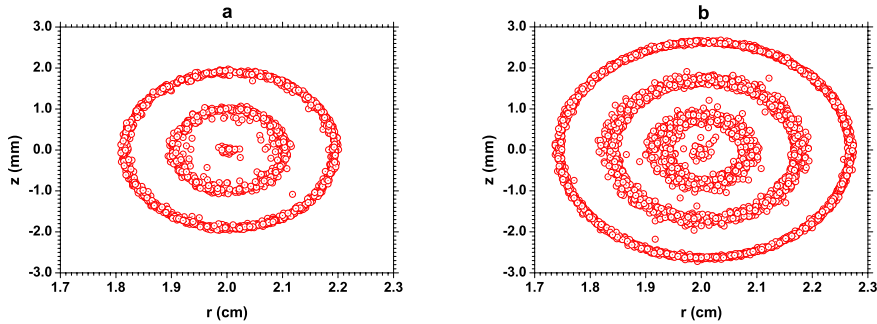
Figure 7.2: Projection of the position of 1800 (a) and 3600 (b) particles on the r-z plane for a rotation free force.

Figures 7.2a and 7.2b show the result of a simulation with 1800 (a) and 3600 (b) silicon (ρ=2200 kg m^{-3}) particles of radius 7.5 μm ($m_p = 3.9\ 10^{-12}$kg) with a charge of 30000 electrons, using a screening length of 2 mm in a rotation free force with $\alpha_z=\alpha_r=160$, $\alpha_f=1$, $\beta=0$, and r$_{00}$=0.02. The charge and screening length are larger than expected in reality, (typical values 15000 and 0.5 mm) to reduce the number of particles needed in the simulation. Plotted is the projection of the positions of the particles on the r-z plane. The position of the center is dictated by

the value of r_{00}, being slightly different from the situation depicted in figures 7.1a and 7.1b.

As expected the friction causes the particles to go to an equilibrium position determined by the balance of all forces, including the particle-particle interaction forces. When the amount of particles is low, they find enough space in the ϕ coordinate and first form a circle. When this is no longer possible due to the particle-particle interaction the particles fill concentric tori. A similar simulation for a harmonic potential centered at the origin would give concentric spheres [2]. In fact the results presented here resemble those of a particle cloud confined in a cylindrical potential [3] with periodic boundary conditions. There is a slight difference, however, because in our case the distribution is not symmetric around r_{00} because at smaller r values the particles have less volume available than at larger r values.
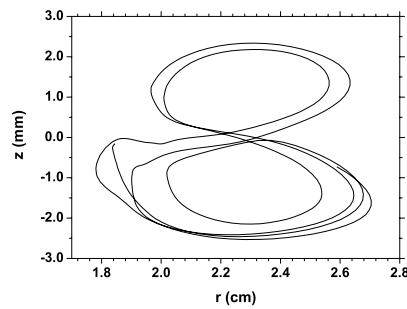

Figure 7.3: Projection of the position of one of the particles on the r-z plane for a force with rotation.
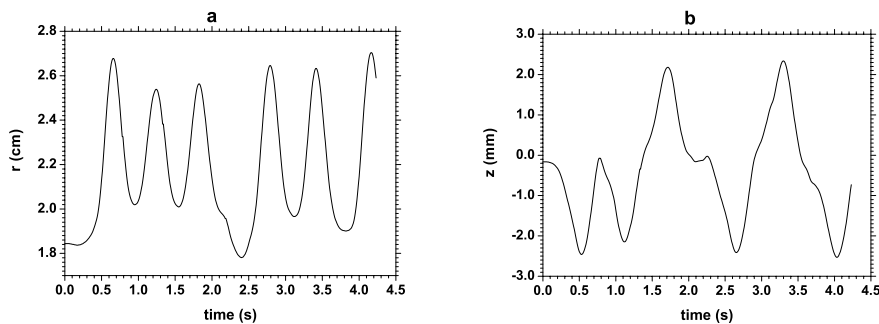

Figure 7.4: r (a) and z (b) position of the particle for a force with rotation.

When the curvature of the lines with constant radial force is introduced, by giving β a value of 10^3, the particles can pick up enough power during one round trip to compensate the losses due to friction (we took α_f=10 in this case) and keep rotating, because $\nabla \times \boldsymbol{F} \neq 0$. This resembles the actual situation depicted in figure 1b. We have followed the 3600 particles in time, starting with the static distribution of the rotation free case. An example of the motion of a particle is shown in figures 7.3, 7.4a, and 7.4b. All particles rotate clockwise in the upper half of the reactor and counterclockwise in the lower half, in agreement with the sign of $\nabla \times \boldsymbol{F}$. The motion is chaotic due to short range interactions with other particles, that also cause the jumping up and down.
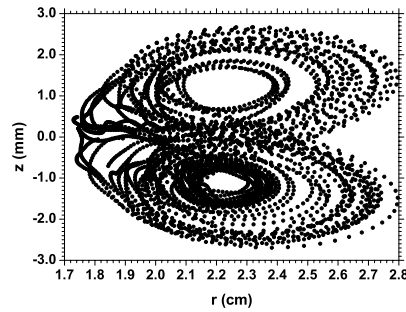
Figure 7.5: Projection of the position of 20 particles on the r-z plane for a force with rotation, showing the two emerging vortices.

Figure 7.5 shows the trajectories of twenty particles during the last two seconds of the simulation. The vortex structure is clearly visible. Note that the up down asymmetry is only due to the selection of the particles for which the data are plotted.

These results are similar to what we found in our previous 2D simulations. The axial and radial component of the force exerted by the discharge on the dust particles are shaped by the charge distribution and the potential distribution (electric force), the positive ion flux (ion drag) and the profile of the gas temperature (thermophoretic force) in such a way that $\nabla \times \boldsymbol{F} \neq 0$. Due to that no equilibrium exists in which the total force, including the inter particle forces, vanishes for all particles. The particles can keep rotating in a vortex-like configuration where the energy loss due to friction with the background gas is compensated by energy gain from the force exerted by the discharge. Since curvature is important in generating a force vector field with rotation, it is plausible that the generation of vortices is favorably triggered by the presence of sharp edges, such as probe tips [9].

Measuring the particle trajectories and comparing them with those obtained

from model forces opens a possibility to unravel the forces inside a dust cloud. This is not restricted to microgravity conditions, but would also apply to experiments where gravity plays a dominant role.

7.4   Conclusions

The behavior of particles in a dusty discharge under microgravity conditions can be analyzed by a molecular dynamics simulation of electrostatically interacting particles in a radially and axially harmonic force. Making the force vector field not rotation free results in the generation of vortex like structures, similar to those observed in experiments. The simulations show that the cloud of particles becomes a dissipative nonlinear system, driven by the applied (harmonic) force and showing chaotic behavior due to the short range particle-particle interaction. Comparing actual trajectories with those obtained from a simulation for a model force (not necessarily harmonic) opens a way to analyze the forces acting on particles in a dust cloud.

References

[1] M.R. Akdim et al., Phys. Rev. E., **67**, 056405 (2003).

[2] J.P. Schiffer, J.Phys. B: At. Mol. and Opt. Physics, **36**, 511 (2003).

[3] R.W. Hasse et al., Annals of Physics, **203**, 419 (1990).

[4] G. E. Morfill et al, Phys. Rev. Lett., **83**, 1598 (1999).

[5] M. R. Akdim et al., Phys. Rev. E., **65**, 015401(R) (2002).

[6] H. Totsuji et al., Phys. Rev. E **58**, 7831 (1998).

[7] M. Zuzic et al., Phys. Rev. Lett., **85**, 4064 (2000).

[8] D.B. Graves et al., Plasma Sources Sci., Technol. **3**, 433 (1994).

[9] D.A. Law et al., Phys. Rev. Lett., **80**, 4189 (1998).

8. Modelling of Two Different Size Dust Species in Plasmas under Microgravity

Abstract. *A self-consistent two dimensional hydrodynamic model for a dusty argon plasma has been developed to model more than one dust species. Results for situations where dust particles with two different diameter have been included are presented. The final steady state solution is achieved after three injection steps of the dust particles. At every injection phase dust particles of only one size are let in and the simulation is continued until the steady state solution is achieved. Results show that the differently sized dust particles form crystals at different positions. These dust clouds have an influence on each other by means of positive space charge layers created due to the argon ions which can not match the steep dust crystal boundaries. The screened Coulomb interaction between the two differently sized dust species is neglected. The electric potential, ion density, electron density and electron energy show significant changes after each injection phase, even at an amount of dust that is small compared to that studied during the microgravity experiments.*

8.1 Introduction

Dusty plasma experiments performed under microgravity conditions have shown interesting phenomena like voids surrounded by crystalline regions and rotating dust clouds which usually appear outside the crystalline regions. In their PKE (Plasmakristall-Experiment) chamber (Fig. 8.1) Morfill et al [1, 2] usually injected uniform size dust particles under microgravity. In an earlier paper [3], we used our dust-argon hydrodynamic model to study these plasma crystal experiments. Our modelling results showed good agreement with the experimental results. This offers a sound basis to use our model as a predictive tool.
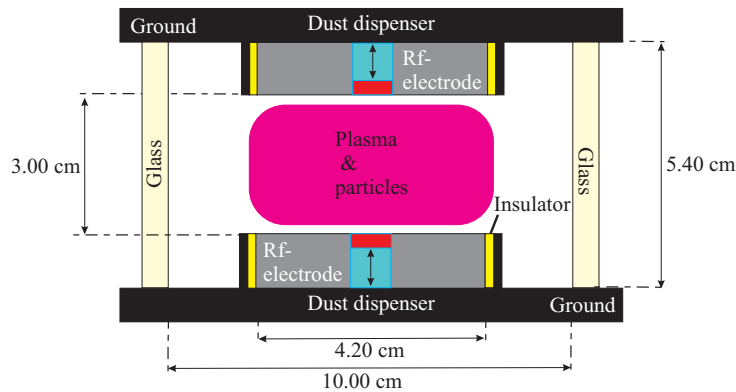
Figure 8.1: Schematic diagram of the PKE reactor.

Theoretical and numerical studies up to now have basically followed dust particles in the electric field and particle fluxes of an undisturbed discharge. An important aspect not covered is the influence of the dust particles on the discharge due to recombination on their surface [4, 5]. In discharges containing a considerable amount of dust, like in the PKE experiments, this approximation is not correct. For this a fully self-consistent model is needed. We have developed such a model for a dust containing radio frequency (RF) discharge in argon and used it to investigate the behavior of dust particles. The model contains a dust-argon fluid part which has been described in a previous article [3]. We have extended the single dust fluid model to a multi-dust fluid and studied the behavior of plasmas containing dust particles of different sizes. Our model accounts for the influence of the different dust fluids on the plasma and for their transport as fluids. This makes it a sophisticated tool for studying dusty discharges which contain dust particles of different sizes. In this paper we describe the multi-dust fluid model and present the results obtained from it.

8.2 Dusty plasma fluid model

In the fluid part of our two-dimensional model the particle balances, the electron energy balance and the Poisson equation are solved, including the transport of the dust fluids. Further details about the algorithms and the set of equations solved in the argon fluid part can be found in [6]. Drift-diffusion expressions are used for the fluxes and in the electron energy balance only Joule heating and energy in inelastic collisions are taken into account. Problems related to the huge difference in the timescale of the dust motion (1-10 s) and the RF period (70 ns) have been solved by a time-splitting technique and an iterative procedure. The charge on a dust particle is calculated from the Orbital-Motion-Limited (OML) probe theory. The (constant) charge on the dust particle is obtained from the balance of the local (OML) electron and ion currents collected by the particle. Recombination of ions and electrons on the dust particle surface is also taken into account. Ion-neutral collisions have been included to simulate a possible gas heating mechanism. For this we have used a simple approximation by assuming that the energy taken up from the electric field by the ions is dissipated locally in collisions with the gas[7]. The heating of the dust particle surface is also taken into account, more details about the used expressions can be found in the following articles [8, 9]. The dust particle (surface) temperature can affect the gas temperature which in turn could affect the other elementary processes in the discharge. The power released by the ions and the dust is the source in the temperature balance of the gas [9]. To obtain expressions for the dust particle fluxes, several forces acting on the dust particle are taken into account, e.g., the ion drag force, the neutral drag force, the electric force and the thermophoretic force.

A dust particle in a discharge is charged up to the floating potential relative to the surrounding plasma. This potential depends on the local ion and electron density and energy distribution. For a spherical dust particle with a radius r_d, the OML theory [10] predicts a positive ion and electron current:

$$I_i = 4\pi r_d^2 e n_i \sqrt{\frac{k_B T_i}{2\pi m_p}} \left(1 - \frac{e V_{fl}}{k_B T_i}\right), \tag{8.1}$$

$$I_e = 4\pi r_d^2 e n_e \sqrt{\frac{k_B T_e}{2\pi m_e}} \exp\left(\frac{e V_{fl}}{k_B T_e}\right). \tag{8.2}$$

Here, n_e is the electron density, n_i the positive ion density, e the elementary charge, k_B Boltzmann's constant, T_i the positive ion temperature , T_e the electron temperature, m_i the ion mass, m_e the electron mass, and V_{fl} the floating potential. All species are assumed to have a Maxwellian energy distribution.

When the ions enter the plasma sheaths near the electrodes, they get a directed velocity $\boldsymbol{v}_i$ due to the electric field. Therefore, we have replaced $k_B T_i$ in the

expression for the ion current by the mean energy E_i, which is:

$$E_i = \frac{4 k_B T_{gas}}{\pi} + \frac{1}{2} m_i v_i^2.$$
(8.3)

Equation 8.3 is obtained by using the mean speed expression of Barnes et al [11] given by:

$$v_s = \left(\frac{8 k_B T_{gas}}{\pi m_i} + v_i^2 \right)^2.$$
(8.4)

By calculating $\frac{1}{2} m_i v_s^2$, equation 8.3 is obtained. The directed velocity v_i is calculated by solving the drift-diffusion equation for the ions.

In the model the charge $Q_d = 4\pi\epsilon_0 r_d V_{fl}$ on the dust is calculated by equating these currents.

The floating potential of the dust is assumed to be constant during an RF cycle. This assumption is justified by the fact that the currents toward the dust surface are too small to change the charge significantly during an RF cycle.

When a dust particle becomes negatively charged, it will attract positive ions, these will recombine with an electron that has to be replaced again by an electron from the discharge to maintain the floating potential. As a result the equilibrium fluxes of positive ions and electrons arriving at the dust surface will recombine and the released energy is used to heat up the dust particle surface [8, 9]. The electron flux (Eq.8.2) results in a recombination rate:

$$R = 4\pi r_d^2 n_d n_e \sqrt{\frac{k_B T_e}{2\pi m_e}} \exp\left(\frac{eV_{fl}}{k_B T_e}\right)$$
(8.5)

In a plasma dust particles undergo a wide variety of forces. Assuming that a dust particle is a perfect sphere the gravitational force can be written as:

$$\boldsymbol{F}_G = \frac{4}{3}\pi r_d^3 \rho_d \boldsymbol{g},$$
(8.6)

where r_d is the dust particle radius, ρ_d is the mass density and $\boldsymbol{g}$ is the gravitational acceleration. For the often used melamine-formaldehyde dust particle ρ_d is approximately $1.51 \cdot 10^3 \ kg/m^3$.

When a dust particle gains a certain velocity relative to the neutral gas, it will experience a drag force due to momentum transfer from/to the gas. This neutral drag force has been discussed in detail by Graves et al [12]. It can be approximated by the following equation:

$$\boldsymbol{F}_{ND} = -\frac{4}{3}\pi r_d^2 n_n \boldsymbol{v}_d v_{th} m_n,$$
(8.7)

where n_n is the density of the neutral with mass m_n, $\boldsymbol{v}_d$ the drift velocity of the dust particle and v_{th} the average thermal velocity of the gas.

Because advection of the neutral gas is not included in the model, this force will only be present as a damping force on the velocity of the dust particles. The assumption is made, that this damping force will be in equilibrium with the sum of all the other forces acting on the dust particle.

Another force caused by momentum transfer is the ion drag. This force results from the positive ion current that is driven by the electric field. It consists of two components. The collection force represents the momentum transfer of all the ions that are collected by the dust particle and is given by:

$$\boldsymbol{F}_I^c = \pi b_c^2 n_i v_s m_i \boldsymbol{v}_i, \tag{8.8}$$

where v_s the mean speed of the ions, $\boldsymbol{v}_i$ the ion drift velocity and b_c the collection impact parameter.

The second component is the orbit force given by:

$$\boldsymbol{F}_I^o = 4\pi b_{\pi/2}^2 \Gamma n_i v_s m_i \boldsymbol{v}_i, \tag{8.9}$$

with $b_{\pi/2}$ the impact parameter that corresponds to a deflection angle $\pi/2$ and Γ the Coulomb logarithm.

$$\Gamma = \frac{1}{2} \ln \left(\frac{\lambda_L^2 + b_{\pi/2}^2}{b_c^2 + b_{\pi/2}^2} \right), \tag{8.10}$$

$\lambda_L = ((1/\lambda_e)^2 + (1/\lambda_i)^2)^{-1/2}$ is the linearized Debye length, which is a combination of the electron Debye length, λ_e, and the ion Debye length, λ_i. The ion drag is discussed in more detail by Barnes et al [11].

Due to their charge, dust particles will experience an electric force. Daugherty et al [13] derived the following expression:

$$\boldsymbol{F}_E = Q_d \boldsymbol{E} \underbrace{\left(1 + \frac{\kappa r_d}{3(1 + \kappa r_d)} \right)}_{\approx 1}, \tag{8.11}$$

where Q_d is the charge on the dust particle, $\boldsymbol{E}$ is the electric field and $\kappa = 1/\lambda_L$. In a discharge the dust particle radius is much smaller than the linearized Debye length, therefore the term between the bracket is approximately 1 and the electric force is given by:

$$\boldsymbol{F}_E = Q_d \boldsymbol{E}. \tag{8.12}$$

This expression holds for situations where the dust particles are not shielded from the plasma by positive ions trapped in orbitals around the dust particle [14]. In that case the particle will behave as some kind of dipole.

When a temperature gradient is present in a discharge, for instance due to cooling or heating of the electrodes a third force driven by momentum transfer will occur. This force is called the thermophoretic force. Atoms impinging from the hot side have more momentum than their companions of the cold side, this can result in a force pointing in the direction $-\boldsymbol{\nabla} T_{gas}$.

For large Knudsen numbers Talbot et al [15] derived the following expression:

$$\boldsymbol{F}_T = -\frac{32}{15}\frac{r_d^2}{v_{th}}\left(1 + \frac{5\pi}{32}(1-\alpha)\right)\kappa_T\boldsymbol{\nabla}T_{gas}, \tag{8.13}$$

$v_{th} = [8k_BT_{gas}/(\pi m)]^{1/2}$ is the average thermal velocity of the gas. κ_T is the translation part of the thermal conductivity. α, the thermal accommodation coefficient of the gas is taken equal to 1.

For a stationary solution the five forces calculated in our model, the neutral drag, the electric force, gravitational force, thermophoretic force and the ion drag, are in equilibrium. With the introduction of a momentum loss frequency and a mobility and diffusion coefficient for the dust particles given by:

$$\nu_{md} = \sqrt{2}\frac{p_{tot}}{k_BT_{gas}}\pi r_d^2\sqrt{\frac{8k_BT_{gas}}{\pi m_d}}, \tag{8.14}$$

where p_{tot} is the static pressure and m_d the dust particle's mass.

$$\mu_d = \frac{Q_d}{m_d\nu_{md}}, \tag{8.15}$$

$$D_d = \mu_d\frac{k_BT_{gas}}{Q_d}, \tag{8.16}$$

it is possible to define a "drift-diffusion" expression for the flux

$$\begin{aligned}\boldsymbol{\Gamma}_d &= -\mu_d n_d\boldsymbol{E}^{eff} - D_d\boldsymbol{\nabla}n_d - \frac{n_d}{\nu_{md}}\boldsymbol{g}\\ &+ \frac{n_d m_i v_s}{m_d\nu_{md}}\left(4\pi b_{\pi/2}^2\Gamma + \pi b_c^2\right)\boldsymbol{\Gamma}_i\\ &- \frac{32}{15}\frac{n_d r_d^2}{m_d\nu_{md}v_{th}}\kappa_T\boldsymbol{\nabla}T_{gas},\end{aligned} \tag{8.17}$$

of the dust particles and treat them with the same numerical procedures as the other charged particles in the fluid model, hence that in this case we neglect the inertia of the dust particles.

Because of the low mobility of the dust particles the effective field $\boldsymbol{E}^{eff}$ can be approximated by the time averaged rf-field. With the use of the Einstein relation, the diffusion can be defined as a function of the mobility (Eq. 8.16).

The drift velocity and the diffusion coefficient of the dust fluids are much smaller than those of the ions and electrons. Therefore it would rather take a lot of computational effort to achieve a steady state solution for the dust when it is followed during an RF cycle. We therefore have developed a method to speed up the convergence toward the steady state solution by introducing a different calculation cycle with a different time step for the dust. Our model thus consists of two calculation cycles. In the first one, the transport equations of the ions, electrons and the Poisson equation are solved during an RF cycle, during the RF cycle the dust does not move. After a number of RF cycles, the transport equation of the dust is solved with a greater time step, using the time averaged electric field, electron and positive ion fluxes. During the second calculation, space charge regions are created, because the electron and positive ion densities are kept constant. These space charge regions will give instabilities in the Poisson equation. To solve this problem, we correct the artificial space charge by adapting the positive ion density distributions prior to the next series of RF cycles. With this method the required speed-up is established. Both for the plasma species and for the dust fluids the transport equations are solved using the Sharfetter-Gummel exponential scheme [6].

The internal pressure of the crystal due to the inter-particle interaction has been included by means of a density dependence of the diffusion coefficient for the dust. The diffusion coefficient of the dust is increased by a factor $\exp(N_d/N_c)$ where the reference density N_c is chosen such that the dust density saturates at a value N_{crys}. This models the incompressibility of the crystal. Actually, the (yet unknown) equation of state of the dust crystal should be used to account for the internal pressure. Since we were not primarily interested in the precise structure of the crystalline regions, we have chosen for the simple and computationally robust exponential increase of D_d. Plasma crystal experiments [1] have shown an inter-particle distance of about 300 μm for a dust particle with diameter of 15 μm. This results in an average "crystal" density N_{crys} of $3.7 \cdot 10^{10}$ m^{-3}. For the smaller dust particle we used a reference density that is a factor 200 higher than for the bigger dust particles.

8.3   Results and discussion

We have modelled the PKE chamber used by Morfill et al [1]. The reactor is cylindrically symmetric. The simulation starts with zero dust density profiles. During the simulation the dust is injected from both electrodes by adding source terms in the dust particle balances for the first grid points below/above the electrodes, the injection rate is about 750.000 particles per second. Both electrodes are driven by a radio-frequency power source at a frequency of 13.56 MHz. The peak-to-peak
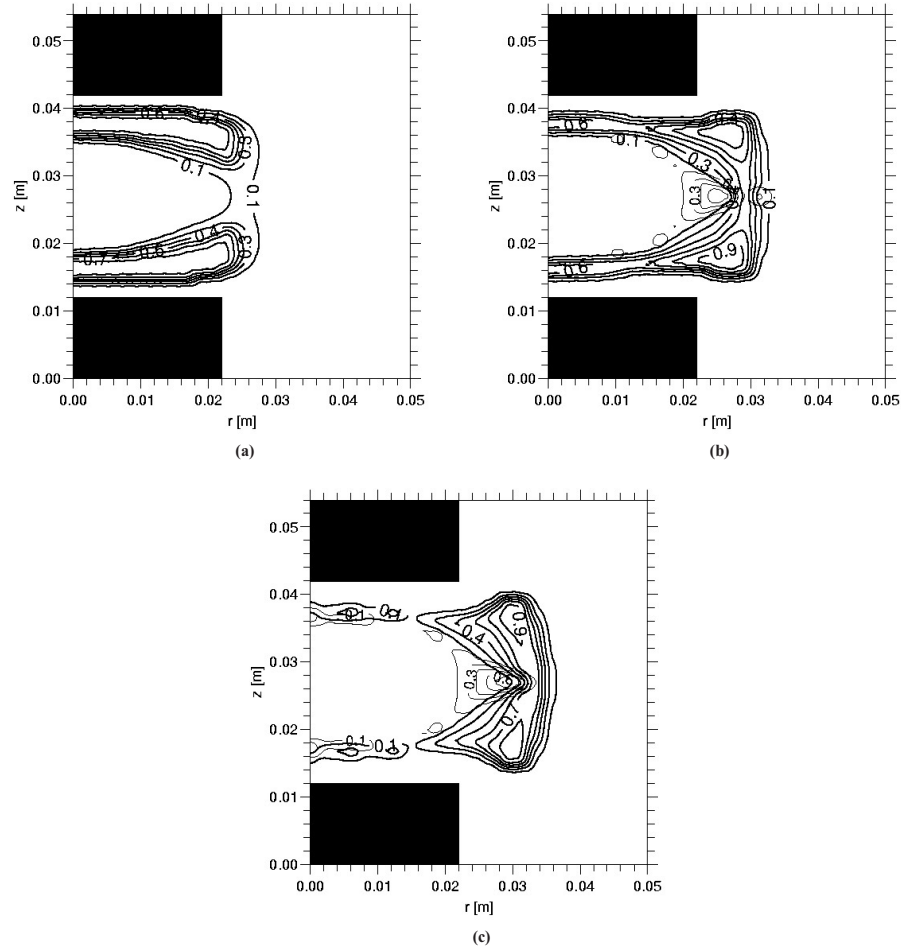
Figure 8.2: (a) Dust density profile after injection step ONE, normalized with a factor of $1.49 \cdot 10^{10}$ in m^{-3}.

(b) Dust density profiles after injection step TWO , normalized with a factor of $9.70 \cdot 10^{10}$ in m^{-3} for the 2 μm sized dust particles and $1.29 \cdot 10^{10}$ in m^{-3} for the 15 μm sized dust particles .

(c) Dust density profiles after injection step THREE, normalized with a factor of $1.44 \cdot 10^{11}$ in m^{-3} for the 2 μm sized dust particles and $1.12 \cdot 10^{10}$ in m^{-3} for the 15 μm sized dust particles.

The thick contours represent the dust density profile of the 15 *μm sized dust particles and the thin contours represent the dust density profile of the* 2 *μm sized dust particles.*

voltage is 70 volts, this results in a power dissipation of about 0.04 W. The pressure is 40 Pa. The equation of motion for the dust fluids (Eq. 8.17) is solved for the time-averaged electric field, plasma densities and fluxes.

First the simulation is started for a dust-free discharge and is run until it reaches steady state. After that, the total amount of dust is injected in three steps. These steps are as follows: In step ONE, the injection of dust particles that have a diameter of 15 μm is started until an amount of 350.000 particles is reached, after that the simulation is run to achieve a steady state solution. In step TWO, 350.000 dust particles of 2 μm diameter are injected to the above steady state solution. This gives a mixture of small and big dust particles [16, 17]. This simulation is also run to the steady state. Eventually, in step THREE, again 350.000 dust particles of 2 μm are injected. This results in a total amount of 1.05 million dust particles, after that the sources are switched off and the simulation is continued until it reaches the final steady state.
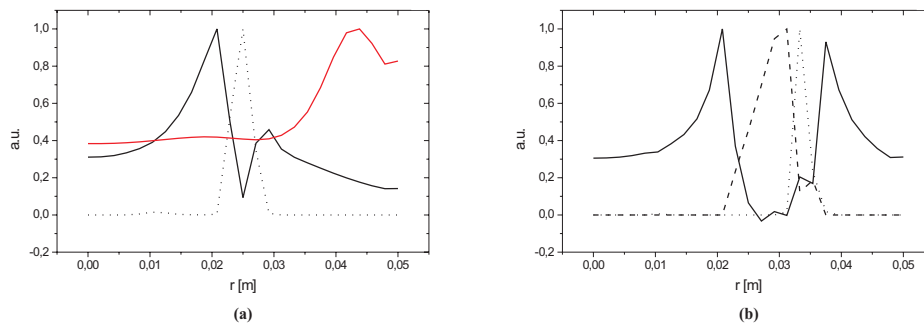

Figure 8.3: (a) Dust density profile and the net space charge profile after injection step ONE at the axial symmetry axis. The thick curve represents the space charge, normalized with a factor of $3.72 \cdot 10^{13}$ in elementary charges m^{-3}. The dotted curve represents the dust density profile of the 15 μm sized dust particles, normalized with a factor of $2.35 \cdot 10^9$ in m^{-3}. The gray solid curve represents the net space charge for a dust-free discharge at the axial symmetry axis, normalized with a factor of $1.84 \cdot 10^{13}$ in elementary charges m^{-3}.
(b) Dust density profiles and the net space charge profile after injection step THREE at the axial symmetry axis. The thick curve represents the net space charge, normalized with a factor of $2.46 \cdot 10^{13}$ in elementary charges m^{-3}. Dashed curve represents the dust density profile of the 2 μm sized dust particles, normalized with a factor of $1.44 \cdot 10^{11}$ in m^{-3}. The dotted curve represents the dust density profile of the 15 μm sized dust particles, normalized with a factor of $1.04 \cdot 10^{10}$ in m^{-3}.

Figures 8.2a, 8.2b and 8.2c show the dust densities of both dust species (big and small) after each injection step. After injection step ONE, the larger dust particles arrange themselves in a crystal around a central void [1]. The crystal is

formed due to the balance of forces acting on the dust particles. When the smaller dust particles are injected in step TWO, the crystal consisting of the 15 μm dust particles moves radially outwards towards the reactor wall. Also the crystalline regions between the electrodes become narrower due to an increase of the ion drag force and electric force acting on the bigger dust particles. The smaller dust particles are pushing the bigger particles to move radially towards the reactor wall. After step THREE, this effect becomes more obvious. The shape of the crystal of the bigger particles seems to be dictated by the smaller dust particles cloud and the dust crystal is pushed more in the radial direction towards the wall. This
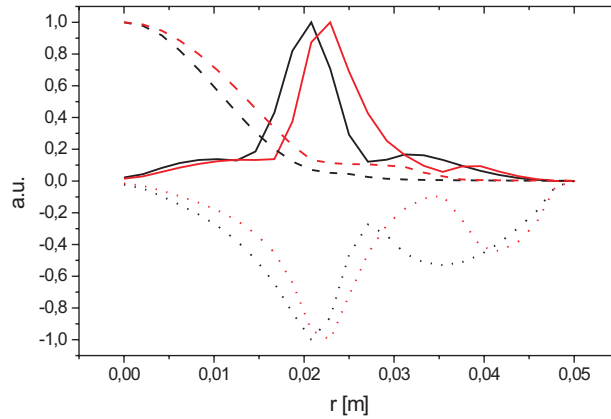

Figure 8.4: Ion drag force, electric force and ion density profiles after injection step ONE and THREE at the axial symmetry axis. Black solid curve represents the ion drag force acting on the 15 μm dust particles after step ONE, normalized with a factor of $8.07 \cdot 10^{-12}$ in N. The gray solid curve represent the ion drag force acting on the 15 μm dust particles after step THREE, normalized with a factor of $8.73 \cdot 10^{-12}$ in N. The black dotted curve represents the electric force acting on the 15 μm dust particles after step ONE, normalized with a factor of $5.99 \cdot 10^{-12}$ in N. The gray dotted curve represent the electric force acting on the 15 μm dust particles after step THREE, normalized with a factor of $5.61 \cdot 10^{-12}$ in N. The black dashed curve represents the ion density after step ONE, normalized with a factor $2.89 \cdot 10^{15}$ in m^{-3}. The gray dashed profile represent the ion density after step THREE, normalized with a factor of $3.50 \cdot 10^{15}$ in m^{-3}.

movement can be explained by the presence of the smaller dust particles and the space charge layers which are formed by the presence of the dust crystals. Figures 8.3a and 8.3b show the space charge and dust density profiles along the axial symmetry axis (z=0.027 m). It can be seen from figure 8.3b that between the two dust density peaks, a space charge layer is created. The line integrated number

of dust particles of the 2 μm size along the axial symmetry axis is about a factor 40 larger than for the 15 μm size particles. The difference in the charge on the dust particles (Fig. 8.5a and Fig. 8.5b) however is approximately a factor of 6. To maintain quasi-neutrality the charge of the 2 μm dust particles must be compensated by at least a factor of 6 more ions. The increase in ion density is shown in figure 8.4 (Note the different scaling.). The space charge layer accelerates the ions towards the crystal of the bigger particles, this fact and the increase in ion density enhances the ion drag force acting on the larger dust particles by about 10 percent (Fig. 8.4). This enhancement of the ion drag force and a decrease in electric force (Fig. 8.4) acting on the crystal of bigger particles results in moving the dust crystal radially towards the reactor wall.
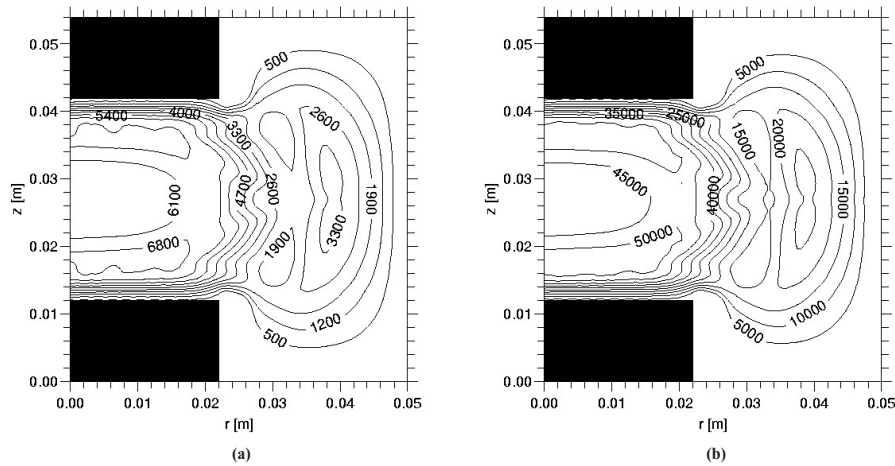

Figure 8.5: (a) Number of electrons on a dust particle with diameter of 2 μm after injection step THREE.

(b) Number of electrons on a dust particle with diameter of 15 μm after injection step THREE.

Figures 8.6a, 8.6b and 8.6c show the time-averaged potential distribution V(r,z) for three different situations. In the three cases the potential has its maximum in the bulk of the plasma between the electrodes. Comparing the potential distributions, a significant change in the plasma potential can be observed. The plasma potential decreases in the center of the discharge after injection step ONE (Fig. 8.6b). Also a decrease of the axial electric field can be observed. After step THREE, the electric potential increases and its maximum becomes almost equal to that for the dust-free situation. From figures 8.6b and 8.6c, it can be seen that the radial electric field has increased after step THREE. This shows that both the dust fluids have their influence on the plasma potential.
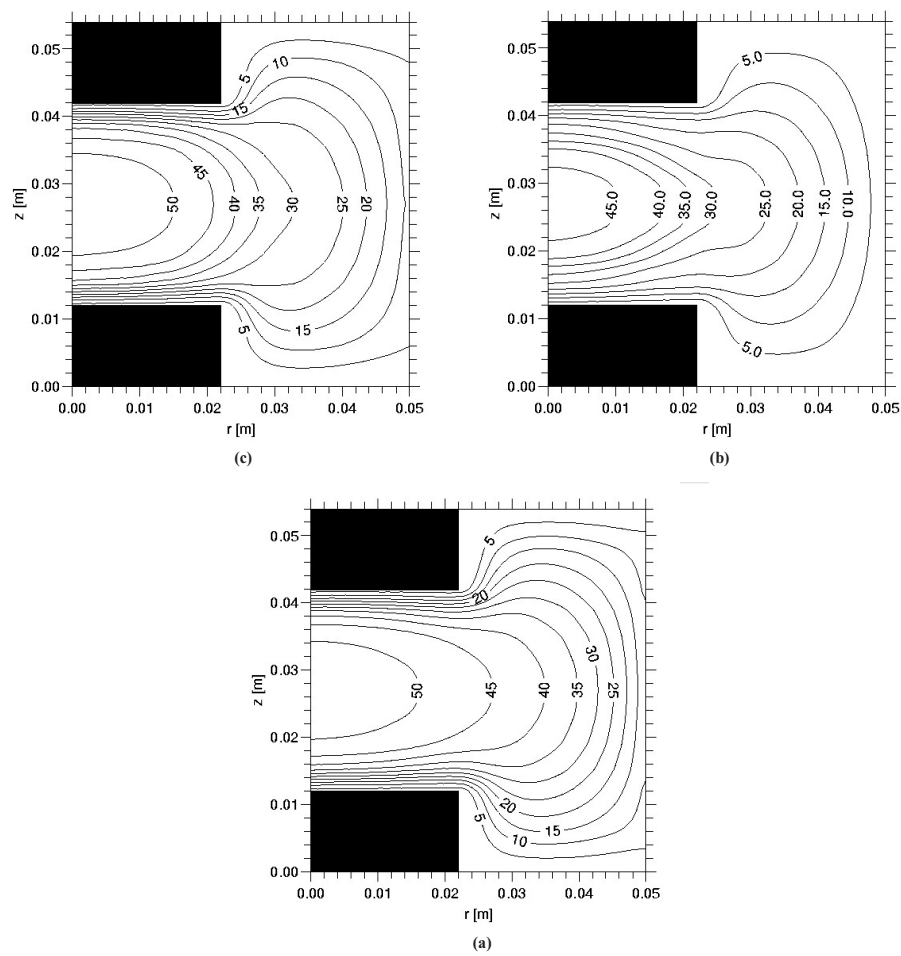
Figure 8.6: (a) Time-averaged electric potential in volts in dust-free discharge .
(b) Time-averaged electric potential after in volts injection step ONE.
(c) Time-averaged electric potential in volts after injection step THREE.

Figure 8.7: (a) Time-averaged electron density after injection step ONE, normalized with a factor of $2.89 \cdot 10^{15}$ in m^{-3}.
(b) Time-averaged electron density after injection step THREE, normalized with a factor of $3.50 \cdot 10^{15}$ in m^{-3}.

Figure 8.8: (a) Time-averaged ion density after injection step ONE, normalized with a factor of $2.89 \cdot 10^{15}$ in m^{-3}.
(b) Time-averaged ion density after injection step THREE, normalized with a factor of $3.50 \cdot 10^{15}$ in m^{-3}.

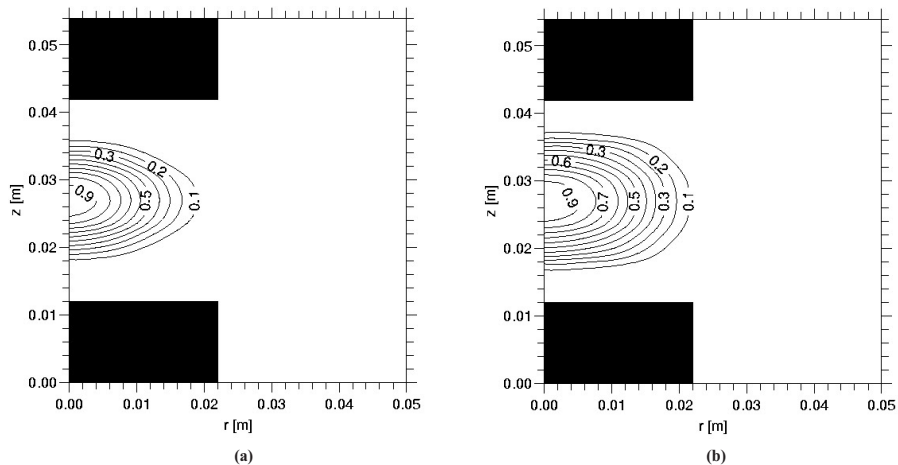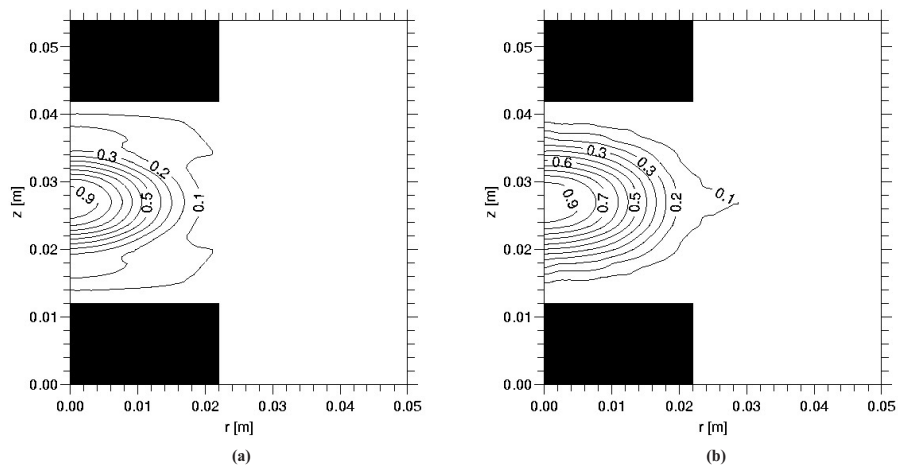The influence of the dust fluids on the plasma parameters can also be observed from figures 8.7a and 8.7b. These figures show the time-averaged electron density profiles after injection step ONE and THREE. After step ONE the electron density decreases. The plasma is confined into the void formed by the larger dust particles (Fig. 8.2a). This drop in electron density is caused by the charging of the
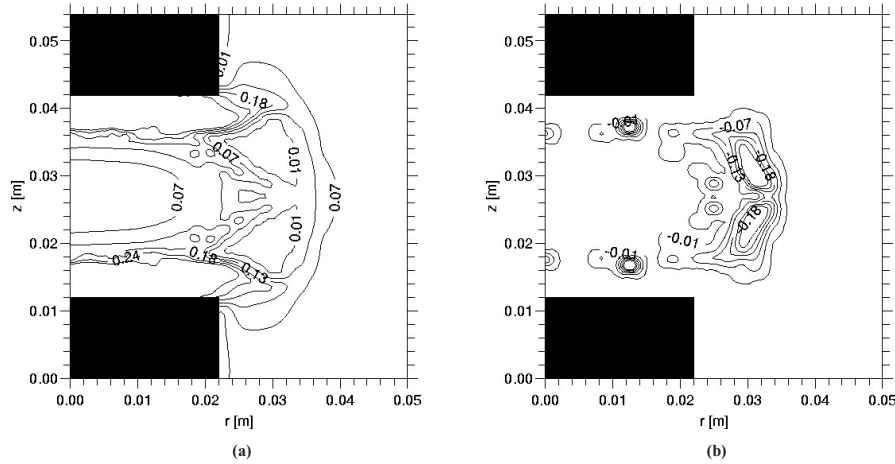

Figure 8.9: (a) Time-averaged positive space charge after injection step THREE, normalized with a factor of $2.12 \cdot 10^{14}$ in elementary charges m^{-3}.
(b) Time-averaged negative space charge after injection step THREE, normalized with a factor of $2.09 \cdot 10^{13}$ in elementary charges m^{-3}.

dust particles and recombination of ions and electrons on the dust surface. After step THREE the electron density increases, which seems quite strange because the amount of dust has increased. The explanation for this phenomenon can be found from figure 8.2b. After injection step THREE the dust crystal formed by the 15 μm particles is pushed radially towards the reactor wall, as a result the dust crystal between the electrodes becomes thinner and moves to a position where there is less plasma. This results in less recombination of ions and electrons on the dust particle surfaces. The same effect is observed for the ion density, after step THREE (Fig. 8.8b) the ion density shows a significant increase compared to the ion density after step ONE (Fig. 8.8a). The ion density profiles have peculiar shapes. After injection step ONE the ions around the midplane in between the electrodes are pushed towards the center. After step THREE (Fig. 8.8b) the opposite effect can be observed. These outer contour lines in the ion density profiles can be explained by examining figures 8.2, 8.3 and 8.9 . These figures show the space charge regions in the plasma and the dust density profiles. After injection step ONE, a dust crystal is formed by the bigger particles. To maintain quasi-neutrality the ions tend to compensate the charge carried by the dust particles this

results in an ion density profile which has the peculiar shape as in figure 8.8a. The steep boundaries of the dust crystal give rise to creation of space charge layers [9] (Fig. 8.9). After injection step THREE, the space charge layer appears (Fig. 8.3b). This space charge layer accelerates the ions in the direction of the reactor wall. This acceleration can be observed in the outer contour line of figure 8.8b.
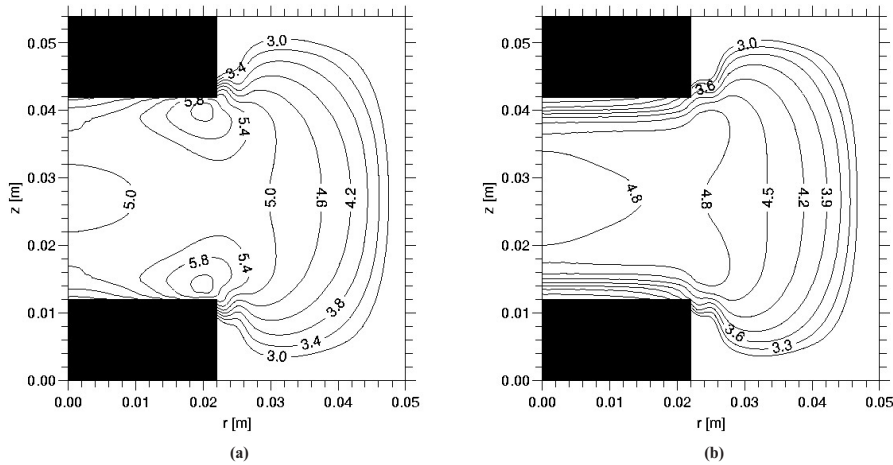

Figure 8.10: (a) Time-averaged electron energy in eV after injection step ONE.
              (b) Time-averaged electron energy in eV after injection step THREE.

Figures 8.10a and 8.10b show the time-averaged electron energy. A Comparison of the figures shows that the electron energy after injection step THREE has decreased. This effect can be explained by an combination of the increase of the electron density (Fig. 8.7a and fig. 8.7b) after injection step THREE and the constraint of constant applied driving voltage, more electrons means less energy per electron. Therefore the time-averaged electron energy decreases.

8.4   Conclusions

The numerical simulation results show that self-consistent modelling of the plasma parameters in a dusty argon discharge is important. We have shown that injection of dust particles with two different diameter results in the formation of dust clouds at different positions, with the cloud of smaller dust particles inside the central void of the crystal of the bigger particles. Neglecting the screened Coulomb force between two dust clouds, these clouds can still interact with each other through the formation of space charge layers, which are formed by the steep boundaries of the dust crystals.

Acknowledgments

References

[1] G. E. Morfill et al, Phys. Rev. Lett., **83**, 1598 (1999).

[2] H. Thomas et al, Phys. Rev. Lett., **73**, 652 (1994).

[3] M. R. Akdim et al, Phys. Rev. E., **65**, 015401(R) (2002).

[4] T. Nitter, Plasma Sources Sci. Technol., **5**, 93 (1996).

[5] Ph. Belenguer et al, Phys. Rev. A., **46**, 7923 (1992).

[6] J. D. P. Passchier et al, J. Appl. Phys., **73**, 1073 (1993).

[7] I. Revel et al, J. Appl., Phys., **88**, 2234 (2000).

[8] G. H. P. M. Swinkels et al, J. Appl. Phys., **88**, 1747 (2000).

[9] M. R. Akdim et al, Phys. Rev. E.,**67**, 056405 (2003).

[10] J. E. Allen et al, J. Plasma. Phys., **63**, 299 (2000).

[11] M. S. Barnes et al, Phys. Rev. Lett., **68**, 313 (1992).

[12] D. B. Graves et al, Plasma Sources Sci. Technol., **3**, 433 (1994).

[13] J. E. Daugherty et al, J. Appl.Phys., **73**, 1617 (1993).

[14] M. Lampe et al, Phys. Rev. Lett., **86**, 5278 (2001).

[15] L. Talbot et al, J. Fluid Mech., **101**, 737 (1980).

[16] L. Boufendi, Private communication.

[17] H. Thomas, Private communication.

9. Modelling of Dust Voids in Electronegative Discharges under Microgravity

Abstract.*Traces of molecular gases, like oxygen influence the size of the void observed microgravity experiments carried out at the International Space Station. These molecular gases produce negative ions via (dissociative) attachment. A considerable amount of negative ions changes the plasma properties, especially the potential distribution, and therefore the forces acting on a dust particle. We have investigated these phenomena by means of a 2D fluid model in which all the plasma parameters are calculated self-consistently. In this model we have included the possibility that negative ions are formed. By changing the attachment rate, we can control the electronegativity of the gas. Heating of the dust particle material by the recombining ions and electrons and subsequent heating of the gas is taken into account, as well as the heating of the background gas by ion-neutral collisions. As in electropositive discharges the resulting thermophoretic force, however, can be neglected at low peak-to-peak voltages compared to the other forces. Results from the fluid model show that indeed the presence of negative ions influences the evolution of the void and its final size. We will show how the relevant forces change with variation of the applied voltage in electropositive and electronegative discharges.*

Authors :
  M.R. Akdim and W.J. Goedheer

9.1 Introduction

Plasma crystal experiments performed under microgravity conditions have shown that dust particles usually arrange in a crystal like structure surrounding a stable void [1, 2]. The experiments are usually carried out in electropositive noble gasses as argon and krypton at static pressures around 40 Pa. Up till now the effects of electronegative gasses like oxygen, have not been studied in these experiments due to safety precautions on the International Space Station (ISS). We have developed a 2D argon-dust fluid model, which we have used previously to explain the appearance of the void in an argon discharge [3]. In this model we can also include the effect of attachment, producing negative ions, thus simulating a dust containing radio frequency (RF) discharge in the presence of an electronegative gas. The model contains a dust fluid part which has been described in [4]. It accounts for the presence of a large amount of dust, changing the plasma parameters. We have extended the model with an equation of state that has been described in [5], leading to a more sophisticated description of the crystalline regions. In this paper we describe the effect of negative ion formation on a discharge containing a significant amount of dust, by comparing the results for electropositive and electronegative discharges at different RF voltages.

9.2 Description of the model

9.2.1 Fluid model for the plasma species

To model the effect of an electronegative gas on a discharge containing a considerable amount of dust, we have used an extension of a previously described two-dimensional model [6], of which only the most important aspects will be summarized here. It consists of particle balance equations for the different species (electrons, ions and meta-stables) and an energy balance equation for the electrons. Ion-neutral collisions have been included to simulate a possible gas heating mechanism. For this we have used a simple approximation by assuming that the energy taken up from the electric field by the ions is dissipated locally in collisions with the gas [7]. This gas heating mechanism has been refined by taking the heating of the dust particle surface into account [4, 8]. The formation of negative ions is included to model the effect of negative ions on the formation of the void in a RF discharge. A discharge has been simulated in which an electronegative gas has been mimicked by adding attachment as a new process. Only the following reactions are considered:

$$A + e \rightarrow A^+ + 2e,$$
$$A + e \rightarrow A^-,$$

$$A^- + A \rightarrow A + A + e,$$
$$A^- + A^+ \rightarrow A + A,$$
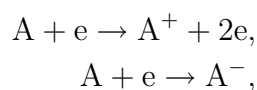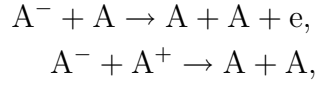
for the first process, ionization, the rate is calculated as a function of average electron energy by solving the two-term Boltzmann equation for the electron energy distribution for an argon plasma. For the second process, attachment by electrons, we have taken the attachment coefficient for a pure CF_4-plasma as given by the following expression [9]:

$$k_{att}(\epsilon) = \begin{cases} 0, & \text{if} \quad \epsilon < 5.3; \\ 2.0 \cdot 10^{-17} \cdot (\epsilon - 5.3)/(0.033 + \epsilon - 5.3), & \text{if} \quad \epsilon \geq 5.3. \end{cases} \tag{9.1}$$

So the attachment coefficient has a threshold energy of 5.3 eV and above this threshold it attains in a few tenths of eV a plateau value of $2.0 \cdot 10^{-17} m^3 s^{-1}$. The third reaction is detachment of the negative ions, for this we have taken a rate coefficient of $1.0 \cdot 10^{-18} m^3 s^{-1}$. The last reaction takes the recombination of positive and negative ions into account. We have chosen a recombination coefficient of $5.0 \cdot 10^{-13} m^3 s^{-1}$. Changing the above mentioned coefficients offers a way to get more or less positive or negative ions in the discharge simulation. This mimics the the degree of electronegativity of the gas.

In the model the density balance for each species j is:

$$\frac{dn_j}{dt} + \boldsymbol{\nabla} \cdot \boldsymbol{\Gamma}_j = S_j, \tag{9.2}$$

where n_j is the particle's density, $\boldsymbol{\Gamma}_j$ the flux of the species, and S_j the local sink or source.

The momentum balance is replaced by the drift-diffusion approximation for the particle fluxes,

$$\boldsymbol{\Gamma}_j = \mu_j n_j \boldsymbol{E} - D_j \boldsymbol{\nabla} n_j, \tag{9.3}$$

with μ_j and D_j the mobility and diffusion coefficient of species j. $\boldsymbol{E}$ is the electric field.

For ions the characteristic momentum transfer frequency is only a few megahertz (MHz). To use the drift-diffusion approximation for positive and negative ions for RF frequencies higher than a few MHz the electric field in equation 9.3 is replaced by an effective electric field. Using this effective electric field $\boldsymbol{E}_{eff}$, inertia effects are taken into account. An expression for the effective electric field is obtained by neglecting the diffusive transport and inserting the expression $\boldsymbol{\Gamma}_i = \mu_i n_i \boldsymbol{E}_{eff}$ in the simplified momentum balance

$$\frac{d\boldsymbol{\Gamma}_i}{dt} = \frac{en_i}{m_i} \boldsymbol{E} - \nu_{m,i} \boldsymbol{\Gamma}_i, \tag{9.4}$$

where $\nu_{m,i}$ is the momentum transfer frequency of the ions given by

$$\nu_{m,i} = \frac{e}{\mu_i m_i}. \tag{9.5}$$

Here e is the elementary charge and m_i the mass of the ions. The effective electric field is then obtained by solving:

$$\frac{d\boldsymbol{E}_{eff,i}}{dt} = \nu_{m,i}\left(\boldsymbol{E} - \boldsymbol{E}_{eff,i}\right) \tag{9.6}$$

The same effective field is used for the positive and negative ions. The electric field $\boldsymbol{E}$ and potential V are calculated using the Poisson equation:

$$\Delta V = -\frac{e}{\epsilon_0}\left(n_i - n_e - n_n - Q_d n_d\right), \tag{9.7}$$

$$\boldsymbol{E} = -\boldsymbol{\nabla}V, \tag{9.8}$$

where ϵ_0 is the permittivity of vacuum, n_e the electron density, n_i the positive ion density, n_n the negative ion density Q_d the number of electrons on a dust particle and n_d the dust density.

The electron energy density $w_e = n_e \epsilon$ (i.e. the product of the electron density and average electron energy ϵ) is calculated self-consistently from the second moment of the Boltzmann equation:

$$\frac{dw_e}{dt} + \boldsymbol{\nabla} \cdot \boldsymbol{\Gamma}_w = -e\boldsymbol{\Gamma}_e \cdot \boldsymbol{E} + S_w, \tag{9.9}$$

with $\boldsymbol{\Gamma}_w$ the electron energy density flux:

$$\boldsymbol{\Gamma}_w = \frac{5}{3}\mu_e w_e \boldsymbol{E} - \frac{5}{3}D_e \boldsymbol{\nabla}w_e, \tag{9.10}$$

and μ_e and D_e the electron mobility and electron diffusion coefficients. The term S_w in the electron energy balance equation is the loss of electron energy due to electron impact collisions, including excitation, ionization, attachment and recombination of electrons on the dust particle's surface. Via the surface charge on the electrodes the plasma can be connected to an RLC circuit. Further details about the algorithms used to solve the above mentioned equations can be found in [6].

9.2.2 Implementing dust as a fluid

Charging of dust

When a dust particle exceeds a certain size it can collect more than one electron and be charged up to the floating potential relative to the surrounding plasma. This

potential depends on the local ion and electron density and energy distribution. For a spherical dust particle with a radius r_d, much smaller than the linearized Debye length, the Orbital-Motion-Limited theory (OML) [10] predicts a positive ion and electron current, at equilibrium given by:

$$I_i = 4\pi r_d^2 e n_i \sqrt{\frac{k_B T_i}{2\pi m_i}} \left(1 - \frac{eV_{fl}}{k_B T_i}\right), \tag{9.11}$$

$$I_e = 4\pi r_d^2 e n_e \sqrt{\frac{k_B T_e}{2\pi m_e}} \exp\left(\frac{eV_{fl}}{k_B T_e}\right). \tag{9.12}$$

Here, n_e is the electron density, n_i the positive ion density, e the elementary charge, k_B Boltzmann's constant, T_i the positive ion temperature , T_e the electron temperature, m_i the ion mass, m_e the electron mass, and V_{fl} the floating potential. All species are assumed to have a Maxwellian energy distribution. The influence of neighboring dust particles is neglected.

When the ions enter the plasma sheaths near the electrodes, they get a directed velocity $\boldsymbol{v}_i$ due to the electric field. Therefore, we have replaced $k_B T_i$ in the expression for the ion current by the mean energy E_i, which is:

$$E_i = \frac{4 k_B T_{gas}}{\pi} + \frac{1}{2} m_i v_i^2. \tag{9.13}$$

Equation 9.13 is obtained by using the mean speed expression of Barnes et al [12] given by:

$$v_s = \left(\frac{8 k_B T_{gas}}{\pi m_i} + v_i^2\right)^{1/2}. \tag{9.14}$$

By calculating $\frac{1}{2} m_i v_s^2$, equation 9.13 is obtained. The directed velocity $\boldsymbol{v}_i$ is the drift velocity of the ions.

In the model the charge $Q_d = 4\pi\epsilon_0 r_d V_{fl}$ on the dust is calculated from the equilibrium of the currents in equation 9.11 and 9.12. The current of negative ions towards the dust particle's surface is neglected, the negative ions do not have enough kinetic energy to overcome the negative floating potential of the dust particle.

The floating potential of the dust is assumed to be constant during an RF cycle. This assumption is justified by the fact that the currents towards the dust particle surface are too small to change the charge significantly during an RF cycle.

Recombination on dust particles

When a dust particle becomes negatively charged, it will attract positive ions, these will recombine with an electron that has to be replaced again by an electron

from the discharge to maintain the floating potential. As a result the equilibrium fluxes of positive ions and electrons arriving at the dust surface will recombine and the released energy is used to heat up the dust particle surface [4, 8]. The electron flux (Eq. 9.12) results in a recombination rate:

$$R = 4\pi r_d^2 n_d n_e \sqrt{\frac{k_B T_e}{2\pi m_e}} \exp\left(\frac{eV_{fl}}{k_B T_e}\right), \tag{9.15}$$

Forces acting on a dust particle

In a plasma dust particles undergo a wide variety of forces. Assuming that a dust particle is a perfect sphere the gravitational force can be written as:

$$\boldsymbol{F}_g = \frac{4}{3}\pi r_d^3 \rho_d \boldsymbol{g}, \tag{9.16}$$

where r_d is the dust particle radius, ρ_d is the mass density and $\boldsymbol{g}$ is the gravitational acceleration. For the often used melamine-formaldehyde dust particle ρ_d is approximately $1.51 \cdot 10^3 \ kg/m^3$.

When a dust particle has a velocity relative to the neutral gas, it will experience a drag force due to momentum transfer from/to the gas. This neutral drag force has been discussed in detail by Graves et al [11]. It can be approximated by,

$$\boldsymbol{F}_n = -\frac{4}{3}\pi r_d^2 n_n \left(\boldsymbol{v}_d - \boldsymbol{v}_n\right) v_{th} m_n, \tag{9.17}$$

where n_n is the density of the neutral with mass m_n, $\boldsymbol{v}_d$ the drift velocity of the dust particle, $\boldsymbol{v}_n$ the velocity of the gas and v_{th} the average thermal velocity of the gas. Because advection of the neutral gas is not included in the model, $\boldsymbol{v}_n = \boldsymbol{0}$, this force will only be present as a damping force on the velocity of the dust particles.

Another force caused by momentum transfer is the ion drag. This force results from the positive and negative ion current that is driven by the electric field. It consists of two components. The collection force represents the momentum transfer of all the ions that are collected by the dust particle and is given by:

$$\boldsymbol{F}_i^c = \pi b_c^2 n_i v_s m_i \boldsymbol{v}_i, \tag{9.18}$$

where v_s the mean speed of the ions, $\boldsymbol{v}_i$ the ion drift velocity and b_c the collection impact parameter.

The second component is the orbit force given by:

$$\boldsymbol{F}_i^o = \sum_i 4\pi b_{\pi/2}^2 \Gamma n_i v_s m_i \boldsymbol{v}_i, \tag{9.19}$$

with $b_{\pi/2}$ the impact parameter that corresponds to a deflection angle $\pi/2$ and Γ the Coulomb logarithm.

$$\Gamma = \frac{1}{2}\ln\left(\frac{\lambda_L^2 + b_{\pi/2}^2}{b_c^2 + b_{\pi/2}^2}\right), \qquad (9.20)$$

λ_L is the linearized Debye length. The orbit force is summed for all ionic species. For the negative ions we have neglected the collection force because their kinetic energy is too low to overcome the negative floating potential of the dust. The ion drag is discussed in more detail by Barnes et al [12]. Previous calculations have shown that the ion drag should be enhanced with at least a factor 5 or the linearized Debye length in the Coulomb logarithm (Eq. 9.20) should be replaced by the electron Debye length, in order to generate a void [3]. We have used the electron Debye length in the calculations presented here. Khrapak et al [13] have studied cases where the ion drag force is underestimated by using the ion drag expression of Barnes with the linearized Debye length in the Coulomb logarithm. These cases are quite similar to ours. Lampe et al [14] have shown that collisions with the background gas may enhance the collection of ions.

Due to their charge, dust particles will experience an electric force. Daugherty et al [15] derived the following expression:

$$\boldsymbol{F}_e = Q_d\boldsymbol{E}\underbrace{\left(1 + \frac{\kappa r_d}{3(1 + \kappa r_d)}\right)}_{\approx 1}, \qquad (9.21)$$

where Q_d is the charge on the dust particle, $\boldsymbol{E}$ is the electric field and $\kappa = 1/\lambda_L$. In a discharge the dust particle radius is much smaller than the linearized Debye length, therefore the term between the bracket is approximately 1 and the electric force is given by:

$$\boldsymbol{F}_e = Q_d\boldsymbol{E}. \qquad (9.22)$$

This expression holds for situations where the dust particles are not shielded from the plasma by positive ions trapped in orbitals around the dust particle [14]. In that case the particle plus ion cloud will behave as some kind of dipole.

When a temperature gradient is present in a discharge, for instance due to cooling or heating of the electrodes a third force driven by momentum transfer will occur. This force is called the thermophoretic force. Atoms impinging from the hot side have more momentum than their companions of the cold side, this can result in a force pointing in the direction $-\boldsymbol{\nabla}T_{gas}$.

For large Knudsen numbers Talbot et al [16] derived the following expression:

$$\boldsymbol{F}_{th} = -\frac{32}{15}\frac{r_d^2}{v_{th}}\left(1 + \frac{5\pi}{32}(1 - \alpha)\right)\kappa_T\boldsymbol{\nabla}T_{gas}, \qquad (9.23)$$

$v_{th} = [8k_B T_{gas}/(\pi m)]^{1/2}$ is the average thermal velocity of the gas. κ_T is the translation part of the thermal conductivity. α, the thermal accommodation coefficient of the gas is taken equal to 1.

To obtain a suitable expression for the flux of dust particles, we assume that the neutral drag force is in equilibrium with the sum of the other forces. This assumption is valid when the final steady state is approached, but should be relaxed, for instance, when the dust is injected at a high velocity. In that case the inertia of the dust should not be neglected. With the introduction of a momentum loss frequency and a mobility and diffusion coefficient for the dust particles given by:

$$\nu_{md} = \sqrt{2}\frac{p_{tot}}{k_B T_{gas}}\pi r_d^2\sqrt{\frac{8k_B T_{gas}}{\pi m_d}}, \tag{9.24}$$

where p_{tot} is the static pressure and m_d the dust particle's mass,

$$\mu_d = \frac{Q_d}{m_d \nu_{md}}, \tag{9.25}$$

$$D_d = \mu_d \frac{k_B T_{gas}}{Q_d}, \tag{9.26}$$

it is possible to define a "drift-diffusion" expression for the flux of the dust particles,

$$\begin{aligned}
\mathbf{\Gamma}_d &= -\mu_d n_d \boldsymbol{E}_{eff} - D_d \boldsymbol{\nabla} n_d - \frac{n_d}{\nu_{md}}\boldsymbol{g} \\
&+ \frac{n_d m_i v_s}{m_d \nu_{md}}\left(\sum_{i=pos}^{neg} 4\pi b_{\pi/2}^2 \Gamma \mathbf{\Gamma}_i + \sum_{i=pos} \pi b_c^2 \mathbf{\Gamma}_i\right) \\
&- \frac{32}{15}\frac{n_d r_d^2}{m_d \nu_{md} v_{th}}\kappa_T \boldsymbol{\nabla} T_{gas},
\end{aligned} \tag{9.27}$$

and treat them with the same numerical procedures as the other charged particles in the fluid model. Because of the low mobility of the dust particles the effective field $\boldsymbol{E}_{eff}$ is approximated by the time averaged RF field. The diffusion originates from the pressure gradient, $k_B T_d \boldsymbol{\nabla} n_d$. The Einstein relation couples the diffusion and the mobility coefficients, see equation 9.26.

The internal pressure of the crystal due to the inter-particle interaction has been included by means of an equation of state for the dust. Gozadinos et al [5] have obtained an expression for the equation of state for a crystalline structure of dust particles. The crystalline pressure is given by:

$$P_{cr} = \frac{(1+\beta\kappa)}{3\beta}N_{nn}\Gamma P_g \exp(-\beta\kappa) \tag{9.28}$$

where $\Gamma = Q_d^2/4\pi\epsilon_0\Delta k_B T_d$ is the coupling parameter, $\Delta = n_d^{-1/3}$ is the mean inter-particle distance, $\kappa = \Delta/\lambda_e, P_g = n_d k_B T_d$, N_{nn} is the number of nearest neighbours (N_{nn}=8 and β=1.09 for bcc lattices, N_{nn}=12 and β=1.12 for fcc and hcp lattices). We take only a fcc and hcp lattices into account in our simulations. With the above equation the effective diffusion coefficient for the crystalline regions becomes

$$D_d = \frac{dP_{cr}/dn}{m_d\nu_m} \tag{9.29}$$

Further details can be found in [5].

The drift velocity and the diffusion coefficient of the dust fluids are much smaller than those of the ions and electrons. Therefore it would require a large computational effort to achieve a steady state solution for the dust when it is followed during an RF cycle. We therefore have developed a method to speed up the convergence toward the steady state solution by introducing a different calculation cycle with a different time step for the dust. Our model thus consists of two calculation cycles. In the first one, the transport equations of the ions, electrons and the Poisson equation are solved during a number of RF cycles. During the RF cycles the dust does not move and its charge does not change. After that, the transport equation of the dust is solved with a greater time step, using the time averaged electric field, and electron and positive ion fluxes. During the second calculation, space charge regions are created, because the electron, positive and negative ion densities do not change. These space charge regions will lead to instabilities in the solution of Poisson equation and the electron transport. To solve this problem, we correct the artificially generated space charge by adapting the positive ion density distributions prior to the next series of RF cycles, in which the ion and electron density profiles adapt themselves to the new dust density profile. With this method the required speed-up is established. Both for the plasma species and for the dust fluids the transport equations are solved using the Sharfetter-Gummel exponential scheme [6]. To model the reactor, we have used a grid of 24 radial gridpoints times 48 axial gridpoints. We make use of a non-equidistant grid. The radial spatial resolution is 0.21 cm and the axial resolution between the electrodes is 0.09 cm. More details about the discretion scheme can be found in [6].

9.3   Results and discussion

In this section the results, obtained with the 2D dust fluid model are presented. The PKE chamber used by Morfill et al has been modelled. The reactor is cylindrically symmetric. The simulation starts with a zero dust density profile. During the simulation the dust is injected from both electrodes by adding source terms in the dust particle balances for the first grid points below/above the electrodes. The

injection rate is about 750.000 particles per second. Eventually a total amount of 1 million dust particles is reached, after that the sources are switched off. The electrodes are both driven by a radio-frequency power source at a frequency of 13.56 MHz. Two peak-to-peak voltages have been chosen, 300 and 600 volts. We have chosen these high values because simulations of electronegative discharges at lower peak-to-peak voltages than 300 volts crashed due to the low electron density. The pressure is 40 Pa. The dust particles have a diameter of 13.6 μm. Comparisons of the plasma parameters are made for electropositive and electronegative discharges.

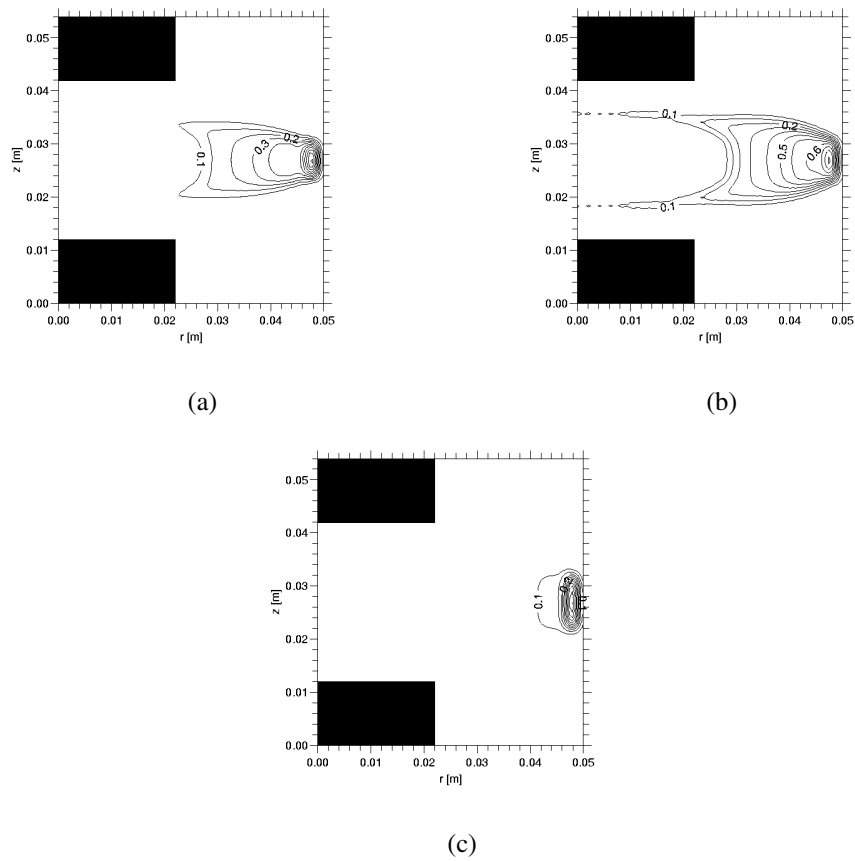(a)   (b)

(c)

Figure 9.1: Dust densities in m^{-3} in different discharges and peak-to-peak voltages.
    (a) Dust density in an electropositive discharge at 300 volts peak-to-peak, normalized with a factor $5.2 \cdot 10^{10}$.
    (b) Dust density in an electronegative discharge at 300 volts peak-to-peak, normalized with a factor $3.1 \cdot 10^{10}$.
    (c) Dust density in an electronegative discharge at 600 volts peak-to-peak, normalized with a factor $1.2 \cdot 10^{11}$.

Figures 9.1a-c show the steady state dust density profiles in different discharges varying the peak-to-peak voltage. In all cases a void (dust-free region) appears during the injection of the dust particles surrounded by a crystalline region as seen in the experiments [1]. After the injection of dust particles is stopped the dust particles move toward the reactor wall due to mainly the ion drag force and the thermophoretic force acting in the radial direction (Fig. 9.2). The forces exerted on the dust particles in the axial direction (Fig. 9.3) in combination with the equation of state speed up the movement of the dust particles toward the reactor wall. Figures 9.2a and 9.2b show that the thermophoretic force becomes more significant at higher peak-to-peak voltages. In the center of the discharge a dust-free region is formed. In figure 9.1b even the remains of the void are still visible.
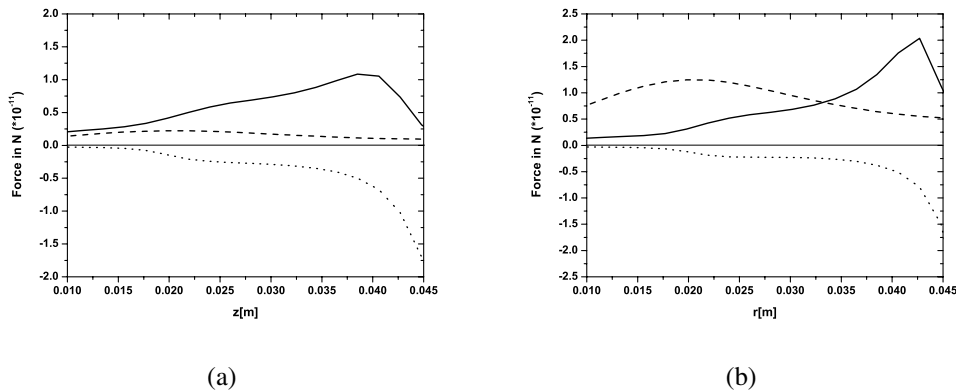

(a)	(b)

Figure 9.2: Forces acting on the dust particle at different peak-to-peak voltages in radial direction at z=0.021 m.
(a) For a dust-free electronegative discharge at 300 volts peak-to-peak.
(b) For a dust-free electronegative discharge at 600 volts peak-to-peak.
The solid line represents the ion drag force, the dotted line the electric force, the dashed line the thermophoretic force.

Figures 9.4 and 9.5 show the time-averaged potential distribution V(r,z) in the dust-free and the dusty discharges with and without negative ions. In all cases the potential has its maximum in the bulk of the plasma between the electrodes. Comparing the potential distributions, a significant change in the plasma potential can be observed. The slope of the plasma potential in the radial direction for the dusty discharges has increased compared with the dust-free cases. This results in a stronger radial electric field. This effect results from taking into account both the contribution of the charge on the dust (Fig. 9.6) in the Poisson equation and the recombination on the dust particle surface. The non-uniform charge distribution
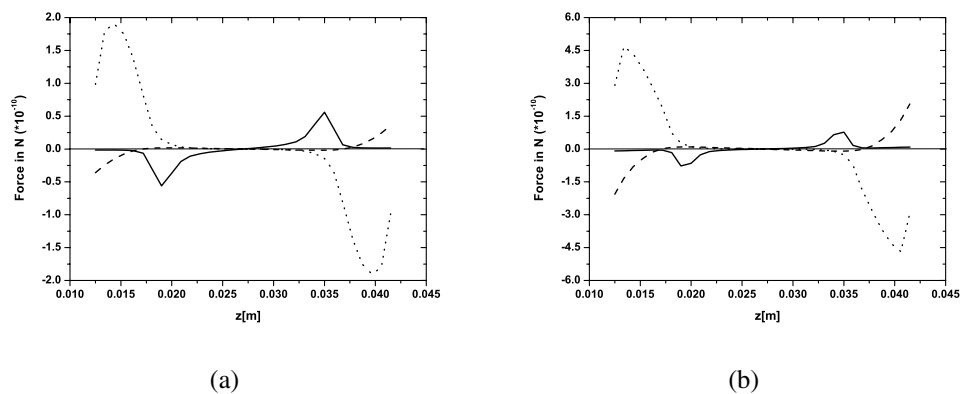
(a)

(b)

Figure 9.3: Forces acting on the dust particle at different peak-to-peak voltages in axial direction at r=0.
(a) For a dust-free electronegative discharge at 300 volts peak-to-peak.
(b) For a dust-free electronegative discharge at 600 volts peak-to-peak.
The solid line represents the ion drag force, the dotted line the electric force, the dashed line the thermophoretic force.
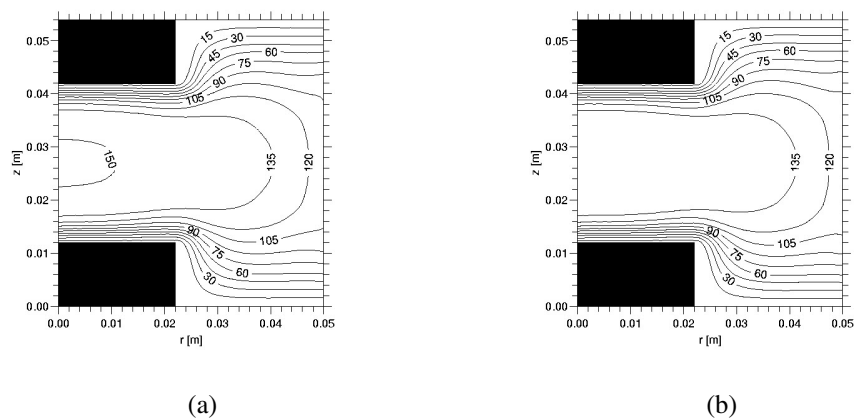

(a)

(b)

Figure 9.4: Time-averaged electric potentials in volts in different dust-free discharges.
(a) In an electropositive discharge at 300 volts peak-to-peak.
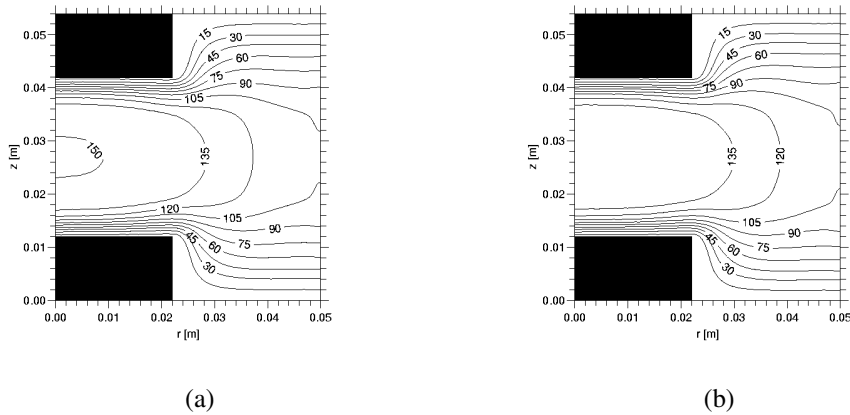(b) In an electronegative discharge at 300 volts peak-to-peak.

Figure 9.5: Time-averaged electric potentials in volts in different dusty discharges.
            (a) In an electropositive discharge at 300 volts peak-to-peak.
            (b) In an electronegative discharge at 300 volts peak-to-peak.

is the result of the spatial distribution of the ions, electrons and electron energy. The enhanced ion density in the dust cloud reduces the dust charge.

Comparing figures 9.7a and 9.7b, shows a lower electron density for an electronegative discharge due to the formation of negative ions. Another effect that can also be observed is the weaker radial electric field in the electronegative discharge resulting in a radially broader electron density profile. After the injection of dust particles, the radial electric field becomes stronger, resulting in a more confined electron density profiles (Fig. 9.8). Due to a higher electron temperature in the case of an dusty electropositive discharge the ionization rate increases resulting in slightly more electrons in the center (Fig. 9.9a). For an dusty electronegative discharge the electron density (Fig. 9.9b) shows even a small decrease due to a lower electron temperature in the center of the discharge. Comparing the negative ion density profiles (Fig. 9.10a and 9.10b) shows an increase of the negative ions density in the center of a dusty discharge due to a steeper electric potential profile (Fig. 9.5b). Due to a lower electron density in an dust-free electronegative discharge, the electrons can gain more energy from the larger oscillating electric field, this gives rise to a higher electron temperature compared to a dust-free electropositive discharge (Fig. 9.11a and 9.11b).

Comparing the positive ion density profiles for dust-free discharges with and without the formation of negative ions (Fig. 9.12a and 9.12b), shows a significant increase of the positive ion density in an electronegative discharge, this is due to the formation of negative ions which have to be compensated by the positive ions to maintain quasi-neutrality in the bulk of the plasma. For the dusty discharges
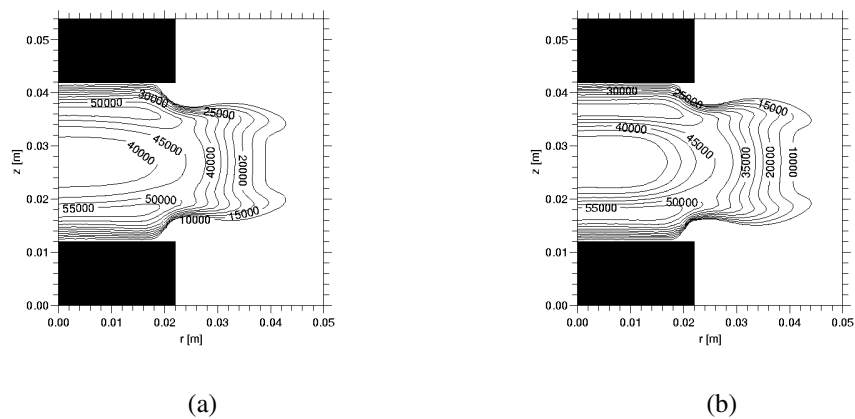
(a) (b)

Figure 9.6: Number of electrons on a dust particle in different dusty discharges.
(a) In an electropositive discharge at 300 volts peak-to-peak.
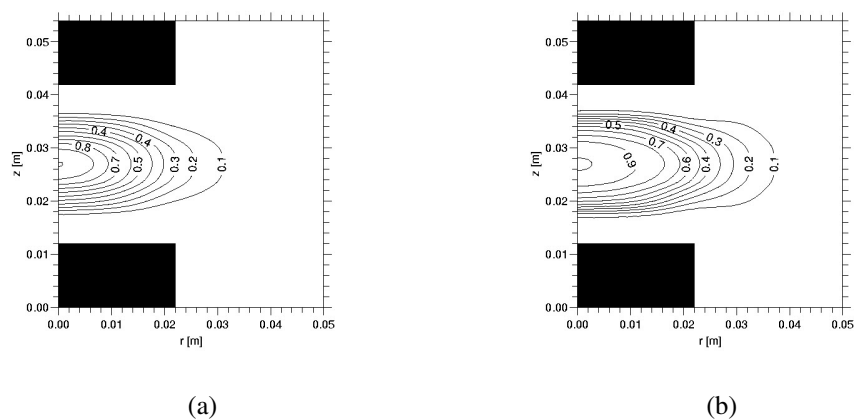(b) In an electronegative discharge at 300 peak-to-peak.

(a) (b)

Figure 9.7: Time-averaged electron densities in m^{-3} in different dust-free discharges.
(a) In an electropositive discharge at 300 volts peak-to-peak, normalized with a factor $1.7 \cdot 10^{16}$.
(b) In an electronegative discharge at 300 volts peak-to-peak, normalized with a factor $0.9 \cdot 10^{16}$.

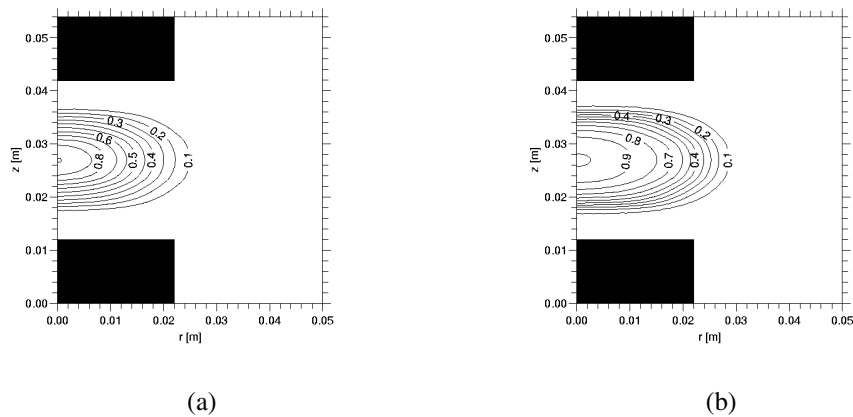(a)   (b)

Figure 9.8: Time-averaged electron densities in m^{-3} in different dusty discharges.
(a) In an electropositive discharge at 300 volts peak-to-peak, normalized with a factor $1.9 \cdot 10^{16}$.
(b) In an electronegative discharge at 300 volts peak-to-peak, normalized with a factor $0.8 \cdot 10^{16}$.

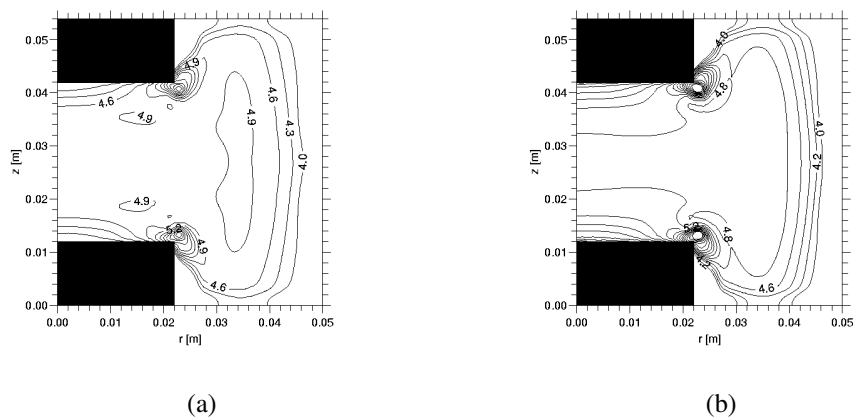(a)   (b)

Figure 9.9: Time-averaged electron temperature in K in different dusty discharges.
(a) In an electropositive discharge at 300 volts peak-to-peak.
(b) In an electronegative discharge at 300 volts peak-to-peak.
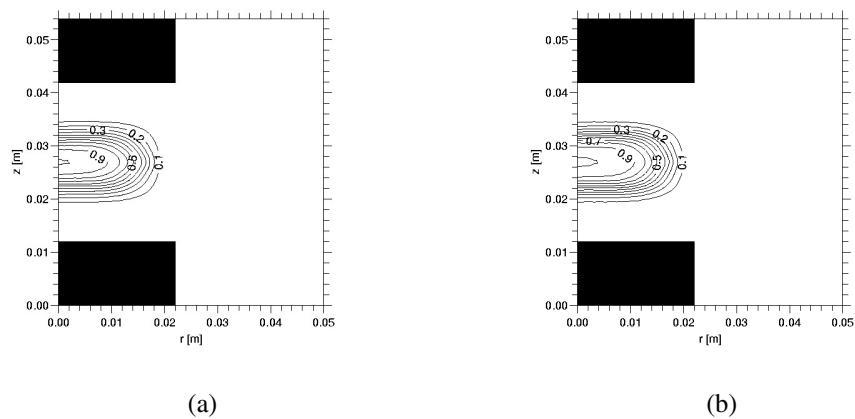
(a)   (b)

Figure 9.10: Time-averaged negative ion densities in m^{-3} in different discharges.
(a) In a dust-free electronegative discharge at 300 volts peak-to-peak, normalized with a factor $1.8 \cdot 10^{16}$.
(b) In a dusty electronegative discharge at 300 volts peak-to-peak, normalized with a factor $2.0 \cdot 10^{16}$.

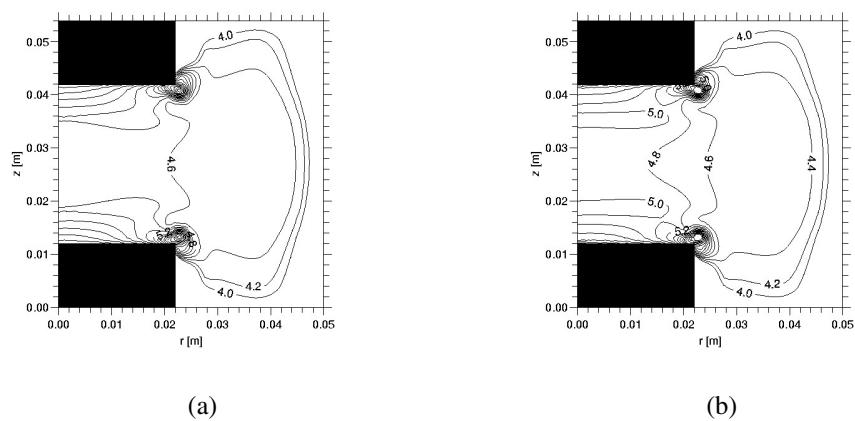(a)   (b)

Figure 9.11: Time-averaged electron temperature in K in different dust-free discharges.
(a) In an electropositive discharge at 300 volts peak-to-peak.
(b) In an electronegative discharge at 300 volts peak-to-peak.

the positive ions (Fig. 9.12a and 9.12b) are more confined due to a stronger confinement of the electrons and negative ions. In the center of the dusty discharges also slight increase of the positive ion density (Fig. 9.13a and 9.13b) can be observed. For the dusty electropositive discharge this effect can be attributed to a higher electron temperature (Fig. 9.11a and 9.9a) resulting in an larger ionization rate. For an electronegative plasma the increase is due to a better confinement of the negative ions (quasi-neutrality).
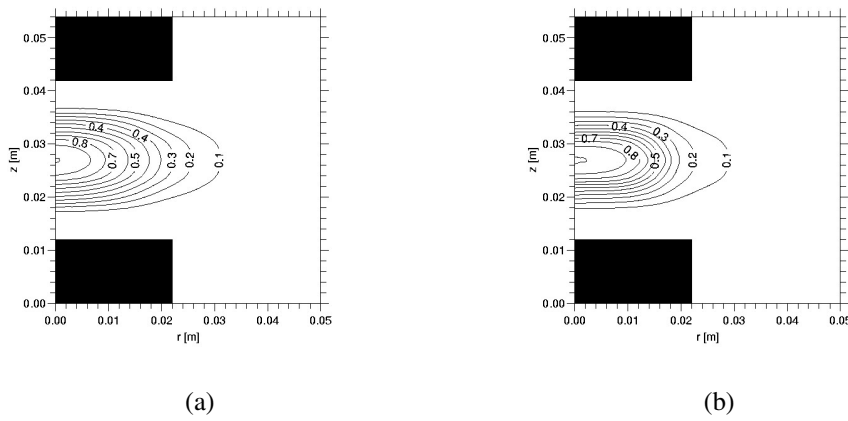

(a)   (b)

Figure 9.12: Time-averaged ion densities in m^{-3} in different dusty-free discharges.
(a) In an electropositive discharge at 300 volts peak-to-peak, normalized with a factor $1.7 \cdot 10^{16}$.
(b) In an electronegative discharge at 300 volts peak-to-peak, normalized with a factor $2.7 \cdot 10^{16}$.

Figures 9.14a and 9.15a show the gas temperature for an electropositive and electronegative dusty discharge. The gas temperature profiles in the dusty plasmas have two maxima of 290 K in the sheaths, which is about 17 K higher than the reactor wall temperature that is kept at 273 K. No significant differences can be observed between the two gas temperature profiles. In figures 9.14a and 9.15a the dust particle (surface) temperature is shown for an electropositive and electronegative dusty discharge, it can be observed that a dust particle would get a maximum temperature in the center of the plasma if it would settle there. This is due to the maximum in the ion and electron density in the middle of the discharge, giving a maximum recombination energy flux towards the dust particles surface. Note that the difference between the gas and dust particle surface temperature would be about 72 K if the particle is at the center of the discharge.

(a)   (b)
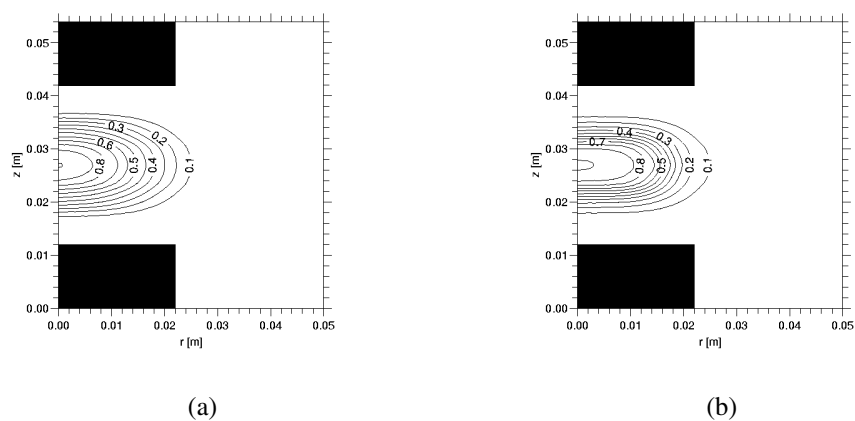
Figure 9.13: Time-averaged ion densities in m^{-3} in different dusty discharges.
(a) In an electropositive discharge at 300 volts peak-to-peak, normalized with a factor $1.9 \cdot 10^{16}$.
(b) In an electronegative discharge at 300 volts peak-to-peak, normalized with a factor $2.8 \cdot 10^{16}$.

(a)   (b)

Figure 9.14: Gas (a) and dust particle material temperature (b) in a dusty electropositive discharge in K at 300 volts peak-to-peak.

Figure 9.15: Gas (a) and dust particle material temperature (b) in a dusty electronegative discharge in K at 300 volts peak-to-peak.

9.4   Conclusions

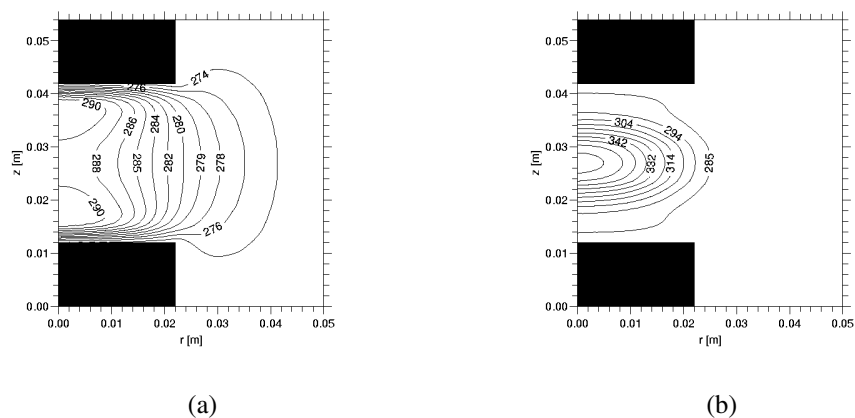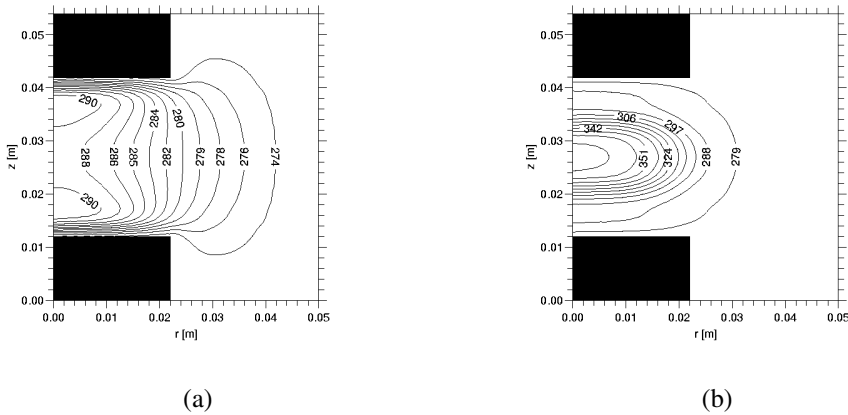Modelling results have shown significant differences in plasma parameters, like the electron densities and ion densities, between electropositive and electronegative dusty discharges. This results in different steady state solutions for the dust density profile. The positive ion density at the center of a dust-free discharge becomes 50% higher in an electronegative discharge compared to an electropositive discharge at the same pressure and peak-to-peak voltage. This significant increase in positive ion density can be attributed to the formation of negative ions and maintaining quasi-neutrality in the bulk of the plasma. The electron density decreases with a factor 2 for the electronegative case. Introducing dust particles at the chosen peak-to peak voltages results for both discharges in the formation of a dust cloud close to the reactor wall. At these positions the influence of this dust cloud on the plasma parameters is very small due to the negligible recombination on the dust particle surface. The results indicate a smaller void in an electronegative discharge than in an electropositive discharge. This can be attributed to the fact that the electric potential in an electronegative discharge is somewhat lower and flatter at the center. The thermophoretic force becomes more significant at higher peak-to-peak voltages.

Acknowledgments

ratom.

References

[1] G. E. Morfill et al, Phys. Rev. Lett., **83**, 1598 (1999).

[2] H. Thomas et al, Phys. Rev. Lett., **73**, 652 (1994).

[3] M. R. Akdim et al, Phys. Rev. E., **65**, 015401(R) (2002).

[4] M. R. Akdim et al, Phys. Rev. E., **67**, 066407 (2003).

[5] G. Gozadinos et al, New J. Phys., **5**, (2003).

[6] J. D. P. Passchier et al, J. Appl. Phys., **73**, 1073 (1993).

[7] I. Revel et al, J. Appl. Phys., **88**, 2234 (2000).

[8] G. H. P. M. Swinkels et al, J. Appl. Phys., **88**, 1747 (2000).

[9] J. P. Boeuf et al, Phys. Rev. A., **36**, 2782 (1987).

[10] J. E. Allen et al, J. Plasma. Phys., **63**, 299 (2000).

[11] D. B. Graves et al, Plasma Sources Sci. Technol., **3**, 433 (1994).

[12] M. S. Barnes et al, Phys. Rev. Lett., **68**, 313 (1992).

[13] S. A. Khrapak et al, Phys. Rev. E., **66**, 046414 (2002).

[14] M. Lampe et al, Phys. Rev. Lett., **86**, 5278 (2001).

[15] J. E. Daugherty et al, J. Appl. Phys., **73**, 1617 (1994).

[16] L. Talbot et al, J. Fluid Mech., **101**, 737 (1980).

Summary

Nowadays plasmas are used for various applications such as the fabrication of silicon solar cells, integrated circuits, coatings and dental cleaning. In the case of a processing plasma, e.g. for the fabrication of amorphous silicon solar cells, a mixture of silane and hydrogen gas is injected in a reactor. These gases are decomposed by making a plasma. A plasma with a low degree of ionization (typically 10^{-5}) is usually made in a reactor containing two electrodes driven by a radio-frequency (RF) power source in the megahertz range. Under the right circumstances the radicals, neutrals and ions can react further to produce nanometer sized dust particles. The particles can stick to the surface and thereby contribute to a higher deposition rate. Another possibility is that the nanometer sized particles coagulate and form larger micron sized particles. These particles obtain a high negative charge, due to their large radius and are usually trapped in a radio-frequency plasma. The electric field present in the discharge sheaths causes the entrapment. Such plasmas are called dusty or complex plasmas. In this thesis numerical models are presented which describe dusty plasmas in reactive and non-reactive plasmas.

We started first with the development of a simple one-dimensional silane fluid model where a dusty radio-frequency silane/hydrogen discharge is simulated. In the model, discharge quantities like the fluxes, densities and electric field are calculated self-consistently. A radius and an initial density profile for the spherical dust particles are given and the charge and the density of the dust are calculated with an iterative method. During the transport of the dust, its charge is kept constant in time. The dust influences the electric field distribution through its charge and the density of the plasma through recombination of positive ions and electrons at its surface. In the model this process gives an extra production of silane radicals, since the growth of dust is not included. Results are presented for situations in which the dust significantly changes the discharge characteristics, both by a strong reduction of the electron density and by altering the electric field by its charge. Simulations for dust with a radius of 2 μm show that the stationary solution of the dust density and the average electric field depend on the total amount of the dust. The presence of dust enhances the deposition rate of amorphous silicon

at the electrodes because of the rise in the average electron energy associated with the decrease of the electron density and the constraint of a constant power input. This increase of deposition rate has also been observed in experiments by others.

To study the behavior of dust in a less complicated environment, experiments in non-reactive plasmas have been carried out by a number of research groups. In these experiments the dust particles are injected through the electrodes in an argon discharge. These experiments have shown very interesting phenomena. Dust particles start to interact with each other in the discharge and form two-dimensional Coulomb clusters. These experiments often show an appearance of a void, a dust-free region in the discharge. Similar experiments have also been carried out under microgravity. These experiments have shown three-dimensional Coulomb clusters of dust particles also with the appearance of a void. Also rotating dust clouds (vortices) near the edges of the electrodes have been observed, that tend to rotate as long as the plasmas is on.

To understand the behavior of the particles, we have developed a two-dimensional fluid model for a dusty argon plasma in which the plasma and dust parameters are solved self-consistently to study the behavior of dust particles. Simulations for dust with a radius of 7.5 μm show that a double space charge layer is created around the sharp boundary of the dust crystal. The inter-particle interaction is taken into account by means of an equation of state for the dust. A central dust-free region (void) is created by the ion drag force. The contribution of the thermophoretic force, driven by the temperature gradient induced by gas heating from ion-neutral collisions and heating of the dust particle material by the recombining ions and electrons, can be neglected in the quasi-neutral center of the plasma. Inside this void a strong increase of the production of argon meta-stables is found. This phenomenon is in agreement with experimental observations, where an enhanced light emission is seen inside the void.

The dusty argon fluid model has been supplemented with a separate dust particle tracing module to study the behavior of dust vortices. Simulation results show that the non-conservative total force exerted by the discharge on the dust particles is responsible for the generation of the vortices. The contribution of the thermophoretic force driven by the gas temperature gradient plays an insignificant role in the generation of the vortices, even when the gas heating via the dust particles is taken into account. The forces related to the electric field, including the ion drag force, are dominant.

We have upgraded the above mentioned dusty argon fluid model plasma to model more than one dust species. Dust particles with two different diameters have been studied. The final steady state solution is achieved after three injection steps of the dust particles. At every injection phase dust particles of only one size are let in and the simulation is continued until the steady state solution is achieved. Results show that the differently sized dust particles form crystals at

different positions. These dust clouds have an influence on each other by means of positive space charge layers created due to the argon ions which can not match the steep dust crystal boundaries. The screened Coulomb interaction between the two differently sized dust species is neglected. The electric potential, ion density, electron density and electron energy show significant changes after each injection phase, even at an amount of dust that is small compared to that studied during the microgravity experiments.

Experiments done under microgravity have shown that traces of molecular gases, like oxygen influence the size of the void. These molecular gases produce negative ions via (dissociative) attachment. A considerable amount of negative ions changes the plasma properties, especially the potential distribution, and therefore the forces acting on a dust particle. We have investigated these phenomena by means of a two-dimensional fluid model. In this model we have included the possibility that negative ions are formed. By changing the attachment rate, we can control the electronegativity of the gas. As in electropositive discharges the resulting thermophoretic force, however, can be neglected at low powers compared to the other forces. Results from the fluid model show that indeed the presence of negative ions influences the evolution of the void and its final size when the applied voltage is varied.

A natural extension for the silane model would be to include a growth model for the dust and taking the deposition of small dust grains into account. At high power inputs, the chemistry on the dust particle surface should also be accounted for, this may explain the high deposition rates seen in experiments which could not be explained by our model. In the case of the two-dimensional dusty fluid models comparison with kinetic models could result in an improved treatment of the charging of dust. Kinetic modelling of dust particles in a discharge on a microscopic level could also give more information about the Debye spheres surrounding the dust particles. This is important for the calculation of the ion drag force and of course the equation of state for the dust crystal.

Samenvatting

Tegenwoordig worden plasma's gebruikt voor verschillende applicaties, zoals de fabricage van silicium zonnecellen, geïntegreerde schakelingen, coatings en gebits-verzorging. In het geval van een plasma voor bijvoorbeeld de fabricage van amorf-silicium zonnecellen, wordt een mengsel van silaan en waterstof gas geïnjecteerd in een reactor. Deze gassen worden ontleed door het maken van een plasma. Een plasma met een lage ionisatiegraad (typische waarde 10^{-5}) wordt meestal gemaakt in een reactor met twee electrodes die bekrachtigd worden door een ra-diofrequente (RF) spanningsbron in het megahertz bereik. Onder de juiste om-standigheden kunnen de radicalen, neutralen en ionen verder reageren tot deelt-jes met een grootte van enkele nanometers. Deze deeltjes kunnen zich aan het substraat hechten en bijdragen aan een hogere depositiesnelheid. Een andere mo-gelijkheid is dat de deeltjes met een grootte van enkele nanometers gaan samen-klonteren en deeltjes gaan vormen met een grootte van enkele micrometers. Deze deeltjes krijgen een grote negatieve lading door hun grote straal en worden meestal gevangen gehouden in het radiofrequente plasma. Het aanwezige elektrische veld in de grenslagen zorgt voor het isolement. Zulke plasma's worden stoffige of com-plexe plasma's genoemd. In dit proefschrift worden numerieke modellen gepre-senteerd voor het beschrijven van stoffige plasma's in reactieve en niet-reactieve plasma's.

We zijn eerst begonnen met de ontwikkeling van een eenvoudig een-dimen-sionaal vloeistofmodel waarmee een stoffige radiofrequente silaan/waterstof ont-lading gesimuleerd wordt. In het model worden plasma grootheden als fluxen, dichtheden en elektrisch veld zelf-consistent uitgerekend. Een straal en een ini-tieel dichtheidsprofiel voor de bolvormige deeltjes worden opgegeven, de lading en dichtheid van het stof worden dan met een iteratieve methode berekend. Gedu-rende het transport van het stof, wordt zijn lading constant gehouden. Het stof heeft invloed op het elektrische veld en de plasmadichtheid door zijn lading en door recombinatie van positieve ionen en elektronen op zijn oppervlak. Dit pro-ces geeft in het model een extra productie van silaan radicalen omdat er geen groeimodel voor het stof is ingebracht. De resultaten hebben betrekking op si-tuaties waar het stof het plasma aanzienlijk verandert, door een sterke verminder-

ing van de elektronendichtheid en door het beïnvloeden van het elektrische veld middels zijn lading. Simulaties van stof met een straal van 2 micrometer laten zien dat de stationaire oplossing van de stofdichtheid en het gemiddeld elektrisch veld afhangt van het totaal aantal aanwezige stofdeeltjes. De aanwezigheid van stof verhoogt de depositiesnelheid van amorf-silicium op de elektroden doordat de gemiddelde elektronen energie toeneemt wat op zijn beurt veroorzaakt wordt door vermindering van de elektronendichtheid en constante vermogen toevoer. Deze verhoging van de depositiesnelheid is ook door anderen geobserveerd in hun experimenten.

Om het gedrag van stof te bestuderen in een minder ingewikkelde omgeving, zijn er in een aantal onderzoeksgroepen experimenten in niet-reaktieve plasma's uitgevoerd. In deze experimenten worden stofdeeltjes in een argon plasma via de elektroden geïnjecteerd. Deze experimenten laten een scala aan interessante verschijnselen zien. Stofdeeltjes beginnen elkaar te voelen in de ontlading en vormen dan twee-dimensionale Couloumb clusters. Deze experimenten laten vaak een stofvrij gebied zien, omgeven door een zone met stof. Ook zijn er soortgelijke experimenten uitgevoerd onder gewichtloosheid. In deze experimenten zijn er drie-dimensionele Couloumb clusters van stofdeeltjes waargenomen met wederom de verschijning van een stofvrij binnengebied. Ook zijn er roterende stofwolken (wervels) waargenomen dichtbij de randen van de elektroden, deze blijven roteren zolang het plasma in stand wordt gehouden.

Om het gedrag van stofdeeltjes te begrijpen, hebben we een twee-dimensionaal vloeistofmodel ontwikkeld voor een stoffige argon plasma waarin de plasma-en stofgrootheden zelf-consistent worden opgelost. Simulaties voor stof met een straal van 7.5 micrometer laten zien dat een dubbele grenslaag wordt gecreëerd rond de scherpe rand van het stofkristal. De interactie tussen de deeltjes wordt door een toestandsvergelijking voor het stof berekend. De centrale stofvrije zone wordt door toedoen van de postieve ionen veroorzaakt, deze slepen het stof naar buiten. De bijdrage van de thermoforetische kracht die wordt gedreven door een temperatuur gradiënt veroorzaakt door het verwarmen van het gas door ion-neutraal botsingen en verwarming van het materiaal waar het stof van gemaakt is door recombinatie van ionen en elektronen, kan worden verwaarloosd in het quasi-neutrale centrale gedeelte van het plasma. In het stofvrije binnengebied wordt een sterke verhoging van de productie van argon metastabielen waargenomen. Dit verschijnsel is in overeenstemming met experimentele observaties, waar een verhoogde lichtemissie uit dit gebied wordt waargenomen.

Het stof-argon vloeistofmodel is uitgebreid met een module waarmee het gedrag van stofwervels bestudeerd kunnen worden. Simulaties laten zien dat de totale niet-conservatieve kracht veroorzaakt door de ontlading en werkend op de stofdeeltjes, verantwoordelijk is voor het ontstaan van wervels. De bijdrage van de thermoforetische kracht speelt wederom geen rol. De krachten die gerelateerd

zijn aan het elektrische veld, waaronder de kracht uitgeoefend door de ionen zijn dominant.

We hebben het bovengenoemde stof-argon vloeistofmodel uitgebreid tot een model dat meerdere verschillende stofdeeltjes kan volgen. Stofdeeltjes met twee verschillende diameters zijn bestudeerd. De uiteindelijke oplossing wordt bereikt na drie injectiestappen van het stof. Gedurende elke injectiefase wordt er stof met één grootte geïecteerd, de simulaties wordt dan vervolgd tot er een stationaire oplossing bereikt is. Resultaten met stof van grootte laten zien dat deze kristallen vormen op verschillende posities. Deze stofwolken beïnvloeden elkaar doormiddel van positieve grenslagen die ontstaan omdat de argonionen de steile stofkristal randen niet kunnen volgen. De gescreende Couloumb interactie tussen de verschillende stofdeeltjes groottes is verwaarloosd. De elektrische potentiaal, ionendichtheid, elektronendichtheid en elektronen energie veranderen significant na elke injectiefase, zelfs al is de totale hoeveelheid aan stof dat wordt gesimuleerd veel minder dan het stof aanwezig in experimenten onder gewichtloosheid.

Experimenten verricht onder gewichtloosheid hebben laten zien dat fracties van moleculaire gassen zoals zuurstof invloed hebben op de grootte van het stofvrije binnengebied. Deze moleculaire gassen produceren negatieve ionen via (dissocatieve) attachment. Een behoorlijke hoeveelheid aan negatieve ionen verandert de plasma eigenschappen, in het bijzonder het elektrische potentiaal profiel, en daardoor de krachten werkend op een stofdeeltje. We hebben deze verschijnselen onderzocht met een twee-dimensionaal vloeistofmodel. In dit model hebben we rekening gehouden met de mogelijke vorming van negatieve ionen. Door de attachment snelheid te veranderen controleren we de elektronegativiteit van het gas. Zoals in elektropositieve ontladingen kan de thermoforetische kracht worden verwaarloosd bij lage vermogens ten opzichte van andere krachten. Resultaten van het vloeistofmodel laten zien dat de aanwezigheid van negatieve ionen de ontwikkeling van het stofvrije binnengebied en zijn uiteindelijke grootte beïnvloedt.

Een vanzelfsprekende uitbreiding van het silaan model zou een groeimodel omvatten voor het stof en zou de depositie van kleine stofdeeltjes in beschouwing moeten nemen. Bij hoge vermogens, moet rekening gehouden worden met de chemie op de grote oppervlakte van het stof, dit kan verklaren waarom de hoge depositiesnelheden in de experimenten niet verklaard kunnen worden met ons model. In het geval van de twee-dimensionale stof vloeistofmodellen kan vergelijking met kinetische modellen resulteren in een verbeterde omschrijving voor de oplading van het stof. kinetische modelleren van stofdeeltjes in een ontlading op microscopische niveau zou ook meer informatie geven over de Debye bollen rondom de stofdeeltjes. Dit is belangrijk voor de berekening van de kracht uitgeoefend door de ionen en natuurlijk voor de toestandsvergelijking van een stofkristal.

Dankwoord

Aan de totstandkoming van dit proefschrift en mijn onderzoek werkten onder andere mee:

> Wim Goedheer, Chris Schüller, Gerrit Kroesen, Govert Kruijtzer, Zahoor Ahmad, Raj Dahiya, Arja Biebericher, Hugo de Blank, Tarig Abdallah en 'Dusty Plasma Community'.

Verder ben ik veel dank verschuldigd aan (in een bijna willekeurige volgorde):

> Vader, Moeder, Fatima (jongste zusje), Amina (een na jongste zusje), Dalila (oudere zus), Rkia (oma), Mohamed (Louis) (oom), Laila (nicht), Mohamed (neef), Noortje Khan, Brahim Boussadkat, Boubker Ibouhouten, Mohamed Kabir Boumandjel, Benaissa Boukarfada, Rachida Bezzazy, Peter Saveur, Mohamed Savon, Theo de Graaf, Diny de Graaf, André van Kan, Erik Olthof, Hajnal Vörös, Hans Goedbloed, Noud Oomens, Margot Beerlage, Peggy Reimus, Jan Kranenbarg, Bart de Groot, Jan Cornelis Wolff, Gerard van Rooij, Niek Lopes Cardozo, Victor Veremiyenko, Gerard Meijer, Ralph Meulenbroeks, Erik Min, Dick Hogeweij, Josée Kragten, Loes van de Ven, Frits Hekkenberg, Fred Wijnholtz, Kees Theunissen, Stef de Kroon, Rony Keppens, Ben Grobben, Wim Mastop, Paul Smeets, Ben Elzendoorn, Jos Oomens en Frits Hoppe.

Al de personen die bijgedragen hebben aan deze leuke periode en die ik niet bij naam heb genoemd, dank ik bij deze.

Curriculum Vitæ

I was born in Utrecht in The Netherlands on the 27nd of January 1976. In 1994, I received my Atheneum diploma at the Oosterlicht College in Nieuwegein, and started studying Physics at the University of Utrecht. The work for my Masters thesis "Group velocity dispersion compensator" was performed at the University of Utrecht, under supervision of Dr. K. de Grauw and Dr. H. C. Gerritsen. I received my Masters degree on the 30th of June 1999. From 1999 to 2003, I performed my Ph.D. research at the FOM Institute for Plasmaphysics Rijnhuizen under the supervision of Dr. W. J. Goedheer and Prof. dr. F. C. Schüller. This thesis is the completion of that work.